THE EFFECTS OF EXPOSURE TO TRACE ELEMENTS ON THE SKELETAL HEALTH OF AMERICAN MINK

THE EFFECTS OF EXPOSURE TO TRACE ELEMENTS ON THE SKELETAL HEALTH OF AMERICAN MINK

By ARIANA FRASCHETTI, H.B.Sc.

A Thesis Submitted to the School of Graduate Studies in Partial Fulfilment of the Requirements for the Degree Master of Applied Science

McMaster University MASTER OF APPLIED SCIENCE (2021) Hamilton, Ontario

(Biomedical Engineering)

TITLE:	The effects of exposure to trace elements on the skeletal health of American mink
AUTHOR:	Ariana Fraschetti, H.B.Sc. (McMaster University)
SUPERVISOR:	Cheryl E. Quenneville, B.Sc., M.E.Sc., Ph.D.
NUMBER OF PAGES:	xix, 156

Lay Abstract

Environmental pollution in regions across Canada puts the health of communities and wildlife at risk. To better measure the impact of pollution in these regions, the implementation of a species monitoring program would benefit those communities who are at the greatest risk. Therefore, this research was aimed at developing an indicator of harmful pollution exposure in mink, an abundant species in Canada, by investigating their bone health.

A group of mink from Alberta and Quebec were collected and their femur and penile bones tested for a variety of bone health measurements. In addition, information on the heavy metal levels in the mink livers were provided. The bone health measurements and heavy metal levels were then compared to look for any relationships between them.

This research found that selenium, rubidium and iron had the strongest effects on bone health. The methods used have set the groundwork for using minks to monitor pollution levels across North America.

Abstract

The release of pollutants by the oil sands industry and pulp and paper mills has been an ongoing environmental concern for decades. Such toxins have been linked to declining reproductive and skeletal health in wildlife species, as they have known endocrine disrupting properties that interfere with hormones responsible for proper reproduction and bone development. As such, declining population sizes because of pollutant exposure has been correlated with altered bone health in mammals. For the purposes of environmental monitoring, the development of a biomarker of pollutant exposure would be a beneficial tool to assess pollution impact on wildlife populations. Therefore, the purpose of this research was to identify this biomarker in the American mink based on measures of their bone health.

Mink from the Athabasca Oil Sands Region and an area surrounding a pulp and paper mill in Quebec were collected. From each mink, a hindlimb femur and the baculum (for males) were dissected. Bones were evaluated through a series of tests to quantify key cortical and cancellous bone structural and material properties. These included dimensional analysis, three-point bending and micro-Computed Tomography. Toxicology reports of trace element exposure levels in the minks were also provided by ECCC. Principal component analyses and correlation matrices were used to identify potential relationships between the bone metrics and trace element levels, followed by linear regression modeling. Results found that the baculum and femur structural properties were correlated with selenium, rubidium and iron concentrations, suggesting that these elements had the strongest influences on bone health for the mink studied here.

This work provides the basis for future research on identifying a biomarker determinant of bone health to be used in environmental monitoring effects programs. The results here indicate that

baculum bone measures are dominated by trace element effects rather than loading effects and are thus a useful bone to investigate for biomonitoring programs. This will provide a simple and reliable method for determining whether there are unsustainable levels of pollution in regions across North America.

Acknowledgements

This work would not have been possible without the support of my supervisor, Cheryl Quenneville. Thank you, Cheryl for believing in me and for your continued guidance and patience through the last three years. I sincerely appreciate everything you have done for me. You have been so kind and considerate, thank you for being the best supervisor I could have asked for. I would also like to thank Phil Thomas for his assistance with this work. Thank you, Phil for your help and guidance, especially with the toxicology aspect. Thanks for being so patient and working hard to help finish this project, this could not have been done without you. I would also like to acknowledge Kristin Eccles for all her help with the statistical analysis, thank you for making the statistics easy to understand! In addition, I would like to thank Environment and Climate Change Canada for funding this project.

Thank you Yasaman for assisting with the dissecting and bending tests. I sincerely appreciate all the effort you went through to help me finish this. I would also like to thank Beth McNally for all her work in completing the imaging for future research for this project.

To my closest friends, you know who you are – thank you for all your kindness. Everything you did was immensely helpful and meaningful. I am so grateful to have you in my life.

Finally, I would like to thank my family. Mom, Dad and Gabriela – thank you for everything you have done for me in the last two years. I am so fortunate to have such a loving and supportive family, without whom I could not have accomplished any of this. You have always supported me in whatever I have wanted to do. Thank you for all the Dharma, care packages, driving, yoga, textbooks and just listening to me talk and present this research. I love you infinitely.

Table of Contents

List of Figures

List of Tables

List of Abbreviations and Symbols

º	Degree
%	Percent
±	Plus/minus
µCT	Micro-computed tomography
µm	Micrometers
Ag	Silver
Al	Aluminum
AOSR	Athabasca oil sands region
Ba	Barium
BMD	Bone mineral density
BW	Bodyweight
Ca	Calcium
Cd	Cadmium
cm	centimeters
Co	Cobalt
Cr	Chromium
Cu	Copper
ECCC	Environment and Climate Change Canada
ECM	Extracellular matrix
EDC	Endocrine disrupting chemical

EEM	Environmental effects monitoring
Fe	Iron
Hg	Mercury
HSI	Hepatosomatic index
K	Potassium
Li	Lithium
Mb	Molybdenum
Mg	Magnesium
mm	Millimeters
Mn	Manganese
Na	Sodium
Ni	Nickel
OC	Organic compound
PAC	Polycyclic aromatic compound
PAH	Polycyclic aromatic hydrocarbon
Pb	Lead
PCA	Principal component analysis
PCB	Polychlorinated biphenyl
POP	Persistent organic pollutant
PTH	Parathyroid hormone
Rb	Rubidium
ROS	Reactive oxygen species

Se	Selenium
Sn	Tin
Sr	Strontium
Zn	Zinc

Declaration of Academic Achievement

The following is a declaration that I, Ariana Fraschetti, completed the research outlined in this thesis and recognize the contributions of Dr. Cheryl Quenneville, Dr. Phillipe Thomas, Environment and Climate Change Canada, Kristin Eccles, Dr. Elizabeth McNally and Yasaman Golandamian. I performed all mechanical testing, imaging, data analysis, image analysis, statistical analysis and writing of this thesis. Dr. Cheryl Quenneville contributed to developing the project plan and contributed to the review of the experimental method, review of the data analysis and review of this thesis. Dr. Phillipe Thomas added to the project plan, provided the mink specimens and toxicology measures. Environment and Climate Change Canada supplied the funding for this research. Kristin Eccles provided guidance on the statistical analyses. Dr. Elizabeth McNally assisted with the final image collection and Yasaman Golandamian contributed to dissecting of the mink specimens and mechanical testing.

Chapter 1– Introduction

Overview: *Bone presents a unique opportunity for assessing the impact of pollution on wildlife health. This chapter focuses on the pollutants produced by the oil and paper industries, bone anatomy and its properties, methods by which to evaluate bone health and presents the potential of these pollutants to be endocrine disruptors within the context of bone health. It concludes with the study rationale, aims and hypotheses for this work.*

1.1 Persistent Organic Pollutants

1.1.1 Endocrine Disrupting Chemicals

The frequency and severity of reproductive problems for humans and wildlife species are significantly increasing worldwide. Within developed countries especially, there have been increases in the prevalence of reproductive diseases and a decline in reproductive success of human populations since the mid-20th century (Woodruff, Schwartz and Giudice, 2010). Moreover, reproductive failure is increasingly being observed in many wildlife species, resulting in declining population sizes every year that if left untreated, may lead to extinction (Andersson *et al.*, 2012). Without correctly identifying the cause, it is unknown whether these reproductive difficulties will continue to worsen, and what the resulting consequences on human and wildlife development will be (Colborn and Clement, 1992).

Numerous studies have attributed a major contribution to the decline in reproductive success to persistent organic pollutants (POPs) (Fox, 2001; Andersson *et al.*, 2012). Many of these also have known endocrine disrupting properties, and as such are known as endocrine disrupting

chemicals (EDCs). The adverse effects of these on ecosystem and human health have been documented since the widespread implementation of the chemical industry in the 1950s (Fox, 2001). Shortly afterwards, the detrimental environmental effects of pesticides were documented and published (Fox, 2001). This sparked significant research into the effects of human-made chemicals on the environment. Research since has demonstrated that exposure to POPs including heavy metals, polychlorinated biphenyls (PCBs), polycyclic aromatic compounds (PACs), organochlorine (OC) pesticides, and other EDCs are strongly linked with reproductive disorders and dysfunction in many species (Fox, 2001; Andersson *et al.*, 2012).

Despite numerous resulting wildlife preservation initiatives, the release of these compounds into the environment at unsustainable levels by industries continues (Andersson *et al.*, 2012). While safety regulations have been enforced on some industries, many are based on standard models of environmental pollution, which are based on identifications of pollutants in the environment at high concentrations (Masuo and Ishido, 2011). However, many environmental chemicals have adverse health effects at very low doses, rendering these models ineffective for protection of all wildlife species (Masuo and Ishido, 2011).

The persistent nature of POPs is attributed to their ability to withstand biological and photolytic degradation, and hydrolysis; they can exist for years before degrading, and range from being very volatile to semivolatile, so can therefore be transported over long distances (Ritter, 1998; Ritter, Solomon and Forget, 2011). As a result, they are quite mobile compounds and may affect regions far from their source. Generally, the more chlorinated one of these compounds is, the more stable and resistant to all forms of degradation it is (Ritter, 1998). In addition, chlorinated compounds are often ring structures, which increases their stability. Notably, some POPs break

down into more persistent compounds, and these prove to be of even greater concern than their parent compound (Ritter, 1998).

The degree of lipophilicity of a POP influences the degree to which it may bioaccumulate in biological tissue (Ritter, 1998). With high lipophilicity, the POP may bioconcentrate in an organism, and be biomagnified through trophic levels. This can potentially put larger carnivores at greatest risk of harmful exposure to these compounds and implies that very little exposure to certain compounds is needed for toxicologically relevant levels to be achieved in an organism (Ritter, 1998).

The degree to which organisms are at risk to harmful POP exposure depends on a variety of factors, such as in which trophic level the organism is, the concentration of POPs to which they are exposed, the type of POP and its properties, and the length of exposure. These factors depend especially on the industrial process that produced them, since different facilities produce different POPs at varying levels, and into different areas of the environment (air, water, and/or soil). Two categories of facilities that are known to release numerous POPs are oil mines and refineries, and pulp and paper mills.

1.1.2 Oil Sands Operations

The Canadian oil sands are the third largest oil reserve worldwide, and one major region of reserves is the Athabasca Oil Sands Region (AOSR) in the provinces of Alberta and Saskatchewan (Kurek *et al.*, 2013). Despite its economic significance, the processes of oil mining, extraction and upgrading produce harmful POPs that are released into the air, water and soil locally and remotely. This has created controversy regarding water and air quality and what the potential consequences are on local wildlife and communities (Schindler, 2010; Kurek *et al.*, 2013). Moreover, concerns have risen regarding the lack of efficient environmental monitoring

of the effects on freshwater quality, identified by previous scientific reviews of the Regional Aquatics Monitoring Program (RAMP) (Gosselin *et al.*, 2010). Thus, to assess the risk the oil industry poses on wildlife in the AOSR, it is important to know what POPs exist in the region and why.

The process of surface-mining oil sands, extracting bitumen and upgrading bitumen deposit several POPs directly into the atmosphere (Kelly *et al.*, 2009; Zhang *et al.*, 2016). Of these POPs, many of them are listed in the top 15 most hazardous substances according to the US Agency for Toxic Substances and Disease Registry and include: polycyclic aromatic hydrocarbons (PAHs), alkylated PAHs, polychlorinated biphenyls (PCBs), Aroclor 1260, Aroclor 1254, arsenic, lead, mercury, benzene and cadmium (U.S. Department of Health and Human Services, no date). Because they are deposited in the atmosphere they become part of the water cycle as well, eventually being deposited in local lakes and tributaries like the Athabasca river (Kelly *et al.*, 2009; Kurek *et al.*, 2013). In addition, due to their persistence and volatile properties they can travel far outside the AOSR region and affect other regions as well.

Other oil sands operations are also responsible for the release of other PACs and heavy metals into terrestrial and aquatic environments (Kelly *et al.*, 2009). After the sand has been mined, bitumen is extracted using hot water often retrieved from nearby fresh water sources (Masliyah *et al.*, 2004; Allen, 2008). After processing, this oil sands processing water (OSPW) contains the leftover sand, clay, minerals, organic compounds and residual bitumen. Some of the organic compounds include naphthenic acids (NAs), asphaltenes, benzene, creosols, phenols, phthalates, polycyclic aromatic compounds and toluene (Allen, 2008). The OSPW is then capped with clean water and stored in dam and dyke facilities termed “tailing ponds” on site, which will often be recycled for further extraction and processing of new sand (Madill *et al.*, 2001; Syncrude

Canada, 2020). These ponds are significant contributors to local aquatic and terrestrial pollution, as a wide variety of aquatic, aerial and terrestrial organisms are exposed to them. In addition, drainage water from the operations process contaminates soil, groundwater, and nearby tributaries (Headley *et al.*, 2001; Masliyah *et al.*, 2004; Allen, 2008). These tailings ponds also contain trace metals including aluminum, arsenic, zinc, chromium, nickel, copper, iron, lead, molybdenum, titanium, cadmium and vanadium (Allen, 2008). Of these, the first eight have previously exceeded CCME (Canadian Council of Ministers of the Environment) water quality guidelines in oil sands process water from the AOSR and may continue to contribute to chronic toxicity in reclaimed environments (Masliyah *et al.*, 2004; Allen, 2008; CCME, 2021).

1.1.3 Pulp and Paper Mills

In Canada, pulp and paper mills are one of the largest polluters after the oil industry (Ali and Sreekrishnan, 2001; Kamali and Khodaparast, 2015). Through the discharging of gaseous emissions, water and solid waste into the environment, they pose a serious risk to the health of all surrounding wildlife. Of all emissions they produce, the polluting of water bodies is of greatest concern with respect to this industry due to the large volume of wastewater (also known as effluent) produced by processing the wood material (Ali and Sreekrishnan, 2001).

Manufacturing of paper may be divided into three steps: pulp-making, pulp-processing and paper-making (Kamali and Khodaparast, 2015). To make pulp, the wood is first debarked. The process of pulping is next, and involves converting the raw wood into chips, which may be performed by a variety of methods depending on the wood in question (Ali and Sreekrishnan, 2001). This removes all lignin and hemicellulose from the wood fibers into the process water, so there is a cellulose-rich pulp leftover. Depending on the method used to pulp, different effluents will be produced and discharged (*e.g.* terpenes, alcohols, phenols, etc.) (Ali and Sreekrishnan,

2001). The next step involves bleaching the brown pulp to meet the required paper colour standards. The bleaching agents may include: chlorine, hydrogen peroxide, chlorine dioxide, oxygen, ozone and other OCs (Ali and Sreekrishnan, 2001). These chlorinate many of the organic compounds in the pulp that are then discharged in the process water, producing compounds such as chlorate, dioxins, furans, chlorophenols, carbon disulfide, chloroform, adsorbable organic halogens and other volatile organic compounds (Pokhrel and Viraraghavan, 2004). The process of papermaking then produces wastewater containing inorganic dyes, organic compounds, and particulate waste.

1.1.4 Bioindicator Species

To understand the potential impact of POPs on human and wildlife health, it is important to perform ecotoxicological risk assessments that investigate all potential consequences of environmental contamination. While many POPs have well-established consequences on species health, difficulties arise when trying to understand the effects of complex mixtures of them due to the unknown effects of their combined interactions (Sonne *et al.*, 2015). Moreover, the presence of all POPs within an area is unpredictable and often not known. Thus, to assess the adverse effects of POPs on wildlife species the use of bioindicator (*i.e.*, sentinel) species is a valuable tool. These are any species studied from within an area of interest that has some level of pollutant contamination to aid in assessing the degree to which the local environment is affected. They can reveal information on pollutant type, abundance, interactions, availability, direct effects on the species itself and potential implications on other wildlife species (O'Brien, Kaneene and Poppenga, 1993).

There are certain criteria a species must meet to be considered a bioindicator species. These criteria have been defined by the National Research Council and other studies based on a

species' ability to provide steady-state, readily available information on pollution within a defined area of interest (Basu *et al.*, 2007). They must: be biologically sensitive to pollutants, have widespread distribution, have high tropic status, have a known and restricted home range, be able to be captured in large numbers, bioaccumulate toxins, survive in captivity and their biology must be well-documented (O'Brien, Kaneene and Poppenga, 1993; Fox, 2001; Basu *et al.*, 2007). Some species used in previous environmental studies have included birds, rodents and marine mammals (Basu *et al.*, 2007). If a species meets these criteria, the species can reveal how exposure to and bioaccumulation of a variety of toxins may result in possible biological consequences (Basu *et al.*, 2007).

1.1.5 Mink as Bioindicator Species

Terrestrial mammals are one of the more favourable sentinel species for environmental health concerning humans because they best model human exposure. In particular, their physiology is similar to that of humans in terms of uptake, metabolism and elimination of pollutants (Basu *et al.*, 2007). Many organizations have recognized mink as a valuable bioindicator species in this context, including the United States Environmental Protection Agency (USEPA) and the Swedish Environmental Protection Agency (Basu *et al.*, 2007).

Mink are quadruped subaquatic mammals that are opportunistic carnivorous apex predators (Larivière, 1999). As such, their diets are comprised mainly of fish, amphibians, crustaceans, muskrats and other small mammals. However, they will consume other organisms if given the chance and their diets will vary with habitat quality, food supply and season (Basu *et al.*, 2007). They live in temperate aquatic ecosystems and are thus distributed throughout North America. Usually they are found in large wetlands with large areas of open water, or shallow tidal areas in marine environments (Larivière, 1999). They do have defined home ranges averaging at a linear

range of 1-5km, but adult males will have the largest ranges while juvenile females have the smallest (Larivière, 1999).

On average, males are 10% larger than females and 50% heavier (Basu *et al.*, 2007). The average lifespan in the wild is three years, but in captivity they may live up to eight. This lifespan combined with their high trophic status and carnivorous diets leads them to bioaccumulating many notable contaminants of interest to appreciable levels (Aulerich and Ringer, 1977; Basu *et al.*, 2007). This bioaccumulation occurs so readily in the species as 50% of their diet is composed of fish and the water systems from which these fish come from are the primary route by which EDCs accumulate (Chan *et al.*, 2003; Basu *et al.*, 2007). Moreover, studies have measured the extent of the bioaccumulation that occurs in mink from contaminated areas, noting that POP concentrations in their tissues can be upwards of 30 times greater than concentrations in their food sources(Kucera, 1983; Basu *et al.*, 2007)

1.2 Bone Structure

Bone is an intricate and complex organ system serving a variety of important functions in the body, which are reflected in its structure and composition. These include providing structural support, protecting vital organs and creating and supplying red blood cells (Nordin and Frankel, 2001). In addition, see Appendix A for a list of anatomical terms.

1.2.1 Bone Composition

Bone is comprised of a variety of compounds in different proportions. Minerals form 70% of bone volume on average, an organic collagen-based extracellular matrix (ECM) accounts for 20% and water accounts for 10% (Nordin and Frankel, 2001). The majority of the mineral composition is the calcium-based mineral hydroxyapatite, and the ECM is mainly composed of

collagen and water, along with small amounts of other proteins. Most of the water in bone resides in the ECM, around the collagen fibers and in hydration shells around the crystalized mineral structures (Nordin and Frankel, 2001). Bone is classified in two categories based on its structure on the macroscale: cortical and cancellous.

1.2.1.1 Cortical Bone

Cortical bone is very dense, with a porosity ranging between 5-10%. This bone type primarily makes up the diaphysis of long bones, as well as the outermost layer of most bones (Nordin and Frankel, 2001). On the microscale, it is composed of osteons. These are long cylindrical structures with narrow canals at their center termed Haversian canals, through which blood vessels, nerve fibers and water run. Osteons themselves are comprised of lamellae, which are concentric layers of mineralized ECM around the canals (Nordin and Frankel, 2001). The collagen fibers within lamellae are aligned parallel to each other, but in alternating directions between each layer to mitigate crack propagation through the osteon. Moreover, collagen fibers do interconnect between lamellae, further increasing an osteon's resistance to mechanical stress. This intricate network is depicted in Figure 1.1.

Along each lamella are small cavities called lacunae within each resides an osteocyte, a type of bone cell. From each cavity extends numerous small channels called canaliculi that connect to other lacunae and Haversian canals, drawing blood and nutrient supply to the osteocytes (Nordin and Frankel, 2001). Osteocytes themselves are very active, playing a key role in cell signaling and regulating bone composition and structure through remodeling mechanisms.

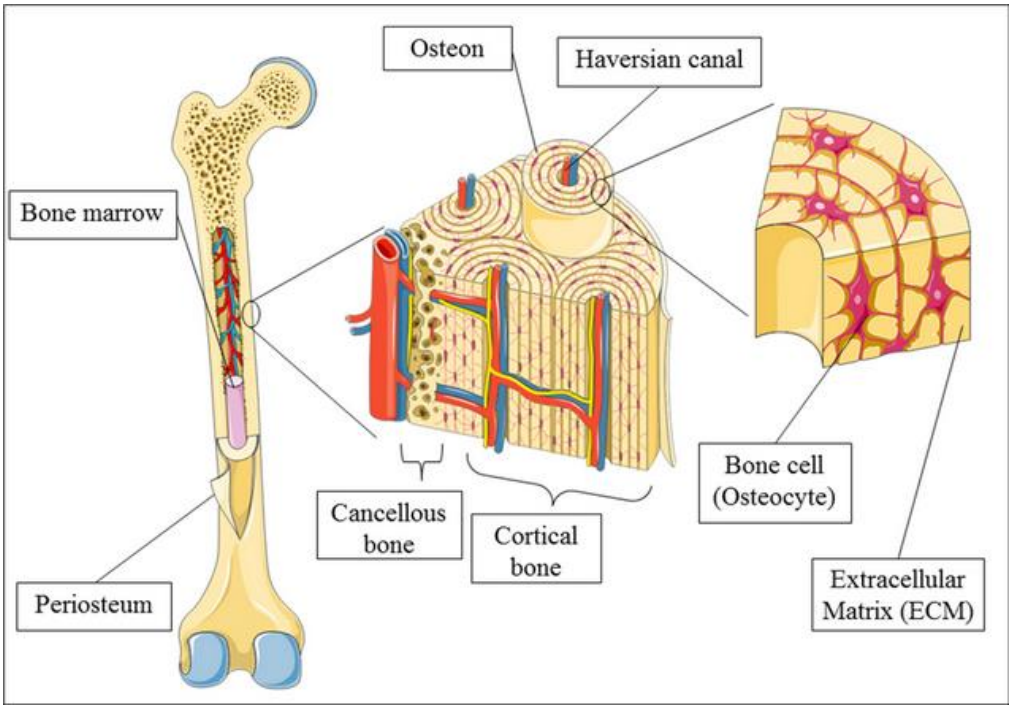

***Figure 1.1**: The osteo-lacunar network of bone tissue.*
A depiction of cortical and cancellous bone is shown here, identifying their components and where they are found in long bones (Meng Bao *et al.*, 2013).

The degree of porosity combined with mineral content and density are significant contributors to cortical bone's mechanical performance. The elastic (or Young's) modulus and ultimate stress are both negatively correlated with porosity and reduced mineral content (Ethier and Simmons, 2007; Morgan, Unnikrisnan and Hussein, 2018). This is because increased porosity consequently means decreased bone volume, thereby reducing the overall mechanical competence of the bone. Moreover, the structure of cortical bone technically makes it anisotropic, but it may be considered transversely isotropic when compared to trabecular (Morgan, Unnikrisnan and Hussein, 2018). So, the elastic modulus and strength are greatest along the longitudinal axis but do not differ strongly between the radial and circumferential directions. With respect to cortical bone's viscoelasticity, loading rate has little to no significant effect on strength and elastic

modulus for loading rates experienced during normal physical activity (Morgan, Unnikrisnan and Hussein, 2018).

1.2.1.2 Cancellous Bone

Cancellous (also known as trabecular) bone is much less dense, with less mineral content than cortical bone and porosity ranging between 50-90% (Currey, 2012). It makes up the epiphyses of long bones and the interior of the vertebrae, pelvis, skull and ribs (Currey, 2012). This bone is arranged in struts and plates called trabeculae (Figure 1.2).

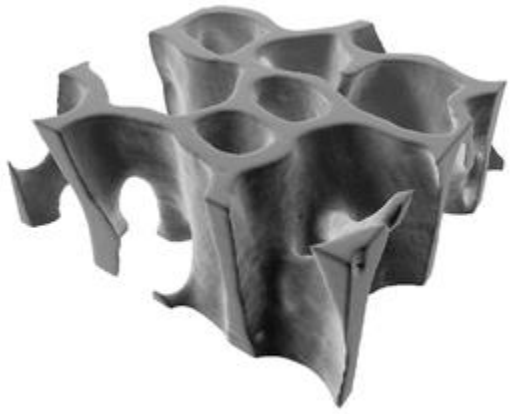

Figure 1.2*: Cancellous bone structure.*
A volume-rendered image of bovine trabeculae from the proximal tibia shows the high degree of porosity of this bone type. The dimensions are 3x3x1 mm^3 (Keaveny *et al.*, 2001).

Cancellous bone behaves similarly to cortical in that a decrease in density results in reduced mechanical performance. However, it is more difficult to quantify material properties for this bone type because the bone volume fraction, related to local bone mineral density (BMD), and anisotropy ratio of trabeculae all affect its properties and vary widely among anatomic locations (Keaveny *et al.*, 2001; Currey, 2012). With respect to BMD, elastic modulus and failure stress of trabecular bone depend on the apparent density (Keaveny *et al.*, 2001). It should be noted that

due to the combination of factors influencing trabecular strength, BMD may only account for 60% of the variation in whole-bone strength (Osterhoff *et al.*, 2016).

For long bones, the trabeculae are arranged following stress lines experienced by the bone under load-bearing conditions; they help to lead large loads away from the joint and into the cortical bone that is more compact (Currey, 2012). Moreover, the degree of trabecular connectivity varies with direction. This all results in significant anisotropy of trabecular modulus and strength, making the trabecular microarchitecture an important factor to consider when evaluating fracture risk (Keaveny *et al.*, 2001). However, in flatter bones trabecular bone resides in the middle, not bearing any major loads, but aids in dealing with shearing loads that may arise (Currey, 2012). Overall, cancellous bone is highly variable, with whole bone mechanical properties that depend on anatomic site, species, age, and other factors (Carter and Hayes, 1977; Keaveny et al., 2001; Nordin and Frankel, 2001).

When comparing the two bone types, the density and isotropy of cortical bone allows it to withstand greater ultimate stresses than cancellous bone. However, it is also more brittle, so can withstand much lower strains (Nordin and Frankel, 2001). In addition, once cortical bone has passed its yield point in mechanical testing, it has low tensile and compressive load-bearing capacities. Cancellous bone behaves as a fluid-filled porous structure, and its strength is proportional to the square of its density (Carter and Hayes, 1977). Moreover, its loading response is also dependent upon the strain rate, as increased rates will result in increased structural properties (Carter and Hayes, 1977).

1.2.2 Bone Remodeling

Bone maintains its structure by undergoing a constant remodeling process, whereby the bone material is resorbed and subsequently replaced with new material. The balance between the

resorption and formation is what allows the bone to repair microdamage, adapt to changes in load-bearing and supply a reservoir of calcium for plasma-calcium homeostasis (Nordin and Frankel, 2001; Robling, Castillo and Turner, 2006). Remodeling is accomplished through the coordination of three bone cell types: osteoclasts, osteoblasts and osteocytes. While osteocytes are interspersed within the ECM, osteoclasts and osteoblasts reside in the inner layer of the periosteum: a fibrous membrane surrounding the bone that is permeated by blood vessels connected to the Haversian canals (Nordin and Frankel, 2001; Robling, Castillo and Turner, 2006). Osteoclasts secrete enzymes that dissolve bone mineral and tissue, thus allowing for these to be resorbed into the blood stream. Osteoblasts synthesize new collagen matrix, so that calcium from the bloodstream can deposit to mineralize the tissue (Robling, Castillo and Turner, 2006). Osteocytes exist within bone or line its surface and are responsible for much of the regulation of osteoclasts and osteoblasts, such as during mechanical loading (Hernández-Gil *et al.*, 2004).

1.2.3 Factors Influencing Homeostasis

The homeostatic balance between osteoclasts and osteoblasts is vital to maintaining and repairing bone structure and function. It is regulated by several factors: genetics, mechanical processes, vascular and nerve factors, nutrition, hormones, plasma-calcium homeostasis and intercellular signaling (Hernández-Gil *et al.*, 2004). While genetic factors are difficult to predict, mechanical factors include loading the bone such as during exercise; when bone is subjected to load, the force is transmitted to the osteocytes that subsequently will produce regulators such as prostaglandins and insulin-like growth factor I (IGF-I). These trigger increased osteoblast activity that results in increased bone formation. This entire process is often termed mechanotransduction. Vascular networks and innervation are also important for proper bone

growth during development, as is diet seeing as there is a minimum intake of calcium needed to maintain a mineralized ECM (Hernández-Gil *et al.*, 2004; Elefteriou, 2008).

Similar to regulators produced during mechanotransduction, many endocrine hormones are also responsible for regulating bone growth during and after early-life development, playing one of the largest roles in osteoblast/osteoclast homeostasis. While the interactive effects of multiple hormones on bone remodeling is not well understood in all situations, individual effects have been studied. For example, thyroid hormones and insulin promote osteoblast activity by encouraging IGF-I synthesis and interruption of this can promote the number of osteoclasts (Hernández-Gil *et al.*, 2004). Sex hormones play very important roles in bone maintenance as well. Androgens generally increase bone density by promotion of osteoblasts in both males and females. Moreover, estrogens play different and important roles in males and females during adolescence, increasing the number and function of osteoblasts and inhibiting resorption. This is in part due to the presence of estrogen receptors on osteoblasts, osteoclasts and osteocytes (Hernández-Gil *et al.*, 2004). Therefore, the interruption of these as well as many other hormones have the potential to disrupt bone remodeling mechanisms, leading to weakened states of bone like osteoporosis.

1.2.4 Biomonitoring and Bone Health

Due to the complex systems of endocrine signaling pathways and biological feedback mechanisms responsible for bone development, bone presents a unique opportunity for investigating the effects of long-term endocrine disruption. As regular bone remodeling is dependent upon proper endocrine functionality, changes in bone development can be used as a predictive marker of insufficient or improper endocrine signaling. Similarly, they could also reflect insufficient mineral and vitamin D absorption. As bone health is reflected in its structural

and material properties, quantifying these properties can be a way to represent and detect changes in bone health that are reflective of changing biological responses. It is in this way that bone has the potential to be implemented in biomonitoring systems looking to evaluate the health of wildlife within a region of interest. Using local wildlife, bone may be used in these systems to measure the effects of environmental circumstances that could be affecting species health, such as through the disruption of endocrine pathways.

1.3 Methods of Determining Bone Properties

Due to the fact that one of the primary functions of bone is to provide support, material and structural bone properties that reflect bone's biomechanical competence may be used as measures to assess bone health (Link *et al.*, 1998; Keaveny *et al.*, 2001). These properties vary significantly between cortical and cancellous bone, primarily because of their different structures. Material properties of bone help to quantify its intrinsic load-bearing capability, including properties determined by a stress-strain relationship and the degree of anisotropy of the ECM. Structural properties of bone are dependent upon its geometry and material and are often determined by force-deformation relationships of the bone under mechanical stress. Some of these properties include stiffness, mineral content distribution and load-to-failure. Both material and structural properties may be obtained to detect diseases hallmarked by bone loss, but changes are often first noticed in the structural properties (Osterhoff *et al.*, 2016). These properties are also generally easier to measure and detect relative to material properties.

1.3.1 Three-Point Bending

A bending test is a form of elastic compression whereby a unidirectional bending moment is applied to the long axis of a specimen (Timoshenko, 1953; van der Meulen, Jepsen and Mikić,

2001). In three-point bending, the specimen is supported by two anvils equidistant from its center. A force is then applied to the center of the specimen, creating a bending moment. This results in the underside of the specimen experiencing tension, while the other side is compressed, until the specimen fractures under the load. From this test, a force-deformation relationship (Figure 1.3) may be established to obtain structural properties of the specimen. From this, the specimen bending stiffness, ultimate strength/force, yield force, yield displacement and work-to-failure can be obtained (van der Meulen, Jepsen and Mikić, 2001). Stiffness is the slope of the force-displace curve, describing the bone's deformation in response to loading. Ultimate strength or ultimate force is the maximum force the bone can withstand under loading. Yield displacement and yield force are the force and displacement of the bone at the yield point, which is defined as the point beyond which the bone is in the plastic deformation range. This point is usually found by taking a line parallel to the linear elastic region of the curve and offsetting it by 0.2% strain. Work-to-failure is the area under the force-displacement curve and is the total energy absorbed by the bone.

Stress may also be calculated using the second moment of area (also known as moment of inertia) of the cross-section of the specimen at the mid-point (Kourtis, Carter and Beaupre, 2014). In addition, strain of the specimen may also be calculated with stress and elastic modulus. Stress, elastic modulus and strain are material properties that do not depend upon the geometry of the specimen, providing insight into the behaviour of the material alone under loading (Timoshenko, 1953; Kourtis, Carter and Beaupre, 2014). However, these properties may be calculated only if certain assumptions about the specimen in bending are held. Some include: the specimen must be of uniform geometry and density throughout, the aspect ratio (ratio of the span to specimen thickness) is at least 10:1 and the material is linearly elastic (Timoshenko, 1953).

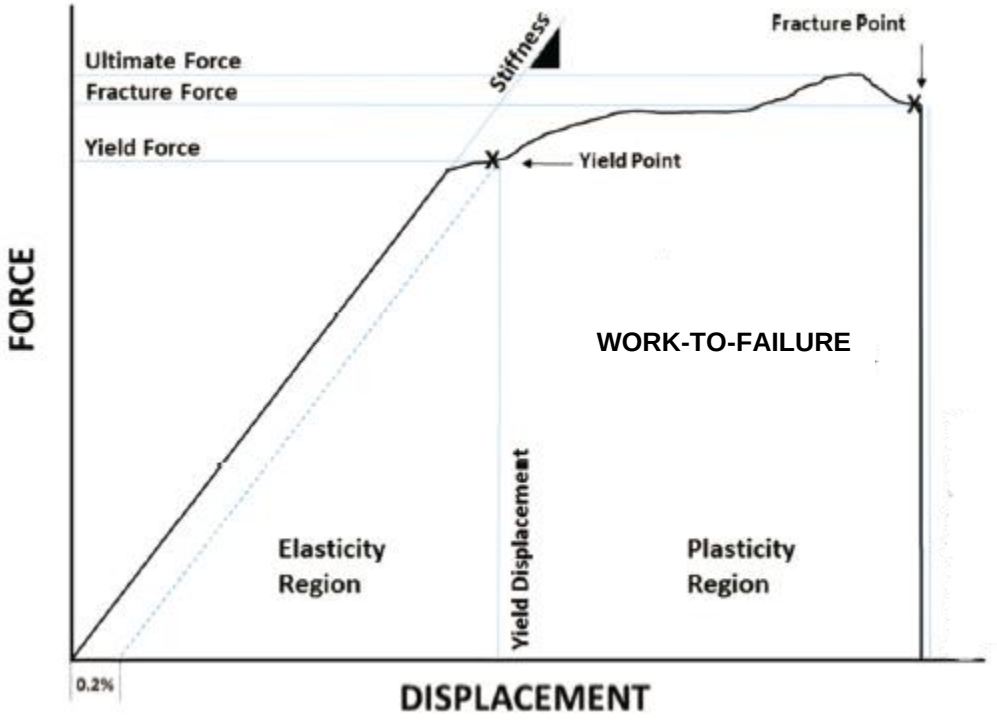

***Figure 1.3**: The force-displacement relationship for a bone in bending.*
An example of a force-displacement relationship for a bone loaded to failure in three-point bending. Included on this graph are properties including stiffness, ultimate force, work-to-failure, yield force, yield displacement and fracture point (Hart *et al.*, 2017a).

1.3.2 Computed Tomography

Computed Tomography (CT) is a non-invasive and non-destructive method for imaging bone (Seeram, 2015). It uses an X-ray source to produce a two-dimensional (2D) image of a specimen. The specimen or source may also be incrementally rotated to obtain images from 360° around the specimen. In this way, the images can be reconstructed to create 2D cross-sectional images of the specimen.

Computed Tomography is the most sensitive of all X-ray techniques to calculate BMD and has been proven to be effective for measuring BMD of cortical and cancellous bone (Silva *et al.*,

1994; Siu *et al.*, 2004; Boutroy *et al.*, 2005). Bone density is measured in Hounsfield Units (HU) from a CT scan. To measure bone density based on HU, water and hydroxyapatite are used as phantoms to calibrate the HU and are scanned alongside the bone. Water and hydroxyapatite have known densities, so the HU of the bone in question can be measured relative to these phantoms in a scan (Silva *et al.*, 1994; Siu *et al.*, 2004). Furthermore, CT it provides more detailed and higher-contrast images than conventional radiography, but with a greater radiation dose than magnetic resonance imaging (MRI).

For small animal specimens, the imaging modality used almost exclusively is µCT (Arnold *et al.*, 2017). Micro-CT has a spatial resolution of 1-100 µm, so it may be used to determine the architectural parameters of cancellous bone (Siu *et al.*, 2004). This includes trabecular number, spacing/separation, thickness and bone volume (Yang, Pham and Crabbe, 2003; Arnold *et al.*, 2017). Due to the increased surface area of cancellous bone relative to cortical bone, changes in bone remodeling may first be reflected here rather than in cortical bone. For example, reduced trabeculae number, thickness, spacing and bone volume may be some of the first signs of osteoporosis (Osterhoff *et al.*, 2016). The consequence of lower surface area in cortical bone is that it takes longer for changes in bone remodeling to be observed, so diseases such as osteoporosis are not identified as early (Osterhoff *et al.*, 2016).

1.4 EDC Exposure

Endocrine disrupting chemicals (EDCs) produced as a result of human activity can have serious repercussions on reproductive health and success, as effects on reproduction are multigenerational and can go unnoticed until population sizes have diminished significantly enough to render investigation. It is important to understand how EDCs pose a risk to wildlife

health and alter reproductive success. What follows is a brief summary of the effects of EDCs on reproductive and bone health, emphasizing heavy metal effects. For further reading on reproductive effects, see Appendix B.

1.4.1 Effects of EDCs on Reproduction

The majority of research on EDCs effects on reproductive health has been conducted on PCBs. However, similar effects are also observed in animals exposed to heavy metals. For instance, cadmium and mercury both reduce female fertility (Rzymski *et al.*, 2015). Cadmium is a metalloestrogen, thus being linked to oestrogen-related diseases and causing subfertility, failed implantation and fetal death (Rzymski *et al.*, 2015). Mercury has been linked to failed implantation, stillbirth and infertility as well (Rzymski *et al.*, 2015). Furthermore, in males, cadmium exposure has been shown to reduce sperm mobility and concentration, suppressing testosterone production and causing damages to the testicles at levels that do not demonstrate adverse effects in any other organs (Wirth and Mijal, 2010).

1.4.2 Effects of EDCs on Bone Health

Bone development is regulated through hormone feedback mechanisms that continue through all stages of life. So, investigating bone for signs of improper or insufficient development could be a direct method of assessing EDC impacts on wildlife and whether they have reached unsustainable levels in a certain area. It should be noted however, that relatively few studies have been performed to evaluate the relationship between EDCs and bone health. Even more so, the literature is very limited with respect to information on mink bone health.

1.4.2.1 Heavy Metals

The presence of heavy metals in mammalian diets has been proven to be associated with several bone diseases, including osteoporosis (Rodríguez and Mandalunis, 2018). Once ingested, they have long half-lives and may bioaccumulate within organs (Rodríguez and Mandalunis, 2018). In general, bone formation may be directly affected by the presence of heavy metals through three processes: the RANK/RANKL/OPG axis, bone mineralization and calcium absorption.

The balance of osteoclasts in bone is primarily controlled through the RANK/RANKL/OPG axis. RANKL is a membrane protein produced by osteoblasts that binds to its receptor (RANK) on hematopoietic precursor cells (Cao *et al.*, 2003). After binding, in the presence of macrophage-colony stimulating factor (MCS-F) osteoclasts will form. OPG is a glycoprotein that will bind RANKL, preventing RANK from binding (Cao *et al.*, 2003). For example, cadmium exposure can increase fracture risk by stimulating RANKL activity, thereby reducing bone mineral content and bone formation (Goyer, 1997; Alfvén *et al.*, 2000; Brodziak-Dopierala *et al.*, 2009). Thus, it is the balance between RANKL and OPG that regulates osteoclast activity (Rodríguez and Mandalunis, 2018).

There are a number of alkaline phosphatases (AP) produced in the body, but tissue non-specific alkaline phosphatase (TNAP) is expressed in the kidney, liver and bone. Generally, APs initiate bone mineralization, but changes in TNAP specifically are connected to defective bone mineralization (Maly, Eppler and Müller-Gerbl, 2018). In addition, calcitriol is a compound necessary for effective absorption of calcium, a metal that is key for formation of the bone mineral hydroxyapatite (Rodríguez and Mandalunis, 2018). For instance, cadmium interferes with the metabolism of calcium and vitamin D in the liver and kidneys and disrupts calcium absorption in the gastrointestinal tract, slowing mineralization of the ECM as evidenced by

reduced BMD (Goyer, 1997; Brodziak-Dopierala *et al.*, 2009). In addition, a correlation between cadmium levels and marrow adipose tissue (MAT) has been established, indicating that cadmium encourages mesenchymal stromal cell (MSC) differentiation into adipocytes rather than osteoblasts (Rodríguez and Mandalunis, 2018).

There are two notable studies that have established relationships between bone biomechanical properties and heavy metal exposure in animal models. A study conducted on rats by Beier et al. (2013) found that after feeding rats low levels of lead in their water supply, beginning before conception through to 18 months old, rats' long bones and vertebrae had significantly reduced BMD and bone mass. Through compression testing, they also demonstrated that vertebrae had reduced maximum strength, stiffness, energy to failure and yield force (Beier *et al.*, 2013). Using micro-computed tomography (µCT) they also found reduced trabecular thickness, connectivity and increased spacing. Another similar study performed by Tomaszewska et al. (2017) exposing rats to low levels of cadmium and lead had nearly identical findings. They demonstrated that there was significant bone loss, weakened trabecular properties, reduced bone length, reduced strength and cortical diameter in the long bones (Tomaszewska *et al.*, 2017). Therefore, evidence of bone health decline due to heavy metals may be observed as weakened biomechanical properties, reduced BMD and reduced bone mass.

1.4.2.2 PCBs

PCBs have well-established adverse effects on bone biomechanical properties. Brankovic *et al.* (2019) intraperitoneally administered PCB-155 and PCB-169 to female rats. Forty-two days after they gave birth, femurs were taken from the offspring and subjected to µCT, 3-point bending and mass spectrometry. The data indicated that the somatic mass and femur size was significantly lower for offspring in the PCB-treated groups compared to the control group. Moreover, the

PCB-169 group had cortical bone that was harder but also more brittle than the other groups. This indicated a high degree of mineralization of the ECM that could be attributed to increased calcification occurring or suppressed osteoclast activation (Brankovič *et al.*, 2019). This and other studies point to PCBs having strong estrogenic activity overall (Lind *et al.*, 2003, 2004a).

1.5 Effects of EDCs on Bone Using Bioindicator Species

Bone is considered a useful biomonitoring tool as is an organ that decays very slowly relative to soft tissue organs and may easily be obtained from licensed trappers. Furthermore, bone is not eaten by scavengers, making collection of the bones relatively easy. The combined effects of multiple EDCs on bone health have been studied and quantified for several different animals. However, the relationship between EDC exposure and bone health is not well-established for all species, as different studies have yielded varying results. For instance, a study conducted by Daugaard-Petersen *et al*. (2018) looked for biomechanical differences in the skulls of polar bears from East Greenland and Svalbard, Norway and from different years: 1892-1932 (the "pre-pollution" period), and 1966-2015 (the "pollution" period). While no geographical differences in BMD were found, the BMD of male skulls was found to decrease significantly from 1892-2015, but this was not the case for females. In addition, from 1966-2004, skulls from Svalbard were significantly larger than those from Greenland. With these findings, they also found that there was a positive correlation between pollutants (including PCBs, chlordanes, and other chlorine-based compounds) and skull size. The reduction in BMD and skull size was not attributed entirely to the presence of POPs, but also to other environmental effects; the presence of POPs was considered a contributing environmental stressor (Daugaard-Petersen, Langebæk, Frank F Rigét, *et al.*, 2018).

Another similar study found opposite results: they studied POP concentrations in polar bear adipose tissue and polar bear penile bone BMD for locations in Greenland and North America from 1996-2015 (Daugaard-Petersen, Langebæk, Frank F. Rigét, *et al.*, 2018). They found positive correlations between BMD and PCB concentrations in the adipose tissues of the polar bears. However, this does not necessarily mean that the bone strength increased, or that increased BMD is a sign of healthy bone (Daugaard-Petersen, Langebæk, Frank F. Rigét, *et al.*, 2018). Lind et al. (2004) collected long bones from female alligators from a pesticide-contaminated lake in Florida. Upon evaluation of their BMD compared to that of a control group, the alligators from the contaminated lake had greater trabecular BMD, total BMD and mineral content. This suggested that these alligators were subjected to compounds that had estrogenic effects that caused them to gain bone mass, but only because they were females whose biological makeup responded well to estrogen-related compounds (Lind et al., 2004). Both studies indicate that while BMD may be useful in identifying the presence of certain chemicals in the environment, the effects of these chemicals on BMD are strongly dependent upon sex and species.

Christian et al. (2004) revealed more compelling findings. They performed a study comparing the femur, lumbar vertebrae and skulls of East Greenland polar bears from 1892-2002. In subadult males, females and adult males, they found significantly reduced BMD correlated with increasing PCB and other OC concentrations in the adipose tissue. However, there was no significant change in BMD for adult females (Christian *et al.*, 2004). A direct correlation between reduced baculum length, baculum weight, testicular size and increasing OCs in the adipose tissue of polar bears has also been demonstrated (Sonne *et al.*, 2006). The same study also found that baculum BMD and OC exposure were inversely correlated for other bone types. Other studies established effects of EDC exposure on reproductive, organ and bone health in

these polar bears as well (Sonne, 2010; Sonne *et al.*, 2012). These studies further support that pollutants categorized as xenoendocrines have significant negative effects on male polar bear genitalia and bone development.

Finally, otter baculums were previously investigated for relationships between pollutant exposure and bone health metrics (Thomas *et al.*, 2021). Otters in northern Alberta collected from sites within oil and gas-extracting regions had lower peak stiffness and ultimate strength values. Thallium exposure was also positively correlated with reduced BMD, cadmium exposure was linked to reduced peak strength values and some PACs were correlated with increased bone BMD and bone stiffness. While these were negative effects, otter exposure to strontium and iron exhibited protective effects (Thomas *et al.*, 2021).

1.5.1 Gaps in the Literature

To date, no known studies have evaluated EDC exposure and bone health on other more viable, widespread bioindicator species. While information on polar bears is available, not all regions have them available for biomonitoring programs. Otter bones were also investigated, but they have large home ranges and are not as widely distributed across central parts of North America. In addition, there are few studies linking pollutant exposure and bone health in smaller mammals, especially from a biomechanical perspective. Thus, information on another species that is more globally distributed but has smaller home ranges, such as mink, could be useful for biomonitoring programs and employed for investigation of pollution near industrial facilities. Furthermore, there are currently no biomonitoring systems that use bone as a measure or indicator of pollutant exposure, even though bone can directly reflect exposure to a variety of toxins. Implementing a biomarker of pollutant exposure in biomonitoring programs may provide a direct measure of the presence of pollutants within a localized region. This would be especially

beneficial for communities and wildlife where there are environmentally-relevant levels of pollution. Moreover, investigating the relationship between mink bones and environmental pollutants will add to the understanding of how pollution may have varying effects on bone growth and development in mammals.

1.6 Thesis Aims and Hypothesis

The overall aim of this thesis was to provide information to inform the development of biomonitoring standards of heavy metal effects on wildlife, through obtaining skeletal measures from a widely abundant and available bioindicator species, the American mink (*Neogale vison*). There were three specific aims of this research:

1. To determine if there is any correlation between skeletal health metrics and heavy metal exposure, and whether a correlation(s) is strong enough to identify at least one metric that could potentially be implemented as a biomarker of exposure to one or more heavy metals.
2. To investigate whether there are differences between the effects of exposure to heavy metals on cortical and cancellous bone.
3. To determine if there is a difference between the effects of exposure to heavy metals on the male reproductive bone (baculum) versus a non-reproductive and weight-bearing bone (femur).

For the above aims, the following hypotheses were made:

1. Skeletal health metrics can be identified that are both positively and negatively related to trace element exposures.

2. Cancellous bone is more affected by heavy metal exposure than cortical bone.
3. There is no difference between the effects of heavy metals on reproductive bones versus non-reproductive long bones.

Chapter 2 – Methodology

Overview: This section outlines the experimental methods used to quantify bone health measures for this research. It includes assessments of cortical and cancellous bone, as well as load-bearing properties of a reproductive and non-reproductive bone. These provided a broad assessment of skeletal health measures of two bone types to be assessed for effects of trace element exposure.

2.1 Dimensional Analysis

2.1.1 Specimens

Mink carcasses were obtained by Environment and Climate Change Canada (ECCC), sourced from registered fur trappers in Alberta and Quebec. Mink were trapped in the winter seasons, so their carcasses were left in approximately -40°C after trapping until collection. The time between trapping and collection was unknown but was not considered as an important factor here since the carcasses were frozen during this time. All mink collected after 2019 were screened for Covid-19 before packaging and shipment to McMaster University. Working with the mink specimens was approved by the McMaster Animal Research Ethics Board (AREB) before shipments arrived.

Eighteen specimens were delivered and included 15 males and three females. Specimens included two bones collected from individual mink: the right hindlimb femur and the baculum (as available). Specimens were stored in their packaging at -20ºC until they were ready for dissection and cleaning. In preparation for dissecting the bones, the baculums were removed from the freezer and left to thaw at room temperature (average 20ºC) for one hour. Femurs were

thawed for two hours because they were larger. Scalpels, dissection scissors and tweezers were then used to clean the bones of soft tissue. To minimize dehydration, all bones were placed back in their packing and sprayed with a 0.9% saline solution before being returned to the freezer when not being tested.

All specimens were dimensioned first. Due to time constraints, the order of imaging and mechanical testing differed among specimens. Seven specimens were imaged first followed by three-point bend testing, and the other 11 underwent three-point bending first followed by imaging. All specimens were sprayed with saline solution prior to bending.

2.1.2 Dimensioning

Measurements for each bone type were collected according to Figure 2.1 and Figure 2.2 using a digital caliper. Bone mass (g) was also measured using a W3200-120 Accuris Instruments precision balance (readability 0.001g). In addition to dimensioning, images of the femurs and baculums were also taken with a 12-megapixel phone camera (Samsung Galaxy S9, SM-G960W) to document their relative size and shape.

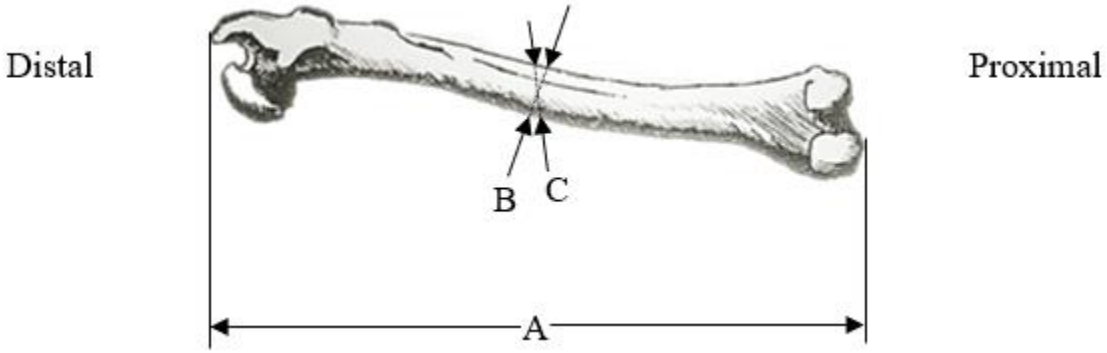

Figure 2.1*: Femur: posterior view.*
An anatomical sketch of the mink right hindlimb femur. Letters A-C depict the different measurements that were collected. A: femur length; B: mid-diaphysis diameter in the anterior-posterior direction; C: mid-diaphysis diameter in the medial-lateral direction.

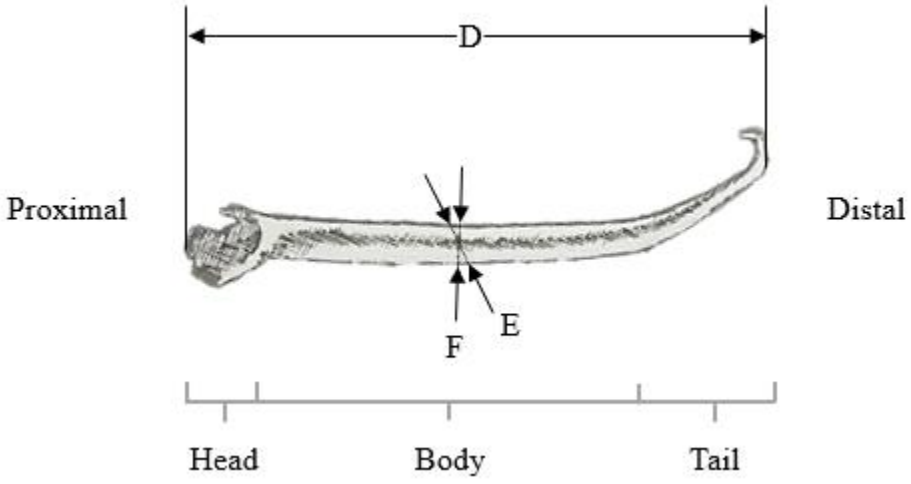

Figure 2.2*: An anatomical sketch of a mink baculum.*
Letters D-F depict the different measurements that were collected. D: whole baculum length; E: mid-diaphysis diameter in the medial-lateral direction; F: mid-diaphysis diameter in the superior-inferior direction.

2.2 Micro-Computed Tomography

All femurs were scanned using Micro-Computed Tomography (μCT) to collect internal geometric, density and trabecular measurements. All scanning was performed with a SkyScan

1172 desktop X-ray microtomograph (Bruker, Burlington, ON, Canada) at the McMaster Automotive Resource Centre (MARC) in Hamilton, Ontario. The bones were stored in a -18ºC freezer at MARC and were removed from the freezer one hour prior to imaging. Initially, bones were imaged before subjected to three-point bend mechanical tests.

Before scanning, each bone was sealed in a small resealable plastic bag to minimize drying. It was then placed in a transparent plastic tube approximately 5cm in height and 1cm in diameter. This tube helped to keep the femur upright during scanning, keeping the long axis of the femur relatively vertical. The base of the tube was then pressed into wax coating the platform of a metal stand. This stand was screwed in place in the desktop scanner for imaging.

The scanner had a 14x14mm field of view, in which the femurs were positioned such that 23-30% of the total bone length was imaged, depending on femur size. The section of diaphysis included varied depending on the size of the femur, but the approximate region is illustrated in Figure 2.3. This location was chosen due to the presence of cancellous and cortical bone in mink femurs at this region (Inkapool, 2018). In addition, imaging this location was ideal as the internal geometry of the diaphysis could be measured from these images as well. While baculums were not imaged, femurs contained sufficient cortical and cancellous bone to assess both structures.

A 0.5mm aluminum filter was put in place to filter out low energy photons. This helped to reduce beam-hardening artifacts and is generally recommended when imaging bones (Li *et al.*, 2008; Bouxsein *et al.*, 2010). The X-ray voltage and current were specified for each individual bone while setting up a scan so that a minimum of 20-40% of the X-rays would be absorbed by the specimen. The flat-field correction was also fine-tuned for every scan. Pilot scanning of one femur specimen was performed to determine the appropriate resolution that could resolve trabeculae; all femurs were thus scanned at 4.8µm/pixel. Once the scanning was complete, the

bone and stand were removed from the scanner, and the bone removed from the plastic tube and plastic bag before being returned to the freezer.

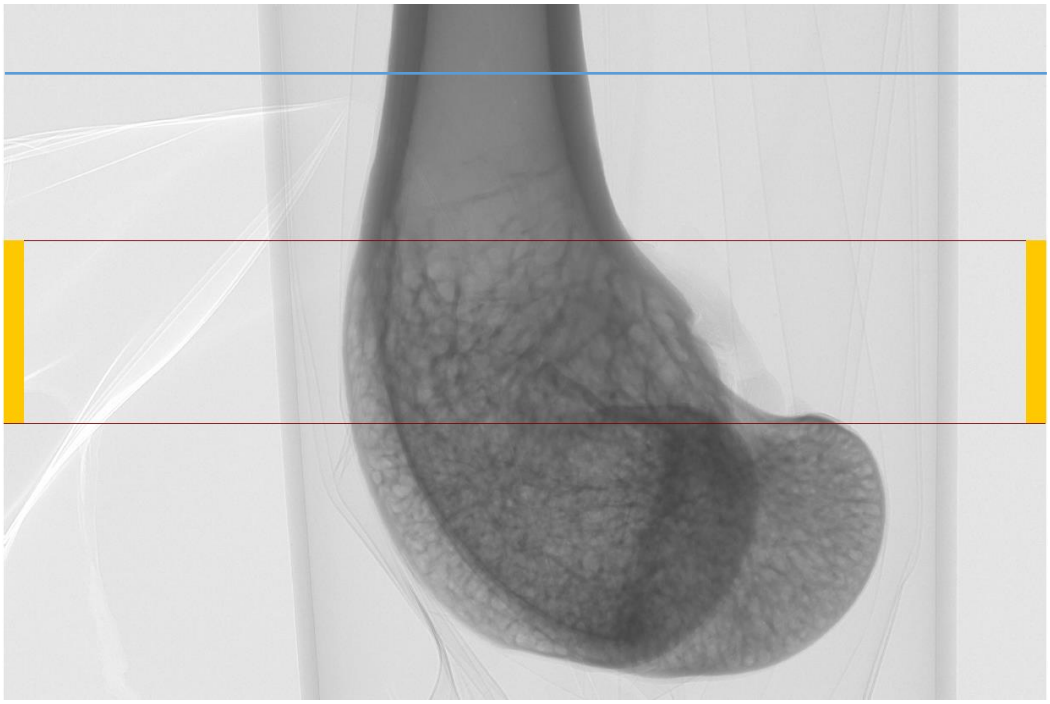

Figure 2.3: *An example of a µCT scan*.
Micro-Computed Tomography of the distal end of mink femurs was used to ascertain trabeculae and cortical measures in the region of interest. The highlighted region corresponds to the region selected for trabeculae analysis (12-20% of total bone length), and the blue line represents 23% of the total bone length.

2.2.1 Image Reconstruction

Image reconstruction was performed using the SkyScan NRecon (2016) (MicroPhotonics, Allentown, PA, USA) software package. For each femur, only the bone containing cancellous bone proximal to the growth plate (epiphyseal plate) was reconstructed for analysis of the trabeculae structure. Generally, the cancellous bone structure is different beyond the epiphyseal plate when compared to other cancellous structures (Bouxsein *et al.*, 2010). This is because during youth the bone grows and extends in the direction beyond the growth plate, so the trabeculae structure here is less developed (Bouxsein et al., 2010).

For each bone, the region of bone chosen for reconstruction began from the top of the medial condyle (at approximately 12% of the total bone length) and ended at 20% of the total bone length. Total bone length was measured moving from the distal end to the proximal end. The opensource software ImageJ (1. 5. 3) (NIH, Bethesda, MD, USA) was used in conjunction with the BoneJ plugin (1. 4. 3) to identify this region for reconstruction on the µCT scans (Doube *et al.*, 2010; Schneider, Rasband and Eliceiri, 2012).

Reconstruction of a single slice at 23% of the length of the bone was also completed for the purpose of obtaining the diaphysis geometry to be used for three-point bending data calculations. Identifying this location for reconstruction on each scan was done using ImageJ.

2.2.2 BoneJ Analysis

The reconstructed images were first assembled into four stacks of an equal number of images to reduce processing time. The number of images in each stack depended upon the length of the bone that was reconstructed, which varied with each specimen. Each stack was analyzed individually using the BoneJ plugin and the results averaged over all four stacks.

The following outcome measures were collected: the internal and external diaphysis diameters at 23% of the length of the femur, trabeculae thickness (µm), trabeculae spacing (µm), trabeculae connectivity (number of trabeculae) and trabeculae connectivity density (μm^{-3}). Connectivity density is the number of trabeculae per unit volume. The measures were then averaged over the stacks for each bone.

2.2.3 Stack Preparation

To begin, a stack of images was imported into ImageJ and the scale set according to the reconstruction resolution (4.80698 µm/pixel). The image resolution was then reduced to one

quarter the original resolution while maintaining the same scale to improve processing time of bone area, a region of interest (ROI) bordering the inside of the cortical bone was drawn using the polygon tool (Figure 2.4). This region was drawn so that it only encapsulated cancellous bone throughout the entire stack. The stack was then cropped to this ROI and the image outside this region was removed. The stack was then binarized using *Process -> Binarize*. This converted pixels into either black (background pixels) or white (foreground pixels).

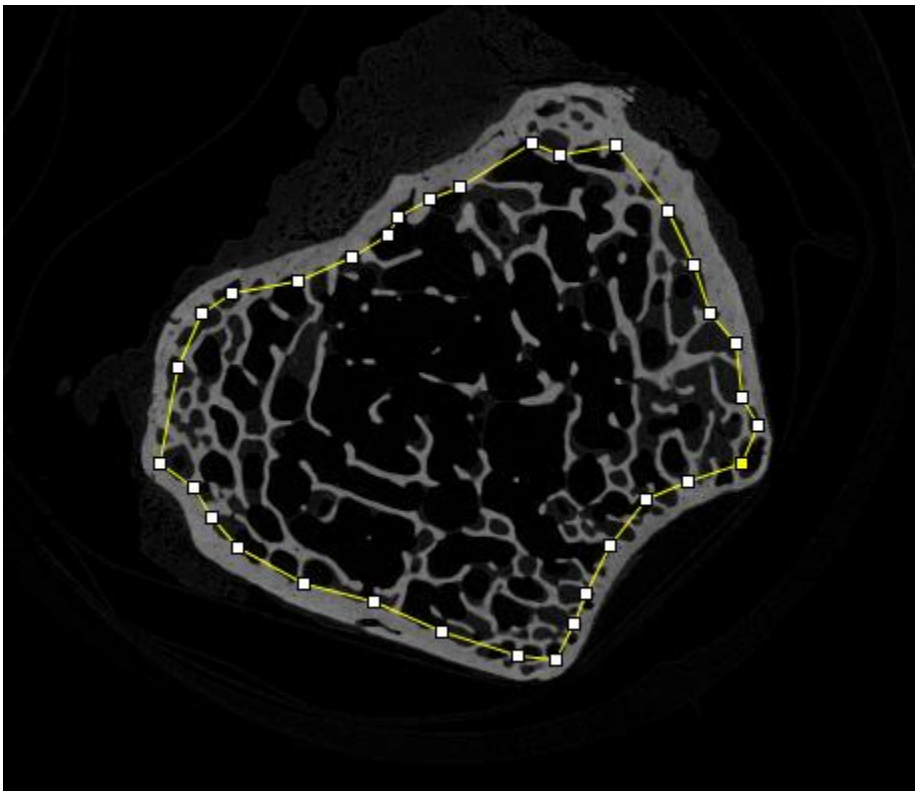

Figure 2.4: *An example of the polygon tool outlining the cancellous bone structure in a slice image.*

2.2.4 Connectivity

Connectivity counts the number of connected trabeculae in a volume of interest. The degree of connectivity of the trabeculae was assessed by first applying *Plugins -> BoneJ -> Purify* to the stack, followed by *Plugins -> BoneJ -> Connectivity*. The Purify function reduced the noise

between stacks so trabeculae could be easily resolved. This reported the connectivity and connectivity density in number of trabeculae and μm^{-3}, respectively. It is important to examine both measures to identify any geometric or mechanical influence on trabeculae.

2.2.5 Trabeculae Thickness

The trabeculae thickness for each stack was quantified using the function *Plugins -> BoneJ -> Thickness -> Trabecular thickness*. This plugin assumes that the trabeculae are the foreground pixels (white) and defines the local thickness as the diameter of the largest sphere that can fit within the bone structure volume. It reported the mean trabeculae thickness (μm), trabeculae thickness standard deviation (SD) (μm) and maximum trabeculae thickness (μm). It also reported a thickness map whereby one can validate that the correct trabeculae structures were measured.

2.2.6 Trabecular Spacing

To assess the trabecular spacing, the original stack was again cropped in the image with the smallest bone area, but the ROI was chosen to include the cortical bone. Further functions had to be applied including subtracting the background using *Process -> Subtract Background*. This functioned to remove the background particles within a certain pixel radius. A radius of 100 pixels was sufficient to ensure that the pixels outside the ROI were subtracted from the image while background pixels (black) within the ROI remained. This was important because the trabeculae spacing function of BoneJ calculates the distance between all foreground particles in a binarized image. Without subtracting the background, the space between the edges of the ROI and the edges of the bounding box would have been calculated. By ensuring that there was no background outside of the ROI, only the spacing between trabeculae within the ROI would be calculated. Additionally, by including the cortical bone, no background pixels were accidentally subtracted from within the ROI (Figure 2.5)

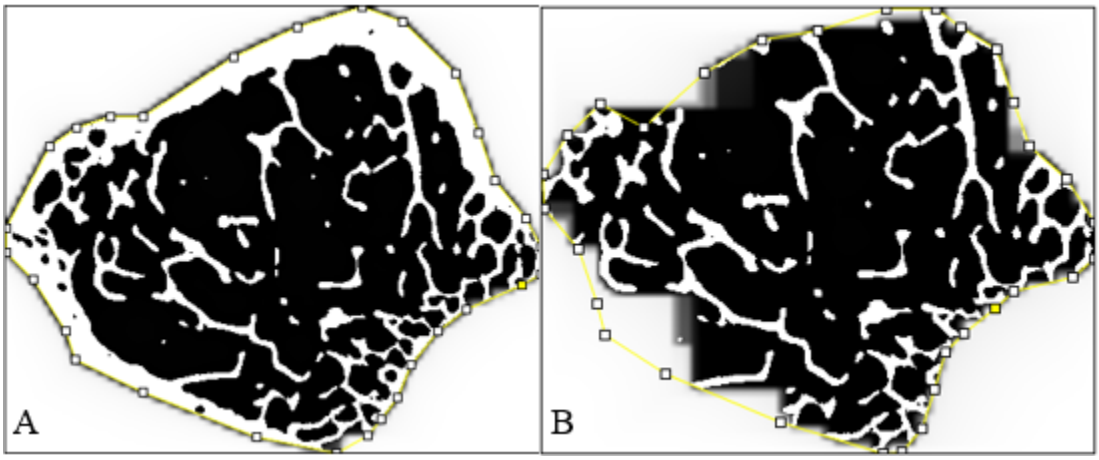

Figure 2.5: *Image subtraction with and without inclusion of the cortical bone.* These images show the advantages of including the cortical bone within the ROI. A: Image subtraction including the cortical bone. B: image subtraction excluding the cortical bone. This leads to sections of the new background bleeding into the ROI, which would offset the trabecular spacing measurements.

The next step was to binarize the image again, and then the spacing was found by following *Plugins -> BoneJ -> Thickness -> Trabeculae Spacing*. This presented a map of the measured spacing as well as mean trabeculae spacing (µm), trabeculae spacing standard deviation (SD) (µm) and maximum trabeculae spacing (µm).

2.3 Three-Point Bending

Three-point bending was performed to quantify the structural and material properties of the bones. Prior to testing the baculums were thawed for a minimum of one hour and the femurs were thawed for a minimum of two hours. After thawing, the bones were each sprayed with a 0.9% saline solution and left to sit in their bags for 20 minutes before being tested to minimize dehydration during storage and previous tests.

2.3.1 Testing Apparatus

Testing was performed with a materials testing machine (Instron Electropuls™ E1000, Instron, Canton, MA, USA) (Figure 2.6). A three-point bend jig with two roller-type parallel anvils upon which the bone rested was used. An upper anvil was located exactly halfway between the two lower anvils and mounted in-line with a 1kN load cell. The testing procedure was controlled and the data collected through a custom-written WaveMatrix program. This program outputted force (N), displacement (mm) and time (s) data at 60Hz.

Figure 2.6*: The Instron E1000 materials testing machine*.
This was used to perform three-point bending tests. The arrow indicates the direction of loading.

The span length (distance between the lower supports and the region subjected to bending) was maximized for each bone type while maintaining stability on the supports. For femurs, this was taken as the length of the diaphysis between the lesser trochanter and medial epicondyle. For baculums it was taken as the length of the body between the head and tail. Due to the varying

arrival dates of different specimens, the span length had to be changed to accommodate the shortest bone among all specimens. This resulted in two male femurs being tested at a span of 28mm and two male femurs tested at 30mm, but the span was kept the same for the other 11 male femurs at 27mm. All baculums were tested at 18mm and all female femurs were tested at 26mm. The jigs were aligned such that the upper anvil would run perpendicular to the long axis of the bone (Figure 2.7).

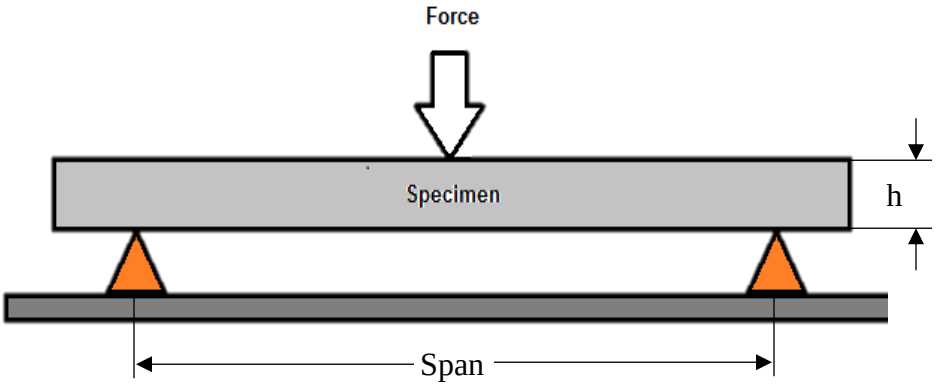

***Figure 2.7**: The three-point bend setup.*
In this diagram, *h* denotes the height of the bone in the direction of loading (medial-lateral diameter). The force was applied at the mid-point of the specimen (mid-diaphysis).

Each bone was aligned such that its diaphysis was parallel with the base. The femurs were oriented so that the direction of loading was in the medial-lateral direction. To do this, the femoral neck was oriented vertically (Figure 2.8A). The baculums were oriented such that diaphysis of the body was subject to bending in the superior-inferior direction (Figure 2.8B).

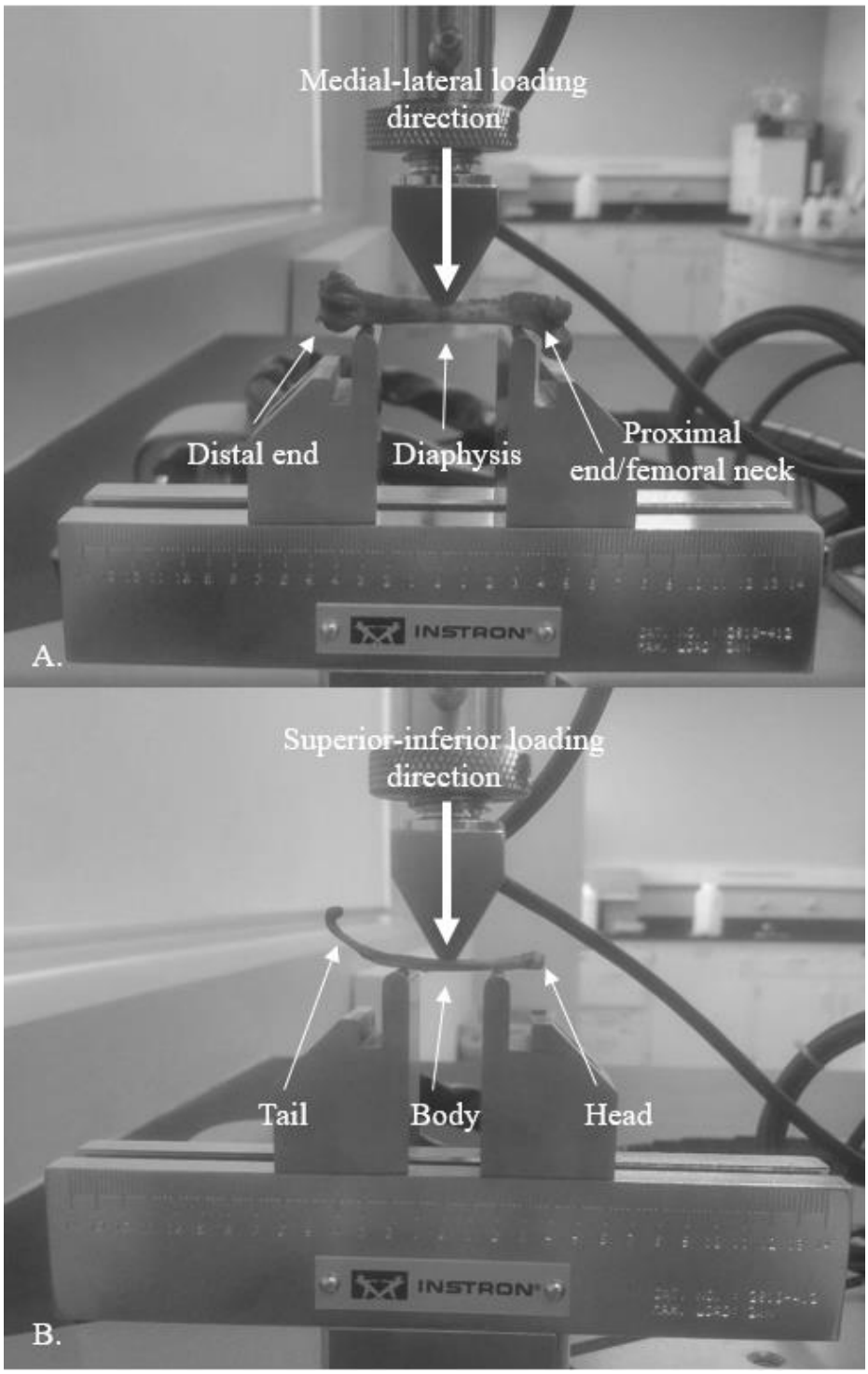

***Figure 2.8**: Three-point bend setups.*
A. A mink femur in the three-point bend jig. Each femur was positioned for loading in the medial-lateral direction. B. A mink baculum in the three-point bend jig. Each baculum was positioned for loading in the superior-inferior direction.

Each bone underwent quasistatic loading for 10 cycles, followed by ramp loading until failure. The displacement rate was determined for femurs and baculums individually so as to have a quasistatic strain rate ($<0.01s^{-1}$). For femurs, the displacement rate was 0.011mm/s and for the baculums a rate of 0.017mm/s was used. For cyclic loading, the femurs were loaded between 0-27.1N, and the baculums were loaded between 0-8.2N. These force values were chosen because they were 10% of the theoretical ultimate force as estimated based on a previous study (Tomaszewska *et al.*, 2016). Once the bone failed (as indicated by a sharp drop in the force-displacement data displayed by the WaveMatrix program), the test was ended.

2.3.2 Analysis

From the Instron, the following were recorded: force, displacement and time. Before extracting any properties, the displacement data were corrected for machine compliance. From these, the following structural properties were obtained: bending stiffness, ultimate strength, yield strength and work-to-failure.

As illustrated in Figure 1.3, stiffness is represented by the slope in the force-displacement curve in the elastic region. To extract this value from a bending dataset, the slope of the last five loading cycles of the force-displacement curve was averaged. The ultimate force is the peak load in the force-deformation curve. Work-to-failure was measured by obtaining the area under the force-displacement curve, from the beginning of the final loading cycle to the point of failure (identified as the point of fracture).

Force-displacement data were converted to stress-strain data to obtain the following bone material properties: ultimate stress (MPa), yield stress (MPa), yield strength (N) and bending elastic modulus (GPa). To convert femur force-deformation data to stress-strain data, the second

moment of area (mm^4) was calculated using measurements of the medial-lateral and anterior-posterior diameters based on μCT scans of the diaphysis at 23% of the total bone length. To align the bending axis with the diaphysis scan correctly, a reconstructed image of the distal end (where the medial condyle and lateral epicondyle were clearly identifiable) was imported into ImageJ and the medial-lateral plane was drawn using the line tool. The angle and position of the line was recorded and then the diaphysis scan was imported into ImageJ. A line at the same position and angle was drawn on this scan, and this was used to measure the diameter of the diaphysis in the anterior-posterior direction. Another line perpendicular to that line was also drawn through the center of the diaphysis to measure the diameter in the medial-lateral direction. This was used to approximate the second moment of area as a hollow ellipse and measure the distance from the neutral axis to the outer diameter of the femur (Appendix C). Force was converted to stress using this distance, the second moment of area measurement and the bending moment. The elastic modulus was calculated using stress and displacement values of the last three cycles of loading. Finally, strain was calculated using the elastic modulus and strain values (Appendix C).

For baculums, the second moment of area was calculated assuming a solid triangular cross-section along the diaphysis. This shape was assumed based on a pilot μCT scan of one of the mink baculums (Figure 2.9) (Appendix C). To assess the contribution of the hollow canal to the overall second moment of area, a manual calculation was performed on a representative sample and the effect was shown to be on the order of <1%, so it was neglected for all subsequent baculums. The calculation was performed using the mid-diaphysis measurements as found during dimensional analysis (section 2.1). Stress, elastic modulus and strain values were calculated in the same way as for femurs.

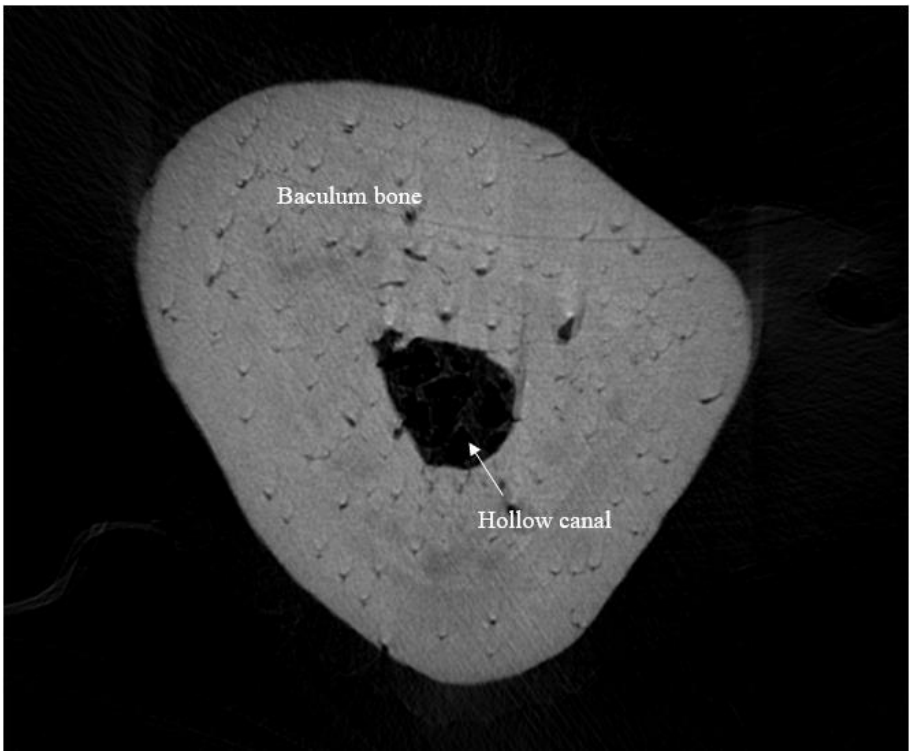

Figure 2.9: *A µCT cross-section reconstruction of a baculum diaphysis*.
The hollow portion of the diaphysis did not substantially contribute to the second moment of area.

From the stress-strain data of both femurs and baculums, yield stress was obtained by drawing a line parallel with the linear portion of the stress-strain curve and offsetting it by 0.002 strain. The point at which the line intersected the curve was taken as the yield stress. The force value at this point was also defined the yield load. Ultimate stress was taken to be the maximum stress the bone experienced. All material properties were calculated based on linear beam theory and were extracted using a Python code (Appendix D).

2.4 Trace Element Exposure

ECCC provided trace element exposure data for each mink from which the bones were dissected, based on trace element analyses of the livers. Analyses were performed at the National Wildlife

Research Center (Ottawa, ON, Canada). The following trace elements were reported: mercury (Hg), aluminum (Al), antimony (Sb), arsenic (As), barium (Ba), beryllium (Be), bismuth (Bi), boron (B), cadmium (Cd), calcium (Ca), chromium (Cr), cobalt (Co), copper (Cu), iron (Fe), lead (Pb), lithium (Li), magnesium (Mg), manganese (Mn), molybdenum (Mb), nickel (Ni), potassium (K), rubidium (Rb), selenium (Se), silver (Ag), sodium (Na), strontium (Sr), tellurium (Te), thallium (Tl), tin (Sn), uranium (U), vanadium (V) and zinc (Zn). Mercury content was expressed on a dry liver weight basis (µg/g), while all other elements were expressed on a wet liver weight basis (mg/kg). In addition, ECCC provided information on the body and liver weights of the specimens. These were used to calculate each specimen's hepatosomatic index (HSI), which is the liver weight as a percent of bodyweight. This is a measure of the energy reserves of an animal and is frequently analyzed when assessing bioindicator species, as it can reflect liver metabolism (Pandit and Gupta, 2019).

For all elements except for mercury, microwave assisted digestion in nitric acid was used to prepare the liver samples and the resulting solutions were analyzed for trace elements with an inductively-coupled plasma-mass spectrometer (ICP-MS). For mercury, samples were analyzed on a DMA-80 (direct mercury analyzer). Each trace element had a concentration level threshold below which they were undetected in the sample. For trace element levels below the non-detect value, the concentration was recorded as half that value. However, for those trace elements where non-detect was recorded for more than 50% of all specimens, those trace elements were removed from further analysis.

2.5 Statistical Analysis

The aim of the statistical analysis was to investigate any relationships between and among bone metrics and trace element exposure levels. To do this, an exploratory analysis was performed to create specific hypotheses about the potential relationships among variables. This was followed by predictive modelling of these relationships, particularly those between trace elements and bone metrics. All statistical analyses were performed using R (4. 1. 2, R Core Team, Vienna, Austria) (R Core Team, 2021). See Appendix D for the script.

To prepare data, all variables (bone metrics and trace element concentrations) were checked for normality. As most variables exhibited non-normal distributions, all variables were log transformed to normalize the spread in data. Two principal component analyses (PCA) were then performed on the data. A PCA can be used to illustrate the variability in a dataset to identify which variables account for the greatest and least variability. This may be used when there are many variables for a dataset to guide hypothesis formation for the relationships between variables (Jolliffe and Cadima, 2016). One PCA considered all baculum bone metrics and trace elements, and the other considered all femur metrics and trace elements. Baculum and femur data had to be separated in this way because PCAs cannot be performed on data with missing values and the female mink specimens as well as two male mink specimens lacked baculum data. This was followed by three correlation matrices: one comparing baculum metrics and trace element data, one comparing femur metrics and trace element data, and one comparing baculum and femur metrics. The correlation coefficient was Pearson's product moment correlation coefficient. A standard p-value of 0.05 was used to determine which correlation coefficients were significant and from these, only those coefficients above 0.5 were considered for predictive modeling.

For the remaining correlation coefficients, individual relationships between two variables were considered for univariate linear regression modeling. Normality was first assessed using the Shapiro-Wilks method. This was followed by a Breusch-Pagan test to test for homoscedasticity and then linear regression was performed. All tests used a p-value of 0.05. The linear fit was assessed based on the R^2 and beta (slope) values. All linear models were plotted with the line of regression and sex differentiated for each data point. However, regressions assessing males and females separately were not performed. Among all relationships, the R^2 and slope of the linear fits were compared to determine which trace elements had the strongest ability to predict bone metrics.

Finally, a power analysis was performed for all significant relationships to determine an appropriate sample size for a power of 0.80.

Chapter 3 – Results

Overview: This chapter provides the bone metrics and trace element concentrations as listed in Chapter 2. Means and standard deviations for each value are reported. In addition, the PCAs, correlation matrices and linear regression models investigating relationships are presented here.

3.1 Dimensional Analysis

In total, 18 mink and their baculums and femurs were measured, three of which were female and 15 were male. Of all male specimens, two were missing their baculums (Table 3.1, Table 3.2). For specific specimen dimensions, span lengths and location see Appendix E.

Table 3.1: *Mean and standard deviations of all baculum dimensions and weight (N = 13).*

Measurement	**Mean**	**SD**
Length (mm)	40.62	3.71
Medial-lateral diameter (mm)	2.28	0.52
Superior-inferior diameter (mm)	2.20	0.43
Weight (g)	0.54	0.70
Second moment of area (mm^4)	2.56	0.91

Table 3.2: *Mean and standard deviations of all femur dimensions and weight. This includes all 18 femurs, 15 of which belonged to male specimens and three of which belonged to female specimens.*

Measurement	Sex	Mean	SD
Length (mm)	Male	50.24	2.42
	Female	43.81	2.09
Medial-lateral diameter (mm)	Male	4.62	0.42
	Female	4.08	0.15
Anterior-posterior diameter (mm)	Male	3.74	0.28
	Female	3.79	0.03
Weight (g)	Male	2.21	0.51
	Female	1.47	0.21
Second moment of area (mm^4)	Male	26.65	13.75
	Female	11.35	2.84

3.2 Micro-Computed Tomography

Scans took anywhere between eight and 13 hours to complete. An example of the cross-sectional images acquired from Micro-Computed Tomography (µCT) before and during image processing (Figure 3.1, Figure 3.2) shows the binarized images for calculating trabeculae thickness, connectivity and spacing, as well as the thickness maps for trabeculae thickness and spacing.

Table ***3.3*** presents the mean and standard deviations for these measures.

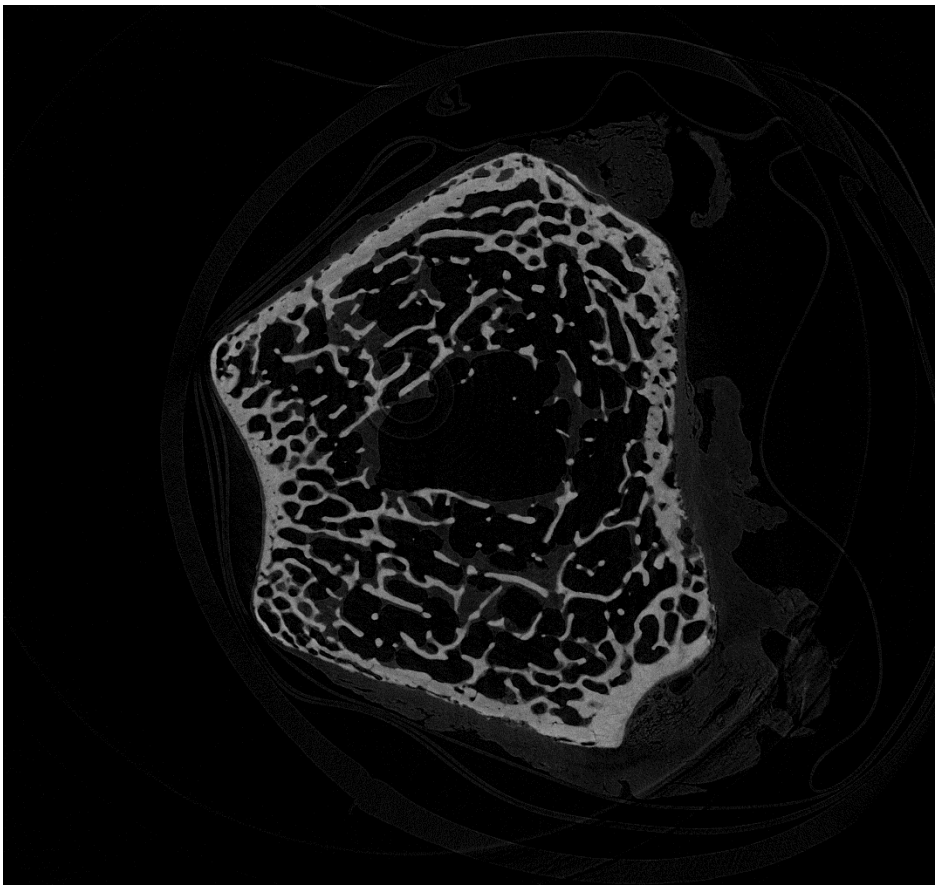

Figure 3.1*: Example of one of the reconstructed images in a stack before analysis with BoneJ.* Grey structures are bone material. The outer boundary (where the bone material is thicker) is the cortical bone that encapsulates the cancellous bone, which is the porous structure.

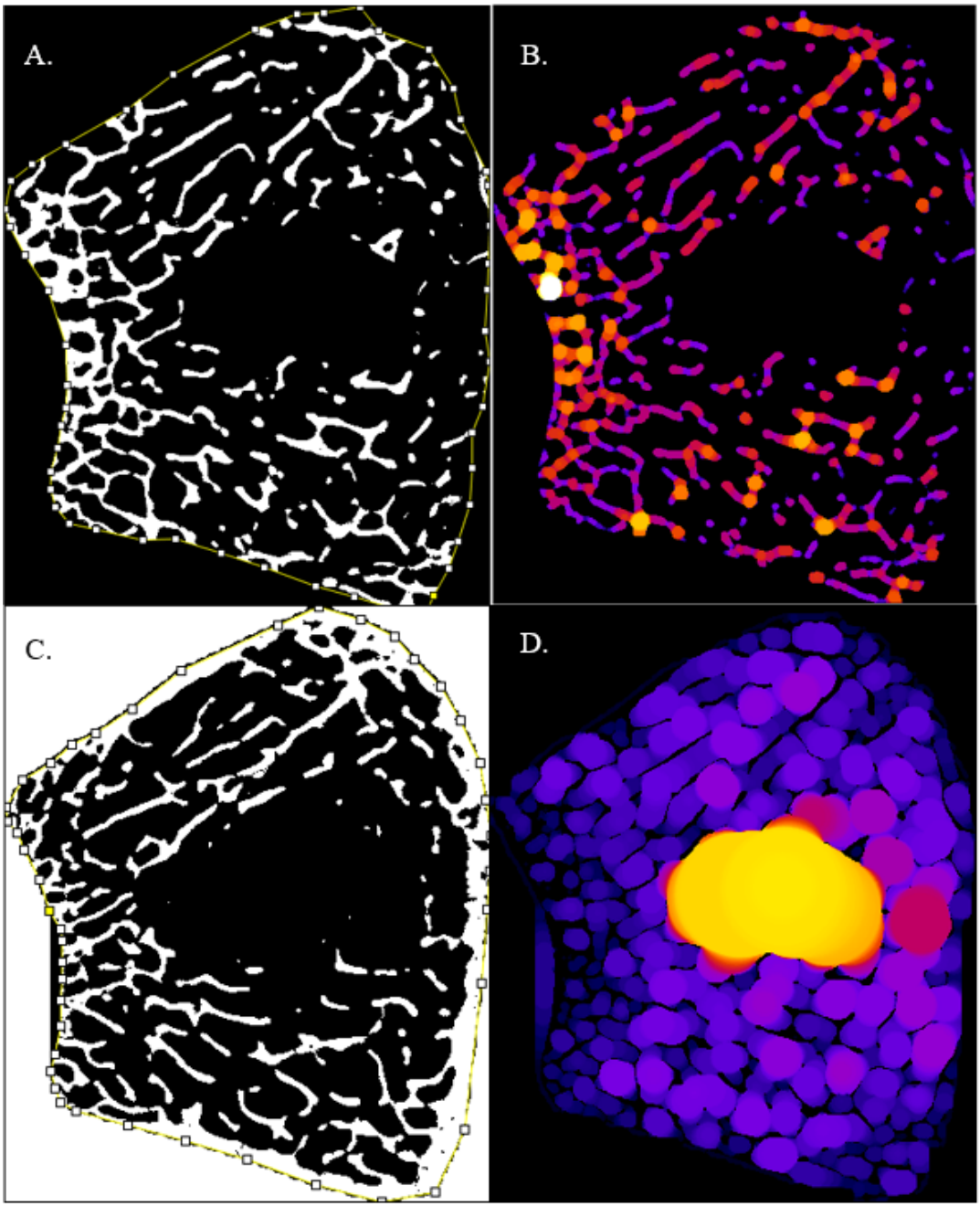

Figure 3.2*: Sample trabeculae ROIs and thickness maps for specimen 1718-451-3.*
A. An example of the ROI used for calculating trabeculae thickness after image processing; B. The map of trabeculae thickness. The colour gradient ranges from white (maximum thickness) to dark blue (minimum thickness); C. The same region after processing in preparation for calculating trabeculae spacing; D. The thickness map of trabeculae spacing. The colour gradient ranges from white/yellow (maximum spacing) to dark blue (minimum spacing).

Table 3.3: *Mean and standard deviation of trabeculae measures for all femurs.*

Measurement	Sex	Mean	SD
Trabeculae thickness (µm)	Male	109.60	39.85
	Female	109.50	37.56
Trabeculae spacing (µm)	Male	644.15	443.50
	Female	549.15	318.28
Connectivity	Male	2194.15	3305.85
	Female	729.56	231.44
Connectivity density (mm^{-3})	Male	40.20	43.80
	Female	27.40	11.70

3.3 Three-Point Bending

The following tables present the mean and SD of baculum (Table 3.4) and femur metrics (Table 3.5) acquired through three-point bend tests.

Table 3.4: *The mean and standard deviations of baculum metrics acquired from three-point bend tests.*

Measurement	Mean	SD
Peak load (N)	47.99	28.40
Stiffness (N/mm)	93.56	63.62
Ultimate stress (MPa)	230.07	80.41
Bending modulus (GPa)	16.76	8.50
Yield stress (MPa)	139.82	72.15
Yield load (N)	28.31	19.15
Work-to-failure (Nmm)	78.31	44.65

Table 3.5: *The mean and standard deviations of femur metrics acquired from three-point bend tests.*

Measurement	Sex	Mean	SD
Peak load (N)	Male	234.45	55.91
	Female	132.76	13.42
Stiffness (N/mm)	Male	445.14	100.48
	Female	252.54	22.73
Maximum bending moment (Nmm)	Male	1617.56	386.13
	Female	862.92	87.26
Ultimate stress (MPa)	Male	181.70	34.37
	Female	187.41	15.39
Bending modulus (GPa)	Male	9.30	1.86
	Female	9.19	12.00
Yield stress (MPa)	Male	160.03	30.08
	Female	171.03	19.27
Yield load (N)	Male	205.81	45.05
	Female	121.47	19.56
Work-to-failure (Nmm)	Male	322.03	115.01
	Female	119.58	34.79

3.4 Trace Element Concentrations

From all trace elements, the following had more than 50% of specimens with non-detect values, so they were removed from analysis: antimony, arsenic, beryllium, bismuth, tellurium, uranium and vanadium. All trace elements for which there were less than 50% non-detect values are reported in Table 3.6 along with mink bodyweight, liver weight and HSI.

Table 3.6: *Mink information and trace element exposure levels acquired from liver toxicology.*

Measure	Mean	SD
Bodyweight (kg) (male)	0.77	0.14
Bodyweight (kg) (female)	0.53	0.10
Liver weight (g) (male)	36.1	11.7
Liver weight (g) female)	25.2	8.44
Hepatosomatic index (HSI) (male)	4.96	1.18
Hepatosomatic index (HSI) (female)	4.81	1.28
Mercury (µg/g)	1.78	1.08
Aluminum (mg/kg)	0.46	0.39
Barium (mg/kg)	0.12	0.06
Cadmium (mg/kg)	0.176	0.120
Calcium (mg/kg)	362	147
Chromium (mg/kg)	0.954	1.01
Cobalt (mg/kg)	0.048	0.022
Copper (mg/kg)	31.0	21.1
Iron (mg/kg)	1213	353
Lead (mg/kg)	0.026	0.016
Lithium (mg/kg)	0.012	0.019
Magnesium (mg/kg)	647	116
Manganese (mg/kg)	9.6	2.7
Molybdenum (mg/kg)	1.73	0.413
Nickel (mg/kg)	0.45	0.63
Potassium (mg/kg)	8560	1080
Rubidium (mg/kg)	39.7	24.5
Selenium (mg/kg)	1.84	0.431
Silver (mg/kg)	0.050	0.046
Sodium (mg/kg)	4870	673
Strontium (mg/kg)	0.27	0.29
Tin (mg/kg)	0.02	0.01
Zinc (mg/kg)	103	27.9

3.5 Statistical Analysis

3.5.1 Principal Component Analyses

All data were first assessed for normality by creating histograms of every variable. The histograms revealed that most variables exhibited non-normal distributions (see Appendix E). To account for this, all variables were log transformed before any further analysis. This was followed by performing the Shapiro-Wilks test on the variables again to confirm they were all normalized.

There was one specimen identified as an outlier from the data, specimen no. 1718-418 (Figure 3.3). This specimen had trabeculae connectivity and connectivity density that was on the order of 10 times greater than the average and four standard deviations larger than the mean. Other baculum and femur metrics for this specimen were also 4-6x greater than the averages. Upon closer examination of the μCT images, the trabeculae structure was visually very different from other specimens. Additionally, the femur material properties, trabecular measures and baculum weights did not pass Shapiro-Wilks tests after log transformation due to this specimen's data. For these reasons, this specimen was removed from all statistical analyses.

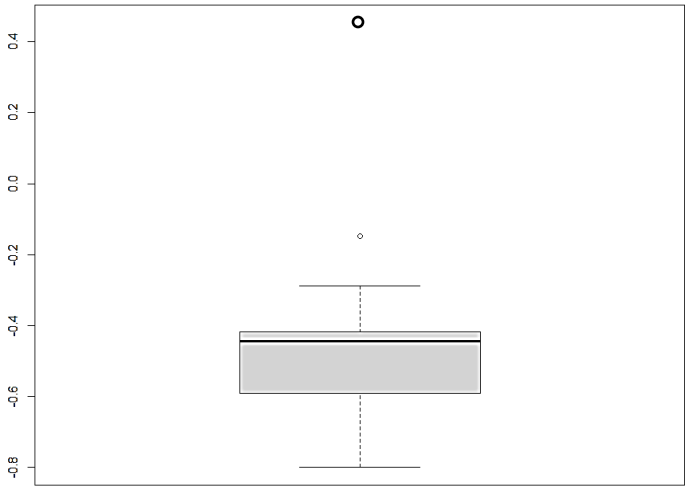

Figure 3.3: *An example of a box and whisker plot of a baculum metric that could not be normalized due to the outlier.*
This was a box and whisker plot of baculum weight. This metric did not pass the Shapiro-Wilks test even after log-transforming the data. The furthest outlier is specimen 1718-418.

To simplify data presentation, each variable was abbreviated (Table 3.7) and all elements were represented by their symbols. For the first PCA, the data on 12 male mink baculums were included along with the mink trace element concentration levels (Figure 3.4).

Table 3.7: *Variable abbreviations used for the analysis and predictive modeling.*

Variable	Abbreviation	Variable	Abbreviation
Bodyweight (kg)	BW	**Liver weight (g)**	LW
Hepatosomatic index	HSI	**Femur length (mm)**	FemL
Femur medial-lateral diameter (mm)	FemML	**Femur anterior-posterior diameter (mm)**	FemAP
Femur weight (g)	FemW	**Femur peak load (N)**	FemPL
Femur stiffness (N/mm)	FemSt	**Femur bending moment (Nmm)**	FemBenMom
Femur ultimate Stress (MPa)	FemUS	**Femur bending modulus (GPa)**	FemE
Femur yield stress (MPa)	FemYS	**Femur yield load (N)**	FemYL
Femur work-to-failure (Nmm)	FemWtF	**Baculum length (mm)**	BacLen
Baculum medial-lateral diameter (mm)	BacML	**Baculum superior-inferior diameter (mm)**	BacSI
Baculum weight (g)	BacW	**Baculum peak load (N)**	BacPL
Baculum stiffness (N/mm)	BacSt	**Baculum ultimate stress (MPa)**	BacUS
Baculum bending modulus (GPa)	BacE	**Baculum yield stress (MPa)**	BacYS
Baculum yield load (N)	BacYL	**Baculum work-to-failure**	BacWtF
Mean trabeculae thickness (µm)	Tb.Th	**Trabeculae thickness SD (µm)**	Tb.Th.SD
Mean trabeculae spacing (µm)	Tb.Sp	**Trabeculae spacing SD (µm)**	Tb.Sp.SD
Trabeculae connectivity	Con	**Trabeculae connectivity density (μm^{-3})**	ConDen

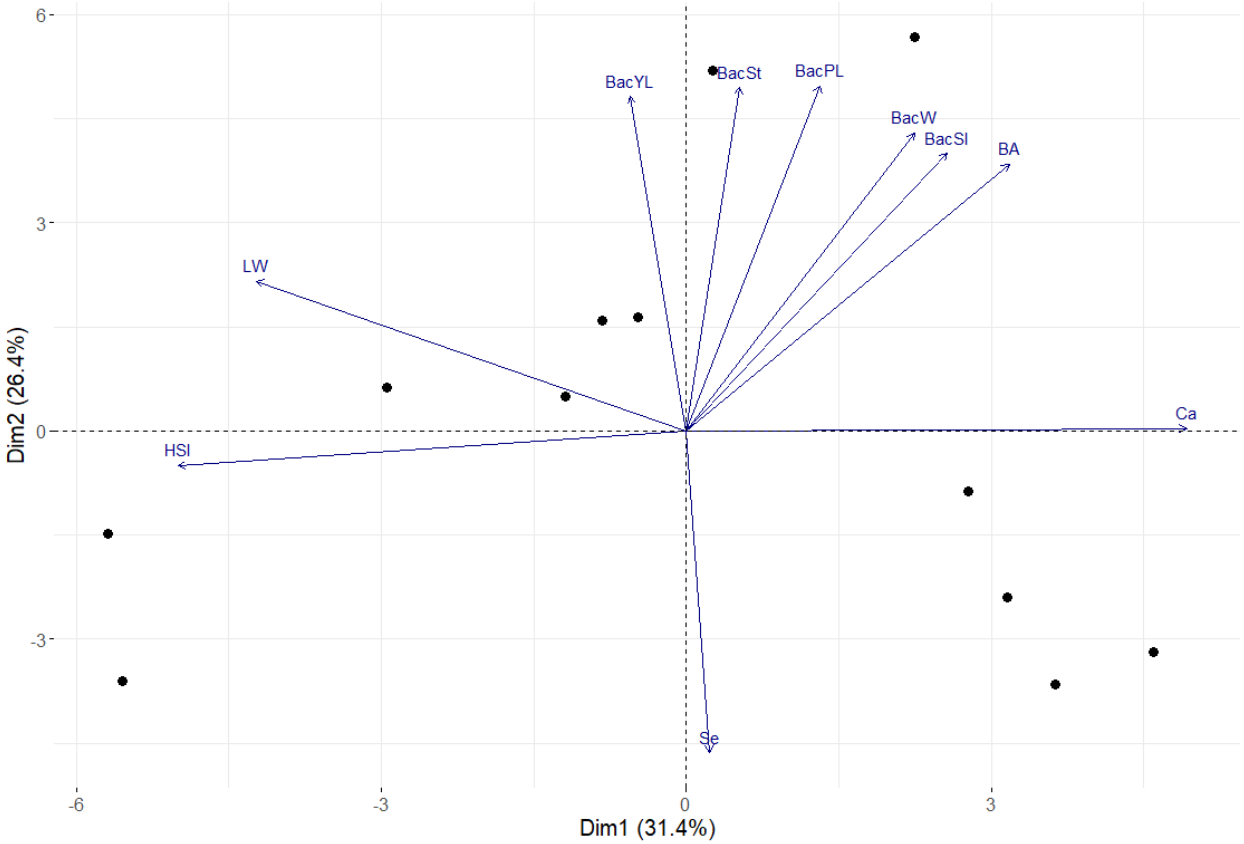

Figure 3.4: *PCA 1: baculum metrics and trace element concentrations*.
The axes represent the first two principal components, labelled here as Dim1 and Dim2. Dim1 is the first principal component and represents the horizontal axis. Dim2 is the second principal component and represents the vertical axis. In brackets, the percent contributions of the components to the variability across all data is given. The black dots are the data points representing each specimen and the blue axes represent the variables and their contribution to each principal component.

Based on the PCA in Figure 3.4, the following variables contributed most to the variability in the data: calcium concentration, selenium concentration, HSI, liver weight, yield load, stiffness, peak load, baculum weight, superior-inferior diameter, and second moment of area. Of the 13 principal components, the first six accounted for 91% of the variance in data. So, following this PCA the percent contributions of each variable to principal components one through six were identified (Appendix E). The variables that contributed the most to the first principal component

were: HSI, calcium, aluminum, liver weight and barium (Figure 3.5). The variables that contributed most to the second principal component were: peak load, stiffness, yield load, selenium and baculum length (Figure 3.6).

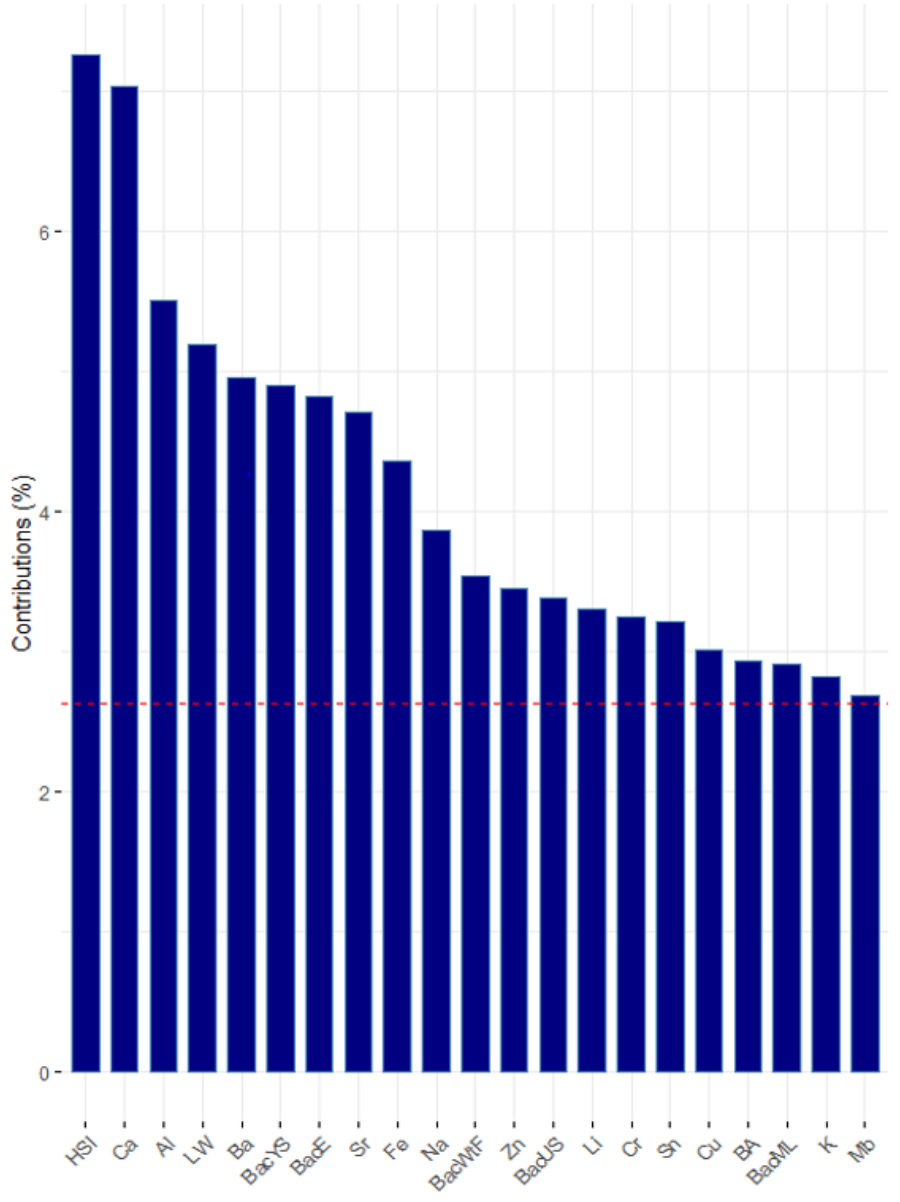

Figure 3.5: *Percent contribution of variables to the first principal component.* This principal component accounted for 31% of the variability in data. The horizontal axis lists the variables in the order of greatest to least contribution to the principal component, while the vertical axis is the percent contribution. The red line indicates the percent contribution that would occur if every variable contributed equally to the principal component. Only those variables whose contributions were greater than this value are presented here.

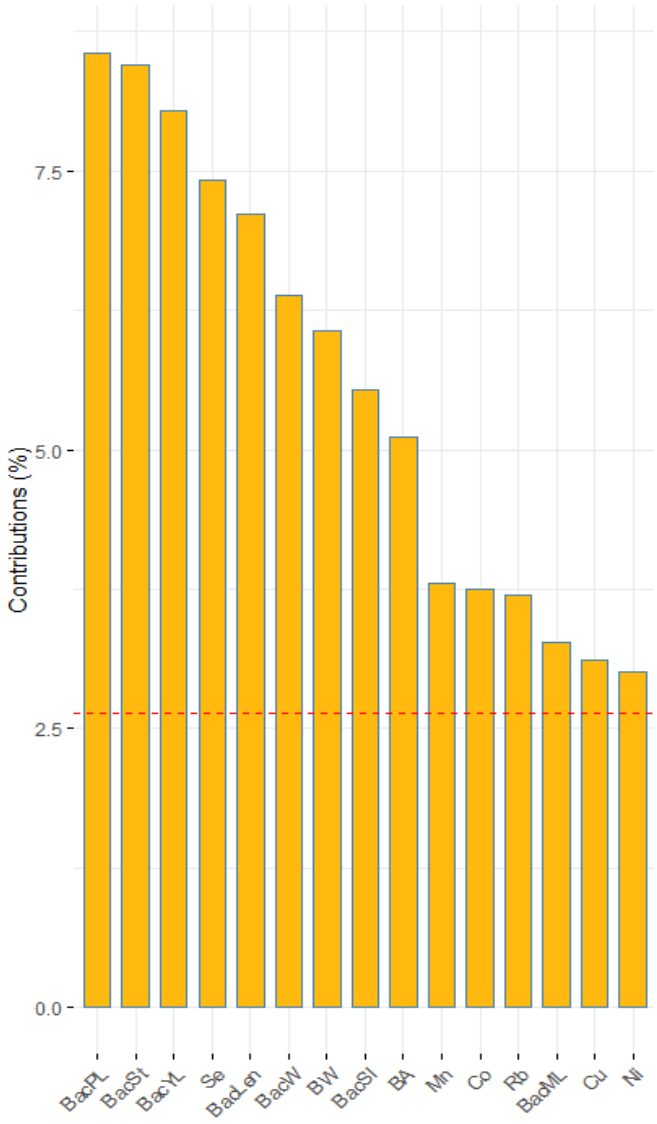

Figure 3.6: *Percent contribution of variables to the second principal component of PCA 1.* This principal component accounted for 26% of the variability in the data. The horizontal axis lists the variables in the order of greatest to least contribution to the principal component, while the vertical axis is the percent contribution. The red line indicates the percent contribution that would occur if every variable contributed equally to the principal component. Only those variables whose contributions were greater than this value are presented here.

The second PCA was run on the femur metrics and trace element concentration levels (Figure 3.7). Percent contributions to the first and second principal components are also included (Figure 3.8, Figure 3.9).

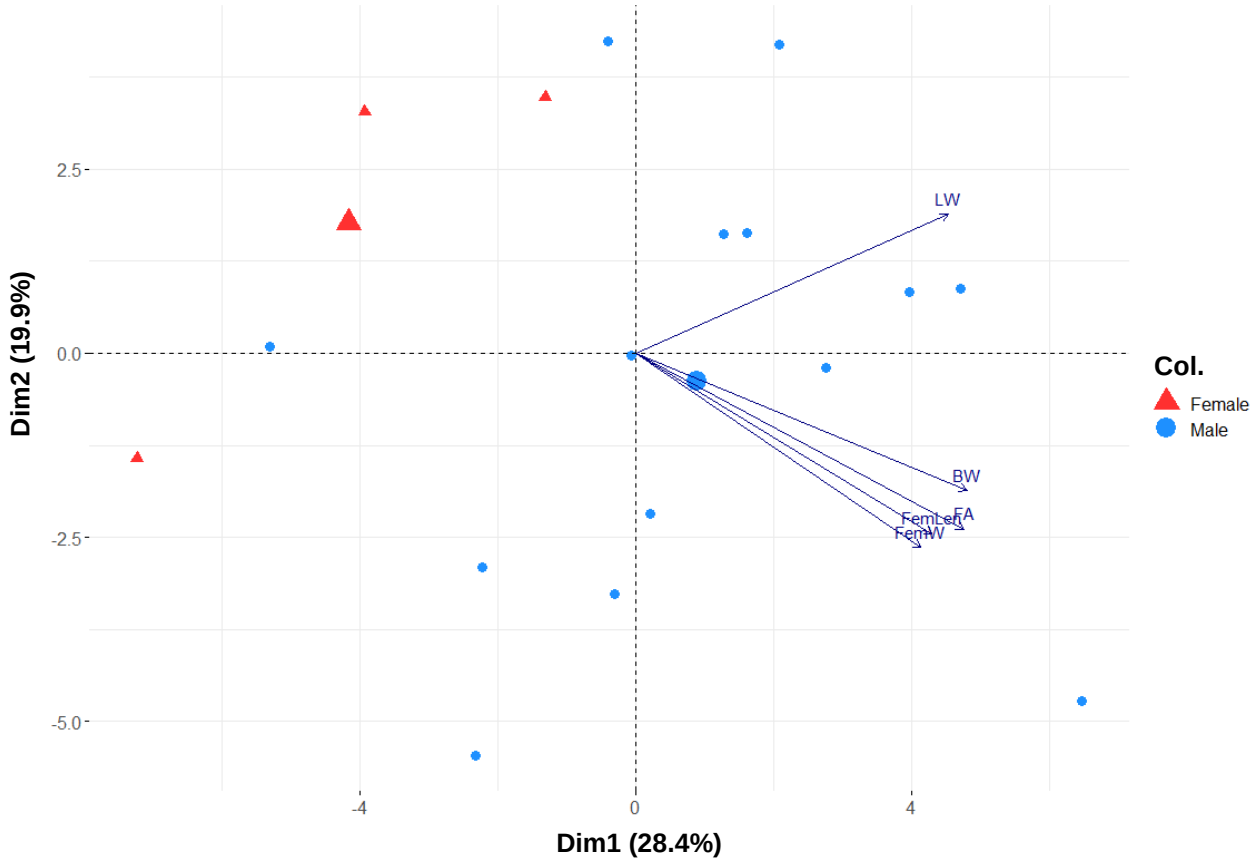

***Figure 3.7**: PCA 2: femur metrics and trace element data.*
The data points representing each specimen were divided by shape and colour to identify male versus female mink (although they were analyzed together, not separately). The large two red and blue points represent the center of the spread in data for male and female specimens and should not be confused with actual data points. The first five most contributing variable axes are drawn and labelled as well.

The variables that contributed most to the first principal component were bodyweight, second moment of area (femur), liver weight, femur length and iron concentration (Figure 3.8). The variables that contributed most to the second principal component were HSI, chromium, zinc, aluminum and magnesium concentrations (Figure 3.9). For further results, see Appendix E.

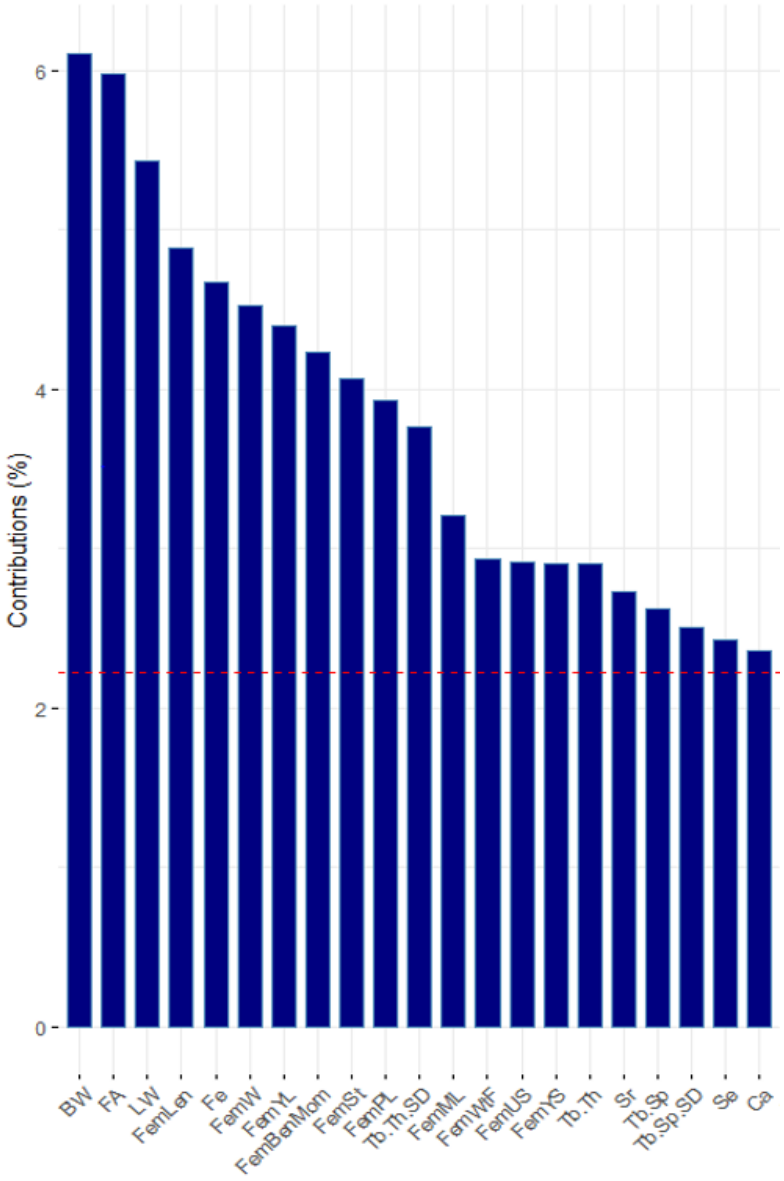

Figure 3.8: *The percent contribution of variables to the first principal component of PCA 2.* This principal component accounted for 28% of the variation in data. The horizontal axis lists the variables in the order of greatest to least contribution to the principal component, while the vertical axis is the percent contribution. The red line indicates the percent contribution that would occur if every variable contributed equally to the principal component. Only those variables whose contributions were greater than this value are presented here.

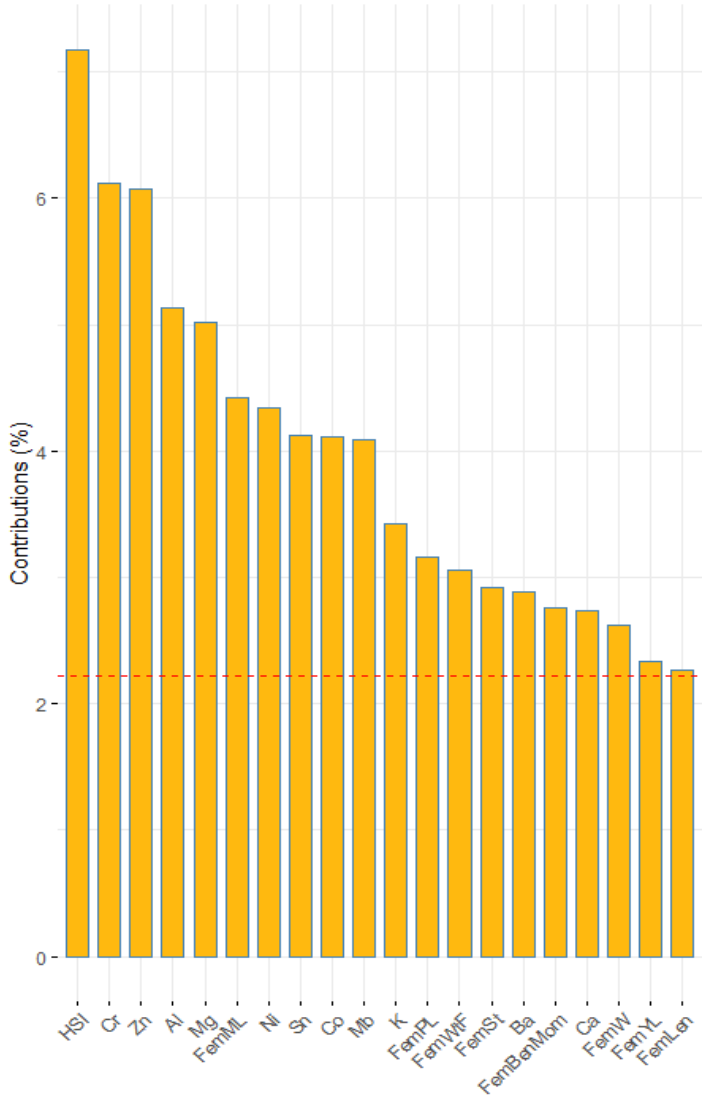

Figure 3.9: *The percent contribution of variables to the second principal component of PCA 2*. This accounted for 20% of the variation in data. The horizontal axis lists the variables in the order of greatest to least contribution to the principal component, while the vertical axis is the percent contribution. The red line indicates the percent contribution that would occur if every variable contributed equally to the principal component. Only those variables whose contributions were greater than this value are presented here

3.5.2 Correlation Matrices

Three correlation matrices were made to compare bone metrics and trace element concentrations.

The first included all baculum bone metrics and trace elements (Figure 3.10). The second matrix

included all femur metrics and trace elements (Figure 3.11). Finally, the third matrix was created to examine relationships between baculum and femur metrics (Figure 3.12).

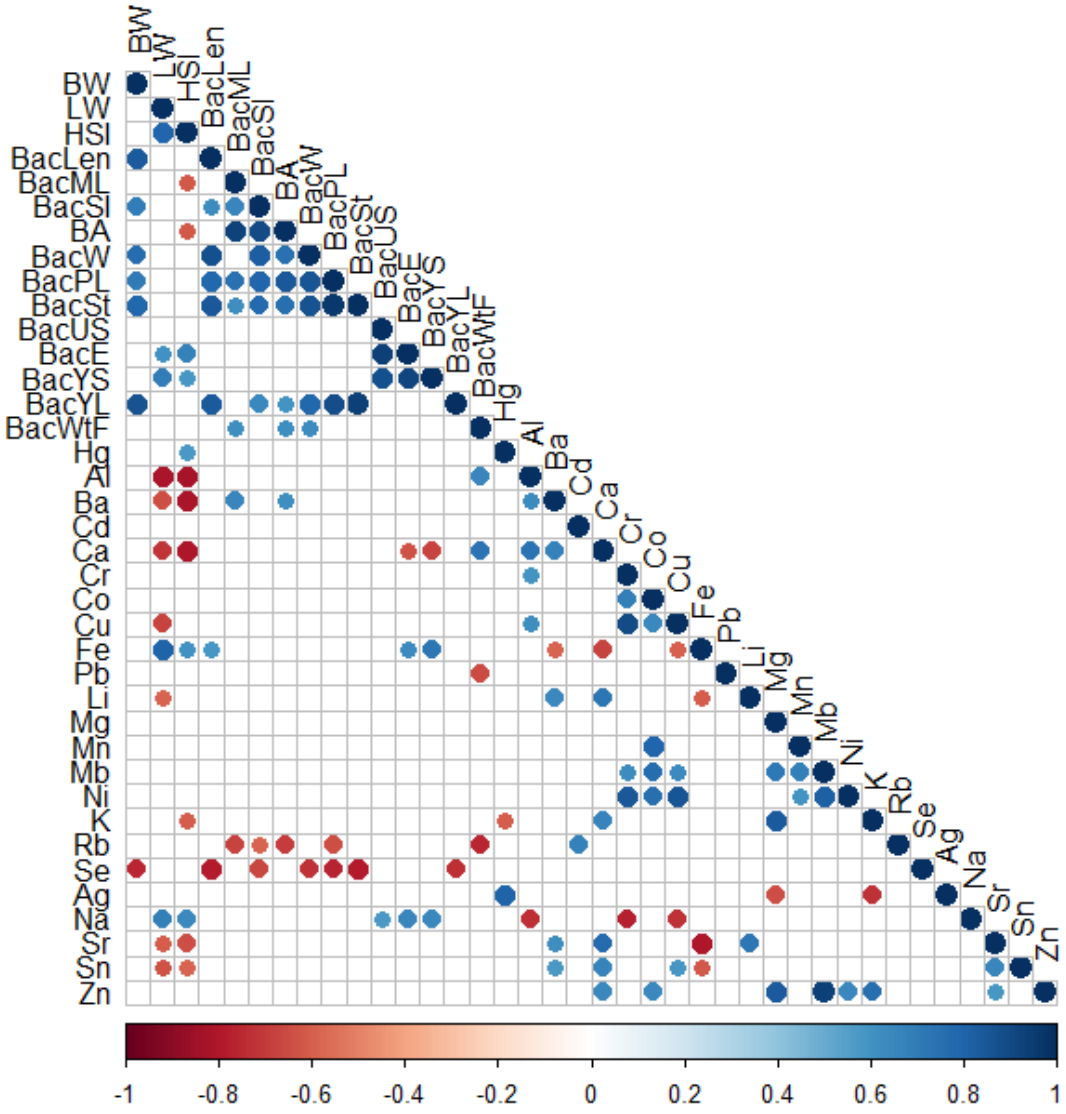

Figure 3.10: *Correlation matrix of baculum metrics and trace elements.* The colour spectrum references the strength of the correlation coefficients on a scale from -1 (negatively correlated) to 1 (positively correlated). The size of the circles also represents the correlation coefficients. The closer to zero, the smaller the circles are, and the closer to 1 or -1, the larger the circle. Only those relationships of significance (p-value = 0.05) are displayed.

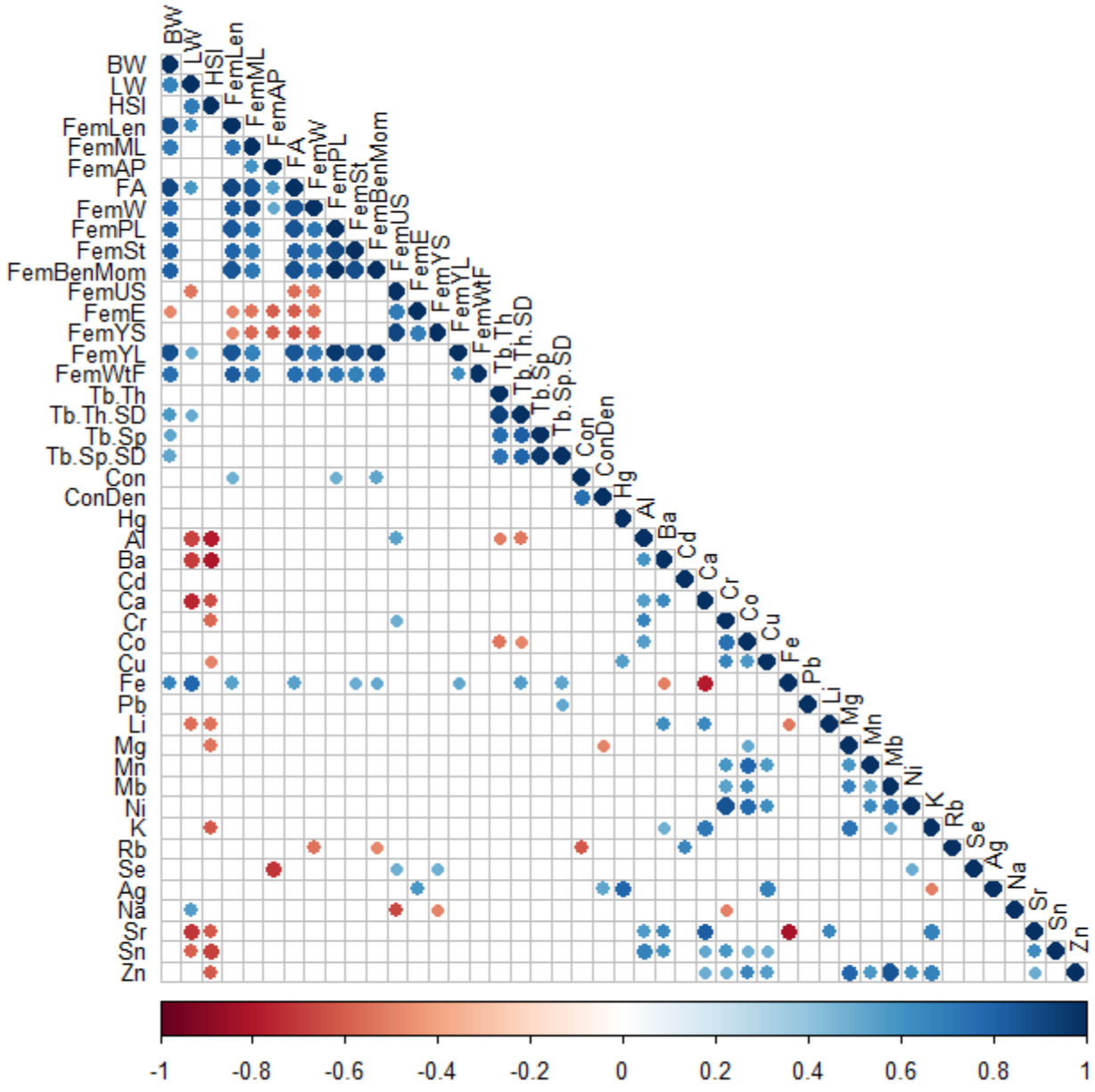

Figure 3.11: *Correlation matrix of femur metrics and trace elements.*
The colour spectrum references the strength of the correlation coefficients on a scale from -1 (negatively correlated) to 1 (positively correlated). The size of the circles also represents the correlation coefficients. The closer to zero, the smaller the circles are, and the closer to 1 or -1, the larger the circle. Only those relationships of significance (p-value = 0.05) are displayed.

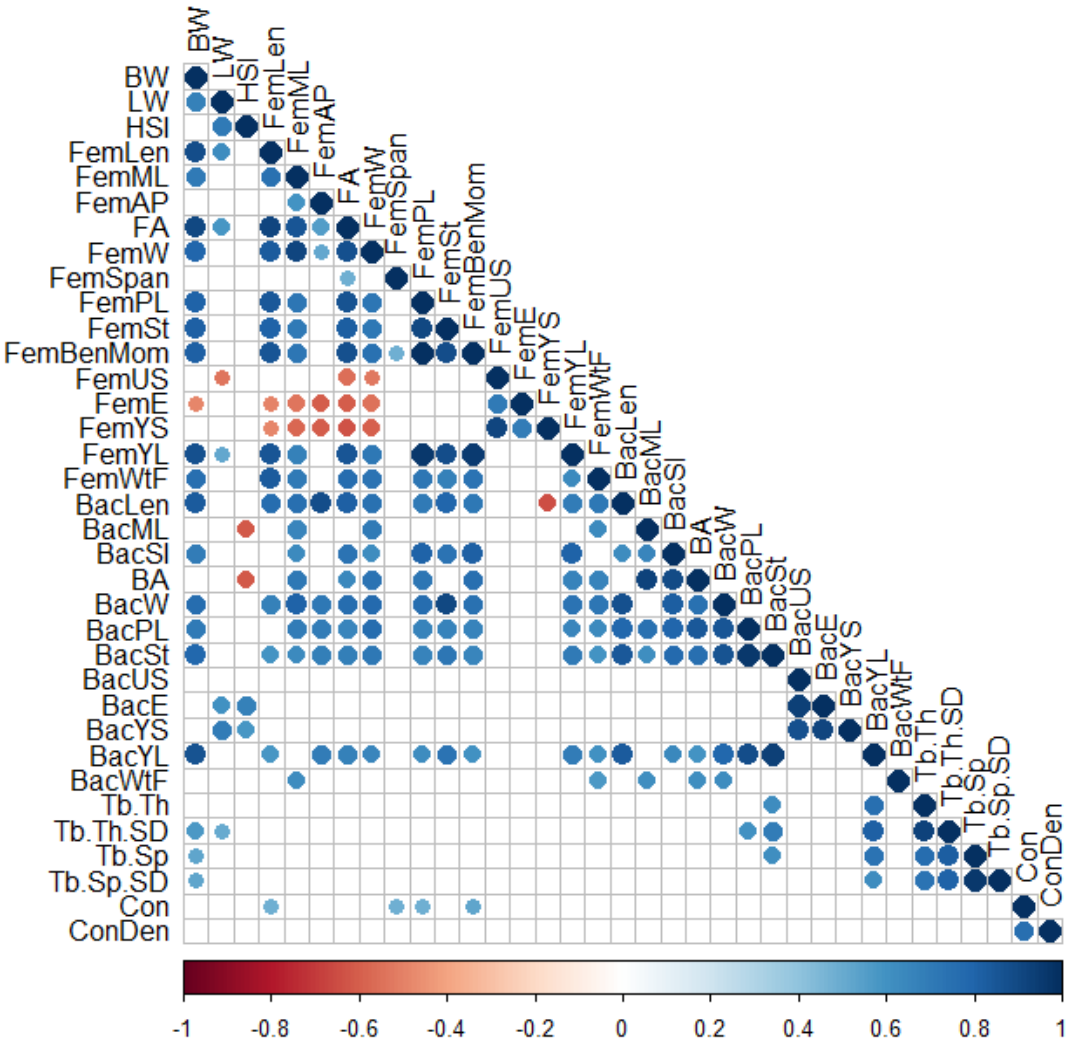

Figure 3.12: *Correlation matrix of femur and baculum metrics.*
The colour spectrum references the strength of the correlation coefficients on a scale from -1 (negatively correlated) to 1 (positively correlated). The size of the circles also represents the correlation coefficients. The closer to zero, the smaller the circles are, and the closer to 1 or -1, the larger the circle. Only those relationships of significance (p-value = 0.05) are displayed.

3.6 Linear Regression Models

The linear regression modelling was driven by the results from the PCAs and correlation matrix.

Only those variables with high correlation coefficients (0.5 to 1) were modelled. Relationships

that did not pass the normality (Shapiro-Wilks) and homoscedasticity (Bruesch-Pagan) tests were not modelled.

3.6.1 Baculum Properties

Baculum structural properties acquired through three-point bend tests were correlated with bone geometry. Among these, the bone weight, length, and diaphysis diameter in both directions were positively correlated with each other as well as other structural properties including peak load, yield load and stiffness (Figure 3.13). Bodyweight and work-to-failure were also positively correlated with bone geometry.

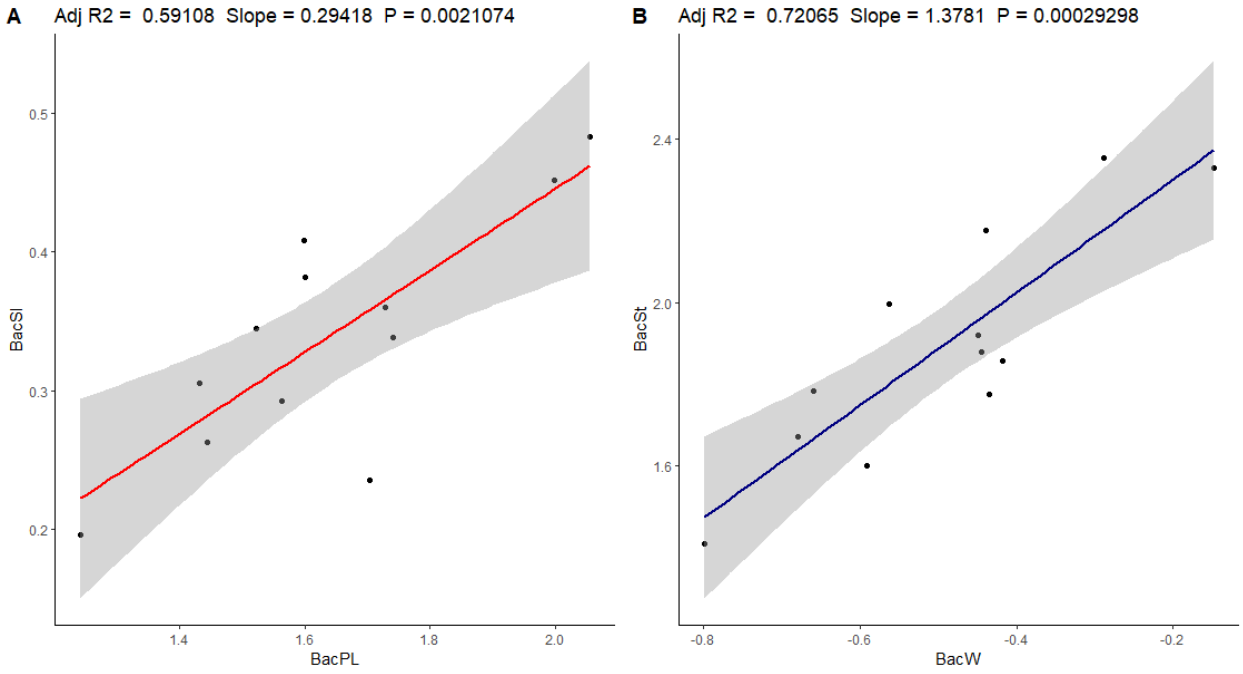

Figure 3.13: *Two examples of baculum dimension and structural property linear regressions*. A. The positive regression between baculum peak load and stiffness; B. The positive regression between baculum bone weight and stiffness. The adjusted R^2, slope of the line and p-values are displayed at the top of each graph. The gray bands around the regression lines are the calculated standard error for the regression in question.

Calcium was negatively correlated with two baculum bone metrics: bending modulus and yield stress. Iron was positively correlated with bending modulus, yield stress and baculum length, and both calcium and iron were positively correlated with work-to-failure (Figure 3.14). In addition, iron and calcium were inversely related with each other. Finally, lead had a negative correlation with work-to-failure while aluminum had a positive correlation with work-to-failure (Figure 3.15).

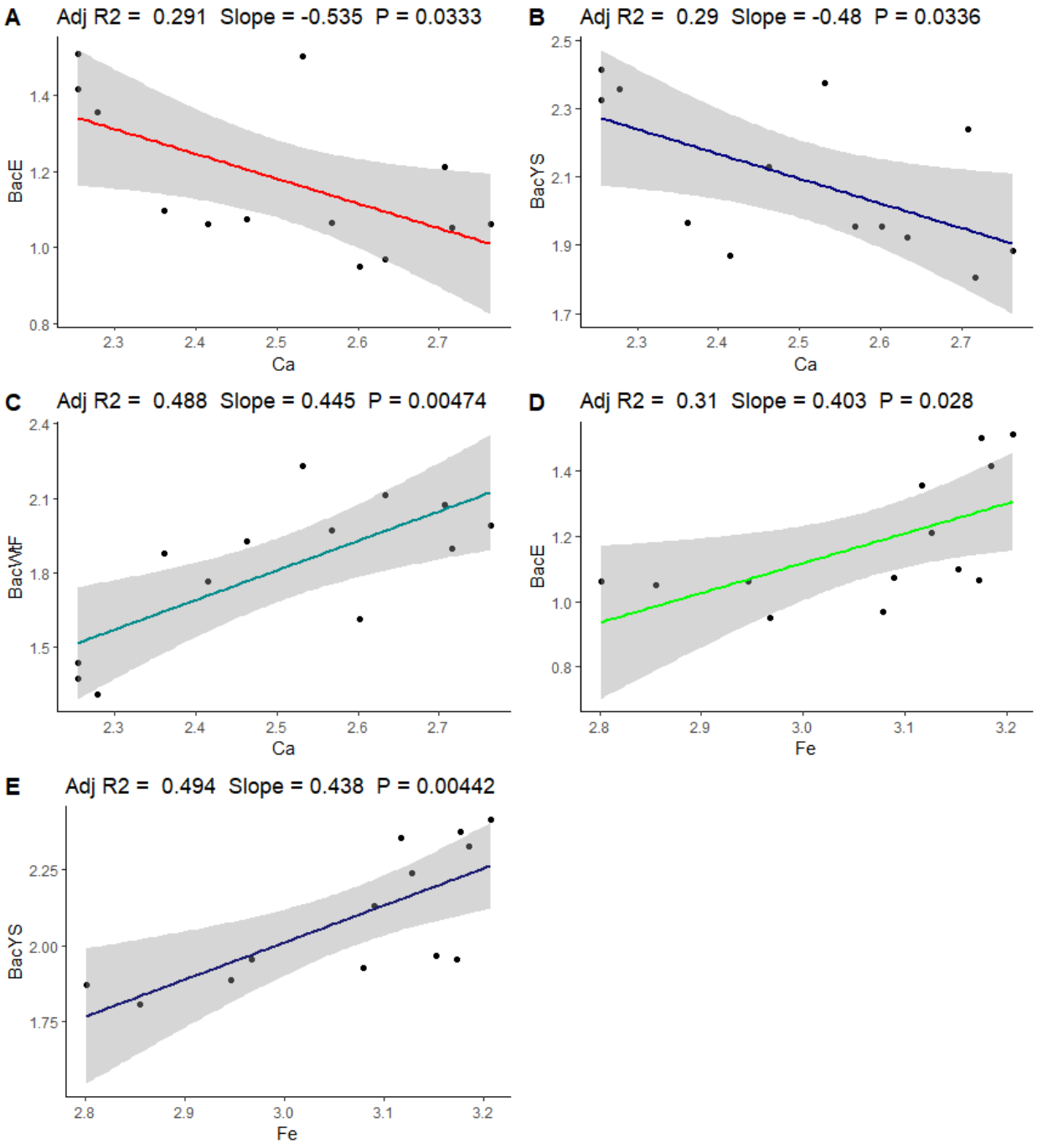

Figure 3.14: *Linear regressions between calcium, iron and bone properties.* The regressions above are: A. Calcium concentration and bending modulus; B Calcium concentration and yield stress; C. Calcium concentration and work-to-failure; D. Iron concentration and bending modulus; E. Iron concentration and yield stress.

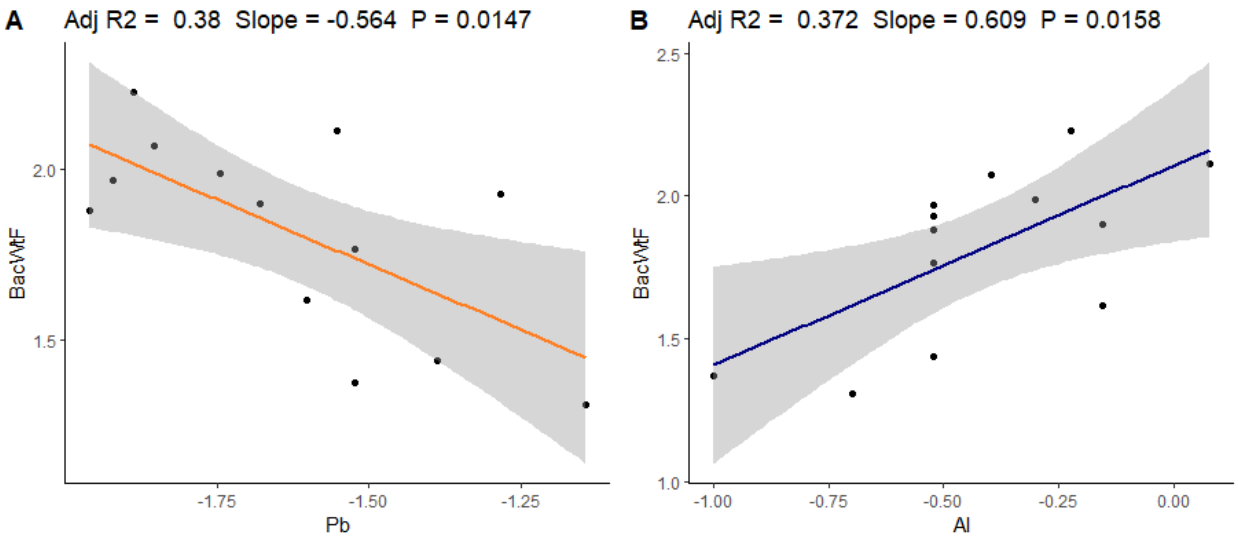

Figure 3.15: *Linear regression between lead and aluminum and baculum work-to-failure*. A. Lead had a negative correlation with work-to-failure; B. Aluminum had a positive correlation with work-to-failure.

Rubidium and selenium had the strongest negative correlations with baculum bone metrics relative to all other trace elements. Rubidium was negatively correlated with both diameters, the second moment of area, peak load and work-to-failure (Figure 3.16). Selenium was negatively correlated with the superior-inferior diameter, bone weight, peak load, stiffness and yield load. It was also negatively correlated with bodyweight (Figure 3.17). Finally, sodium also had positive correlations with baculum material properties including bending modulus and yield stress (Figure 3.18).

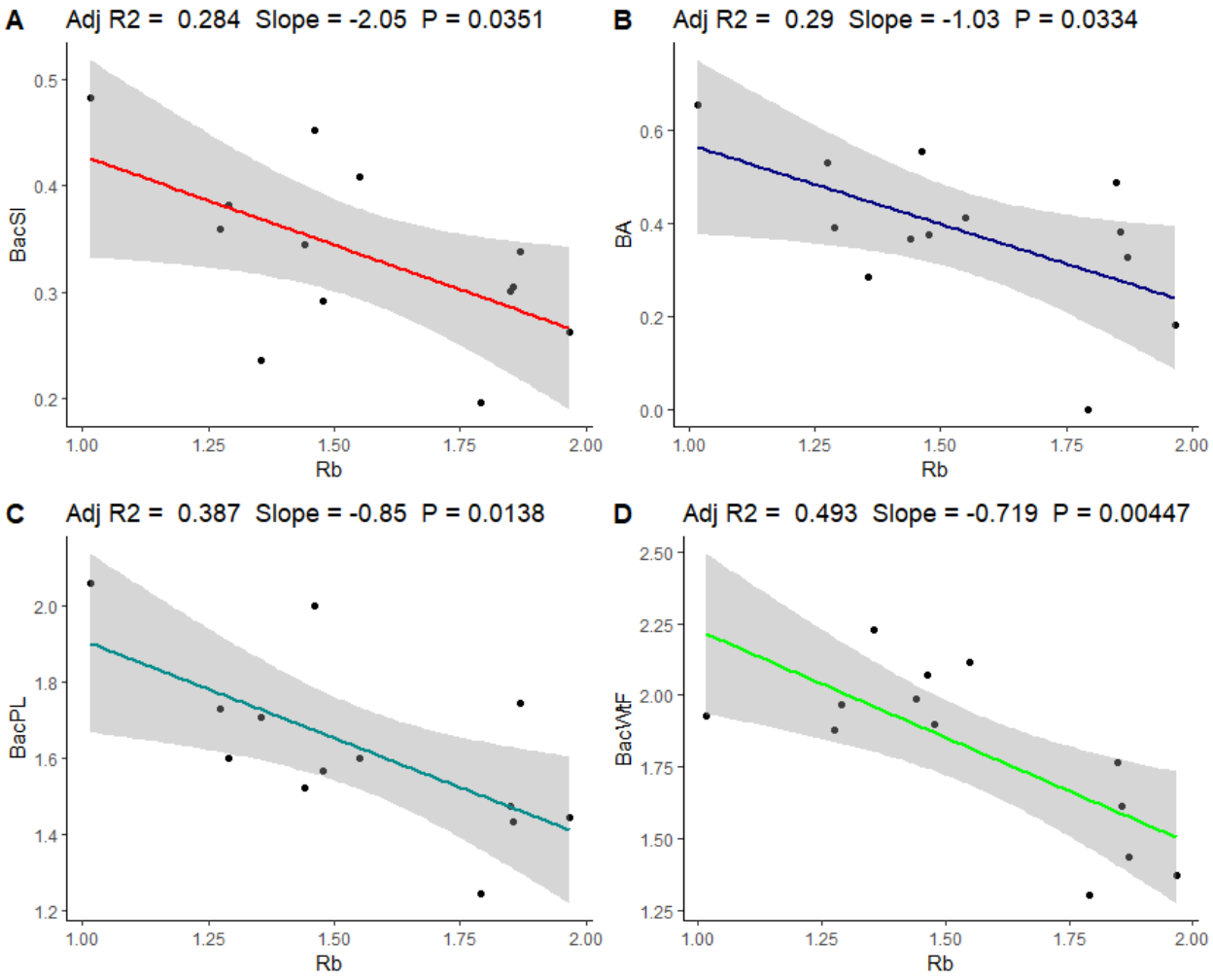

Figure 3.16: *Regression models of rubidium concentration and baculum bone metrics*. A. Rubidium and superior-inferior diameter; B. Rubidium and second moment of area; C. Rubidium and peak load; D. Rubidium and work-to-failure.

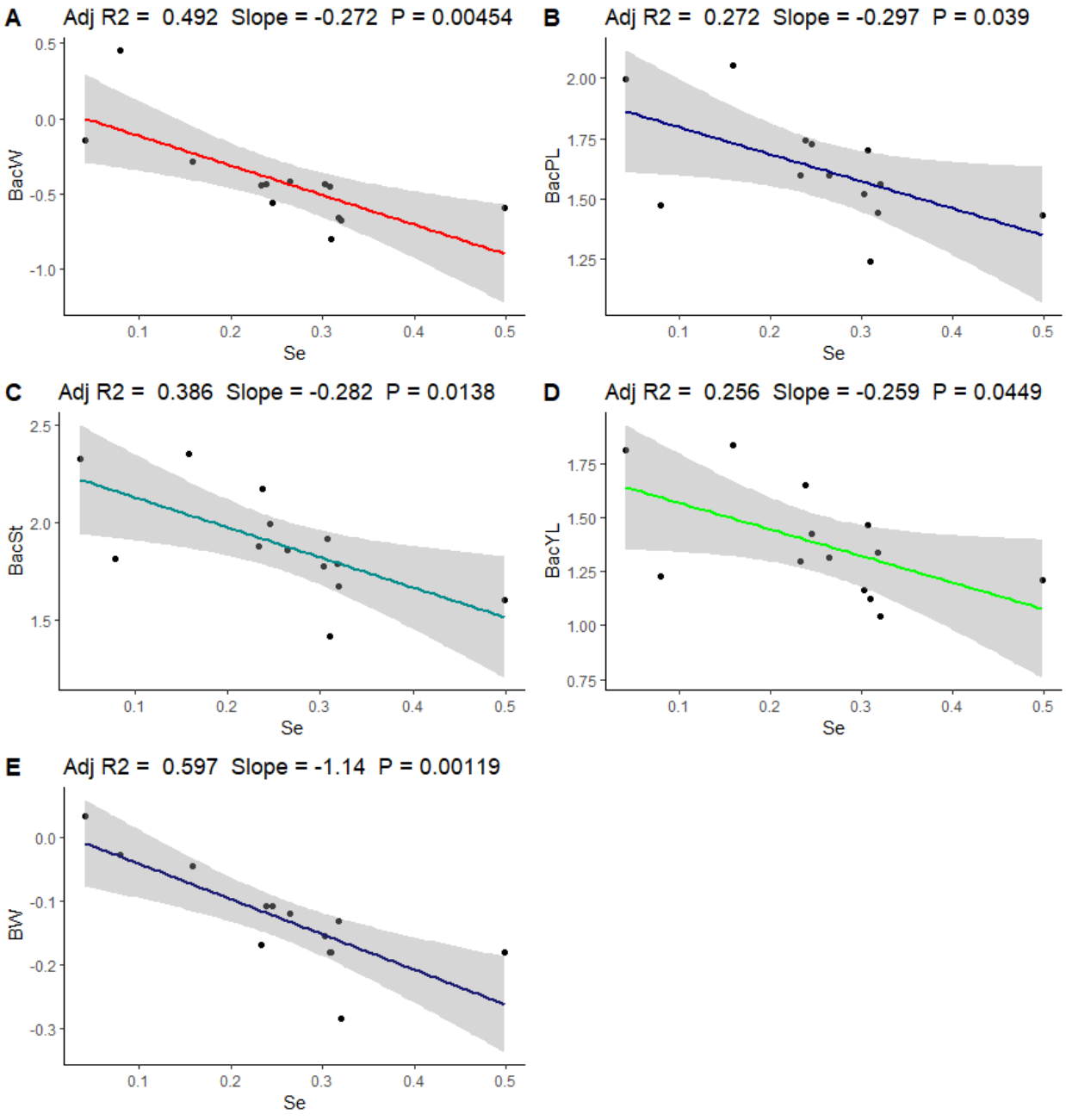

Figure 3.17: *Selenium concentration and baculum bone metrics*.
A. Selenium and baculum bone weight; B. Selenium and peak load; C. Selenium and stiffness; D. Selenium and yield load; E. Selenium and mink bodyweight.

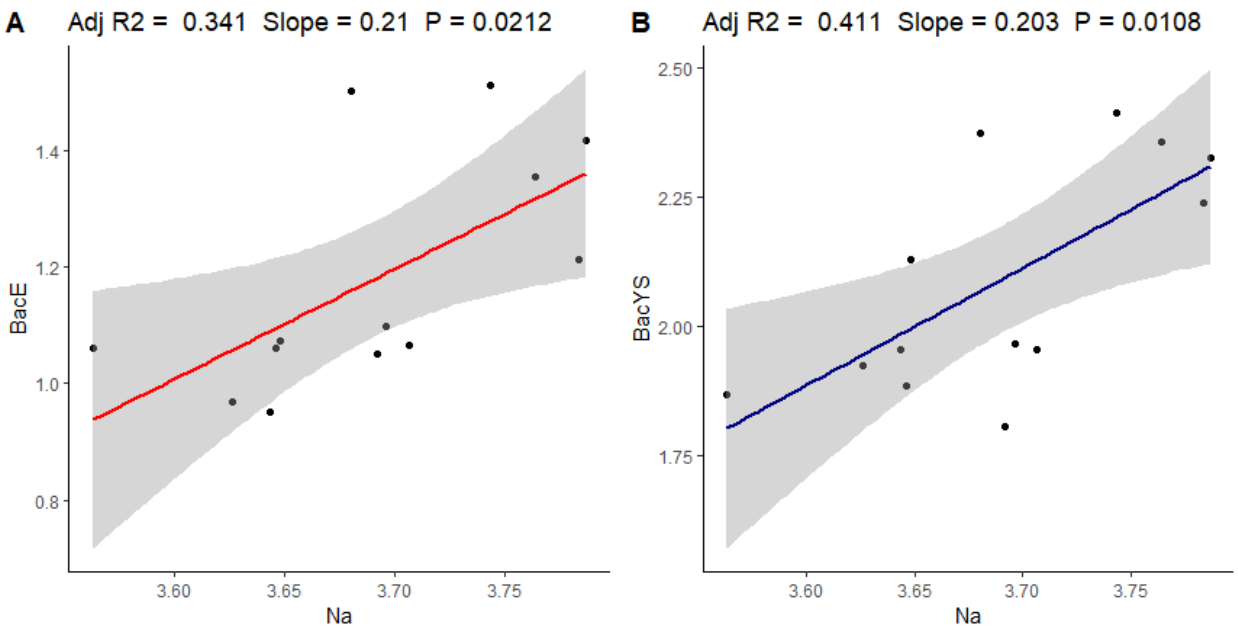

Figure 3.18: *Linear regressions between sodium and baculum bone metrics.*
A. Sodium and bending modulus; B. sodium and yield stress.

3.6.2 Femur Metrics

Like baculums, femurs demonstrated positive correlations among structural properties including geometric measures and bending structural properties (Figure 3.19). In addition, trabeculae connectivity was positively correlated with femur length and peak load. Yield stress was negatively correlated with femur geometric measures. For the linear regressions, male and female data were labelled different so they could be identified graphically but were analyzed in the linear regressions together. They could not be analyzed separately because the sample size of female mink was not large enough. It should be mentioned that even after log transforming every variable, femur bending modulus and ultimate stress did not pass the Shapiro-Wilks test for normality. Thus, they were not included in the linear regression analyses.

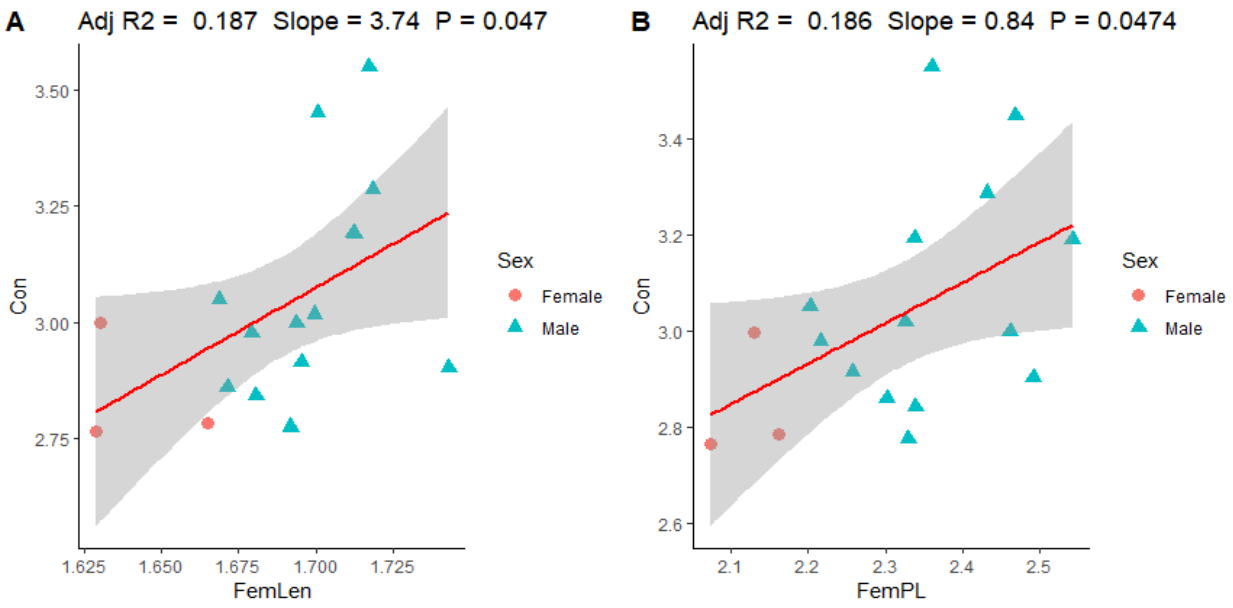

Figure 3.19: *Examples of linear regressions between femur properties.*
A. Trabeculae connectivity and femur length; B. trabeculae connectivity and peak load. In these plots and all subsequent plots representing femur metrics, female and male specimens are distinguished. However, all regressions were performed for all femur specimens regardless of sex. This was because there were not enough female specimens to assess males and females individually.

Iron was positively correlated with the femur second moment of area, stiffness and yield load, but was negatively correlated with yield stress (Figure 3.20).

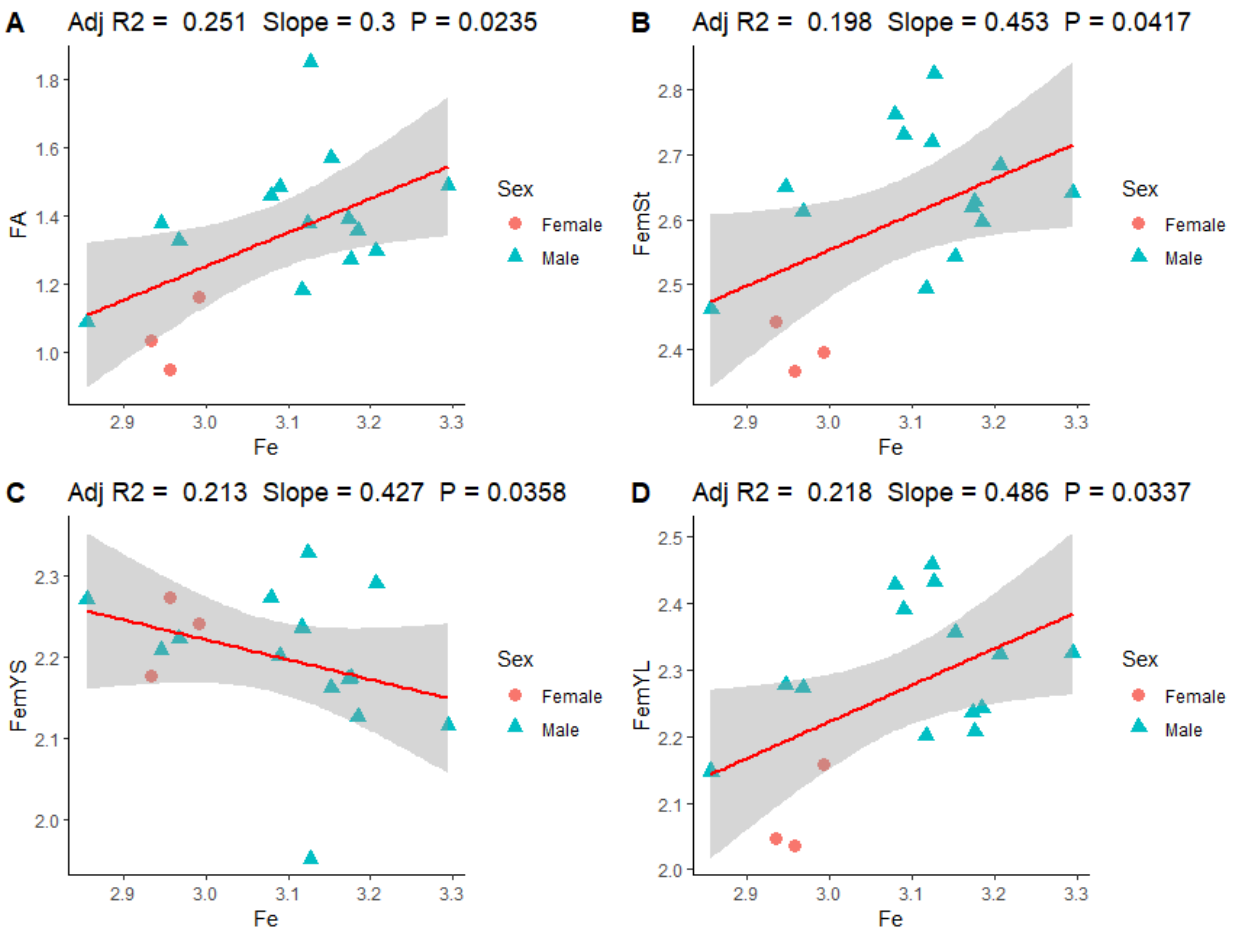

Figure 3.20: *The linear regressions between iron concentration and femur metrics*. A. Iron and second moment of area; B. iron and bending stiffness; C. iron and yield stress; D. iron and yield load.

Other relationships existed between trace elements and bone metrics: magnesium and connectivity density, aluminum and trabeculae thickness (Figure 3.21), rubidium and bending moment, rubidium and femur weight, selenium and yield stress, and selenium with anterior-posterior diameter (Figure 3.22).

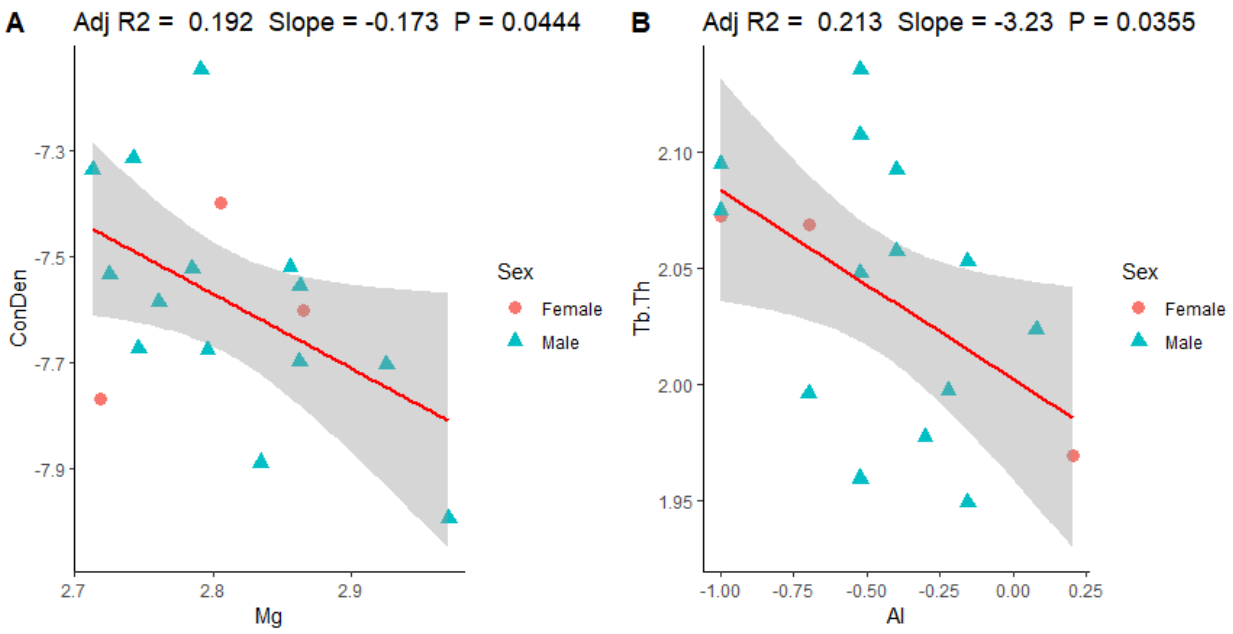

Figure 3.21: *Linear regression between trabeculae measures, magnesium, and aluminum.* A. Magnesium and connectivity density; B. Aluminum and trabeculae thickness.

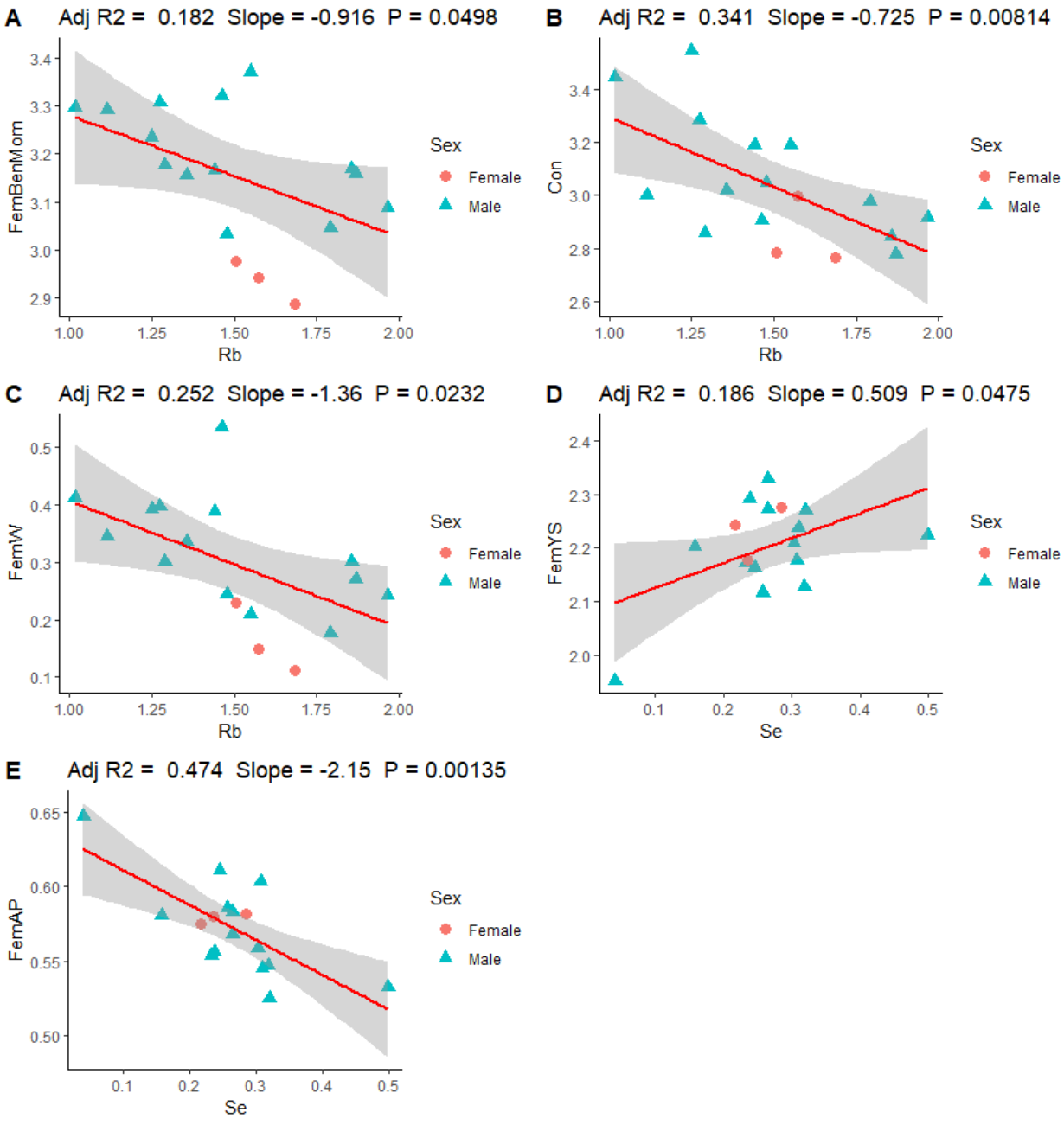

Figure 3.22: *Linear regressions between rubidium, selenium, and femur metrics.*
A. Rubidium and bending moment; B. Rubidium and connectivity; C. Rubidium and femur weight; D. Selenium and yield stress; E. Selenium and anterior-posterior diameter.

3.6.3 Baculum and Femur Metrics

Between baculum and femur metrics, all material properties were unrelated. Additionally, geometric measures and material properties were unrelated among baculums and femurs, except

for baculum length and femur yield stress. However, structural properties between baculums and femurs were nearly all positively correlated. Trabeculae properties were unrelated to most baculum measures, except for trabeculae thickness and spacing with baculum stiffness and yield load (Figure 3.23).

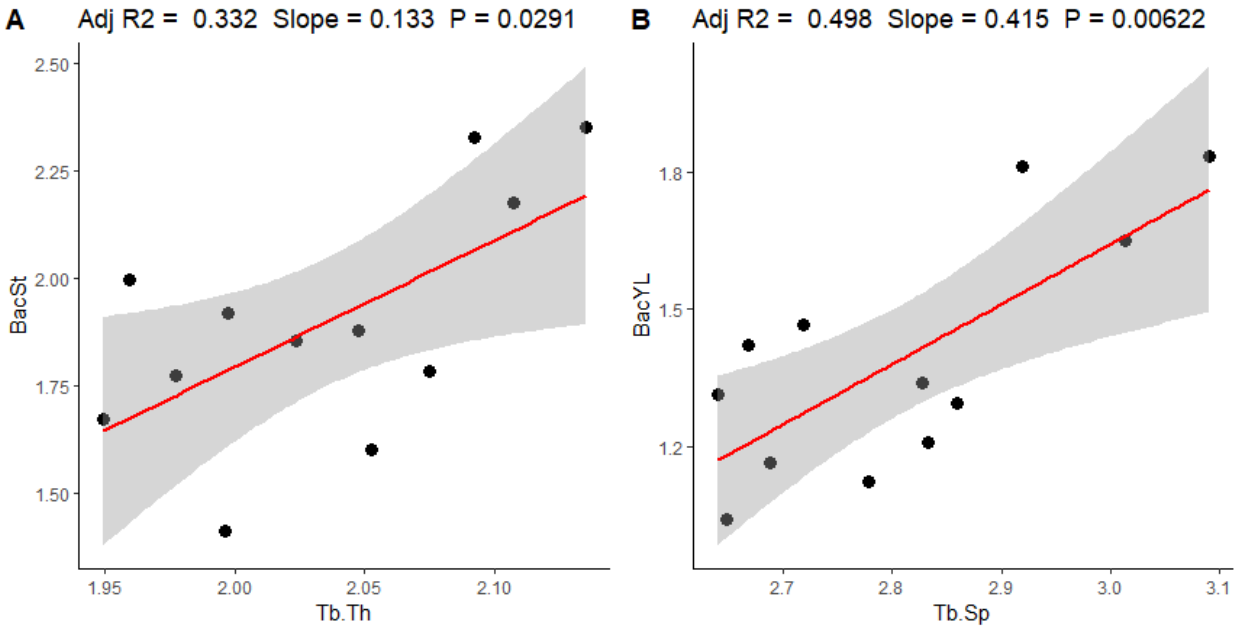

Figure 3.23: *Linear regressions between trabeculae properties and baculum metrics*. A. Trabeculae thickness and baculum stiffness; B. trabeculae spacing and baculum yield load.

3.6.4 Power Analysis

A power analysis was performed for the strongest regressions between bone metrics and trace elements to determine if the relationships were underpowered or not. It was also used to determine what minimum sample size would be needed to for a power above 0.80. To calculate the minimum sample size needed, the R^2 and p-values for each relationship were used. Based on power calculations, a minimum sample size of 20 would provide most significant relationships with enough power (Appendix F).

Chapter 4 – Discussion and Conclusion

Overview: *This chapter outlines the relationships between bone metrics and trace elements found in the mink with respect to their potentiality as biomarkers of pollutant exposure. It describes the strengths and limitations of this research, as well as what it contributes to environmental effects monitoring. Finally, it ends with suggestions for future directions of this work.*

4.1 Summary

This research was the first to evaluate mink bone for biomarkers of environmental pollutant exposure. Relative to other studies, this work was also the first to evaluate different bones and bone types of a bioindicator species within the same study. Both mechanical testing and imaging were performed, to quantify bone health metrics in two bones: the baculum and femur. The baculum is a reproductive bone and is not load-bearing, while the femur is a non-reproductive bone and is load bearing. In addition, cortical and cancellous bone types were assessed here. Obtaining this wide variety of bone health metrics presented insight into the differences between baculums and femurs within the context of evaluating them for biomarkers.

This study was able to demonstrate the ability of mink bone to reflect environmental levels of trace elements. Results indicate that baculums properties had stronger relationships with trace elements than femurs did. Selenium, rubidium, and iron had the strongest effects on both bones, affecting different structural and material properties in each. These bone properties in relation to the trace elements they were affected by, offer the potential for implementation in biomonitoring

programs across Canada. The rationale behind this and its implications will be discussed further in this chapter.

4.2 Metabolism

The principal component analyses (PCA) illustrated that hepatosomatic index (HSI) was one of the largest contributors to variability in the data, as it was strongly correlated with several trace elements including: mercury, aluminum, barium, calcium, iron, potassium, sodium, strontium and selenium. The HSI is a measure of the energy reserves for an animal and is reflective of an animal's metabolism. For aquatic species, the presence of trace elements has been associated with increased HSI and liver weight (Antony Jesu Prabhu *et al.*, 2016; Dane and Sisman, 2020). For terrestrial mammals, there is little in the literature about how HSI may influence metabolism of trace elements. Furthermore, certain trace elements will accumulate in the liver more than others. The HSI also varies largely depending on many biological and environmental factors including season, food availability, food quality, age, sex, and environmental stressors (Tête *et al.*, 2013). Therefore, the HSI could not be used as an indicator of anything related to bone health or trace element exposure without additional information on the mink.

4.3 Geometry

Baculum structural properties were heavily dependent upon bone dimensions. This was expected, as bone geometry is intrinsic to structural properties. For example, increased superior-inferior diameter strongly influenced the peak load values. As the baculums were bent in the superior-inferior direction, this dimension strongly influenced the peak load the baculums could reach in bending. Also, baculum weight was strongly correlated with stiffness. This positive

correlation could be the result of either increased bone density or cross-sectional area. Other similar relationships existed as well and can be identified on the first correlation matrix, including positive correlations between bodyweight and bone geometry.

Like baculums, femur weight and dimensions had the largest influence on bone structural properties, due to the dependence of these properties on bone size. Positive correlations between femur dimensions, bodyweight and structural properties were observed, as larger bone geometry demonstrates greater resistance to stress, exhibiting higher peak loads (Hart *et al.*, 2017b). Overall, these relationships indicate that larger bones have greater structural properties. This could potentially be due to age, as adult minks will be larger than adolescent minks. However, the ages of the mink in this work were not available at the time of writing.

Inverse relationships between yield stress and femur dimensions were also observed. This was contrary to what would typically be observed for femur material properties, suggesting that the calculations were invalid. To calculate the material properties, linear beam theory was applied (Timoshenko, 1953). This theory makes many assumptions about the beam subject to bending including: the aspect ratio must be at least 10:1, the beam has uniform shape and density across the span and the material is linearly elastic (Timoshenko, 1953). Moreover, three-point bend calculations associated with beam theory assume the beam is in pure bending, which means that the top of the beam is in pure tension and the underside is in pure compression. Stress calculations depend upon this assumption. If these requirements are not met for the beam, then not all the load the beam is subjected to is taken by the normal bending stress. Some is taken by the shear stress. So, for larger specimens with greater second moments of area, more load is taken by shear stress. Femurs did not meet any of the linear beam theory assumptions, so stress

calculations for relatively larger femurs were not accurate. Baculums did meet the requirement for a 10:1 aspect ratio, but no other assumptions.

The cancellous bone of femurs was assessed and positive correlations between trabeculae connectivity, femur length and peak load were observed. Besides femur length, there was no relationship between connectivity and any other geometric property. Increased connectivity means there are more trabeculae in the structure, which is expected for longer bones as there is greater bone volume that can contain the cancellous structures. Generally, more bone remodeling occurs at cancellous bone sites due to the increase in bone surface area. As a result, changes in bone remodeling rates are first observed here. The positive relationship between connectivity and peak load may therefore indicate that for bones with greater bone formation, there was increased tolerance to load.

Baculums and femurs exhibited similar relationships with trace element concentrations, but there were more relationships between baculum metrics and trace elements. This suggests that the influence of trace elements may not have been sufficient to observe significant effects in the femurs. This could potentially be due to the difference in size, or the difference in their general functions in the body.

Bone growth is influenced by many factors including sex hormones, diet, stress and more. Femurs have an adaptive response to load, whereby strains experienced within the ECM stimulate intracellular signaling to promote bone growth (Huiskes *et al.*, 2000). In the absence of loading, bone resorption can surpass bone formation, leading to bone loss (Lanyon and Skerry, 2001). Moreover, one of the primary functions of load-bearing bones is to provide structural support. Baculums only have reproductive purposes, so they do not undergo loading; their growth throughout life is primarily due to endocrine signalling by androgens and growth

hormones (Lyons, Abernathy and Gropper, 1950; Nasoori, 2020). Due to these differences, changes or disruptions in endocrine homeostasis may first be observed at the baculum and not the femur, especially if androgens were disrupted. Thus, these findings may mean that load-bearing properties dominated the loading response for femurs but not baculums.

4.4 Calcium and Iron

The correlations between increasing calcium and decreasing yield stress and bending modulus in the baculums could have been caused by elevated calcium blood serum levels, but as previously discussed, the stress calculations may be invalid.

In addition, baculum work-to-failure increased with increasing calcium levels. This indicates that the baculums from mink with high calcium blood serum levels may have been more ductile. Elevated blood calcium serum levels can be influenced by many factors, but in the absence of increased levels of calcium ingestion it could be caused by resorption of bone mineral. As calcium levels in the body are regulated through endocrine-feedback mechanisms primarily involving calcitriol and parathyroid hormone (PTH), the weakened bone metrics indicate that more bone resorption was occurring at the baculum, removing calcium from the hydroxyapatite (Ilich and Kerstetter, 2000). As a result, the baculums became more ductile as more mineral was removed and blood calcium levels increased. There are many reasons as to why more bone resorption could have been occurring and the exact reason here cannot be known without more information on the mink biology and environment.

The relationship between work-to-failure and calcium levels may have also been due to increased loads experienced by baculums as well, but there were no relationships between peak

or yield load and work-to-failure to indicate this. However, to rule out this possibility, a larger sample size would have been needed.

Conversely, femur metrics had no correlations with calcium levels. One explanation could be that because femurs are larger, reductions in calcium within the ECM were not great enough to observe through mechanical testing or imaging. Another possibility may be that because femurs are load-bearing there was less calcium removal at femur sites than the baculums. This also further indicates that the femur's load-bearing properties dominated the loading response.

Iron is closely linked with bone maintenance and in general iron overload can result in bone loss (Zofková, Nemcikova and Matucha, 2013). Seeing as iron levels increased with increasing material properties in the baculums, this could potentially mean that when the calcium levels were low, iron uptake was increased as there was less competition for uptake in the intestinal tract (Ilich and Kerstetter, 2000). This has been demonstrated in previous studies in which rats were fed calcium and iron deficient diets (Ilich and Kerstetter, 2000; Medeiros *et al.*, 2002). These rats exhibited reduced BMD and cortical bone area when fed iron-deficient diets, and this effect was increased for those rats with combined calcium and iron-deficient diets (Medeiros *et al.*, 2002). Thomas *et al.* (2021) also found that iron was positively correlated with otter baculum work-to-failure.

In addition to the positive influence of iron on bone, at excessive levels it may have detrimental effects. A clinical study found that patients with iron toxicity had increased osteoclast activity and dysfunctional osteoblast activity (Skordis and Toumba, 2011). Furthermore, *in vivo* and *in vitro* studies have demonstrated that iron overload stimulates osteoclast differentiation and inhibits the growth of hydroxyapatite (Mandalunis and Ubios, 2005; Guggenbuhl *et al.*, 2008). Overall, a balance of iron and calcium are needed for healthy bone.

Baculums and femurs had different relationships with iron. The increase in baculum material properties was not accompanied by increased femur yield stress. However, the femurs did demonstrate increasing structural properties with increasing iron levels. For baculums, the inverse relationship observed between iron and calcium here means that the increased calcium levels accompanied by reduced modulus and yield stress were also accompanied by reduced iron levels. Similarly, high iron levels were accompanied by greater modulus and yield stress in the baculums, but also low calcium levels, perhaps suggesting a retention in calcium in the bone. This points to the combined positive effects of iron and calcium on bone growth and that without both, bone health declines. This suggests that the iron levels in the mink may not have been at levels high enough to induce serious bone loss but may have been within a healthy range as evidenced by increasing material properties. At this point these relationships are only theoretical, as the material properties are rough estimates and the linear beam theory upon which they were based did not hold. They should be considered lightly, and further investigation into correcting/modifying the material property calculations should be done.

In femurs, the increasing yield load and increasing second moment of area may indicate that as the cross-sectional area increases, so does yield load. This relationship is also found in the early stages of bone disease such as osteoporosis, as bone diameter will increase to accommodate the reduction in bone density (Lanyon and Skerry, 2001). The decline in yield stress may further point to this, as it could mean that bone density was declining in the mink femurs, but without other information like BMD values this is not strongly substantiated. Furthermore, as stiffness is a structural property dependent on bone diameter, the increase in stiffness with iron concentration also supports the observed increase in the second moment of areas and yield load.

Overall, these findings suggest that iron may have had a net positive effect on baculums and femurs, but more information and further study will need to be done to elucidate this. Relationships between iron levels and baculum and femur material properties should be considered cautiously, due to the inaccuracy of the bending material property calculations as discussed previously. Potentially there may have been another causative factor that caused iron levels to drop and increased calcium resorption to occur.

4.5 Lead

Increased lead levels were associated with decreased work-to-failure values in baculums, but this was the only relationship present. Previous studies have demonstrated that lead has negative effects on bone by decreasing cortical width and bone density (Wong *et al.*, 2015). In children, lead causes a decrease in skeletal growth (González-Riola *et al.*, 1997). As there was no relationship between lead and bone geometry in the mink, lead levels may not have been high enough to induce these bone metrics. In fact, the decrease in work-to-failure indicates that with increasing lead levels in the mink, the bones became increasingly brittle. However, there may not have been enough range in the lead levels to observe other relationships with bone metrics.

Lead often deposits in bone as it can displace calcium in the extracellular matrix (ECM) (Rodríguez and Mandalunis, 2018). It also displaces other divalent cations including iron, magnesium and sodium (Lidsky and Schneider, 2003; Flora, Gupta and Tiwari, 2012). However, most clinical and *in vivo* studies investigating the effects of lead on bone health have demonstrated its function as an endocrine disruptor, whereby it inhibits calcium and phosphorous metabolism, disrupts absorption of calcitriol, decreases vitamin D and decreases PTH. This results in reduced BMD and delayed fracture healing (Carmouche *et al.*, 2005; Dongre *et al.*,

2013; Rodríguez and Mandalunis, 2018). Moreover, it is for these reasons that lead can cause hypocalcaemia (Dongre *et al.*, 2013). As lead was not related to any other baculum metric here, this likely means that lead levels in the mink were not high enough to significantly induce bone loss. However, the increase in work-to-failure combined with the increased calcium levels suggests that lead may have been displacing calcium in the ECM.

4.6 Aluminum

Aluminum concentration was positively correlated with work-to-failure. This could potentially indicate a reduction in the bone mineral content, as this increase in work-to-failure means the bones were becoming increasingly ductile. Previous *in vivo* and clinical studies investigating aluminum in bone have demonstrated its ability to reduce BMD and the number of osteoblasts, causing aluminum-induced bone diseases (Yang *et al.*, 2018; Souza-Monteiro *et al.*, 2021). The correlation with aluminum and work-to-failure supports the literature with respect to reducing bone mineral content, but this was the only relationship between aluminum and bone metrics in the baculums.

In the femurs, increased aluminum levels were associated with decreased trabeculae thickness. Aluminum has been demonstrated to damage the cancellous bone structure as it is primarily deposited in the bone mineral once absorbed and can inhibit calcium deposition in the ECM (Yang *et al.*, 2018; Souza-Monteiro *et al.*, 2021). In addition, aluminum has been demonstrated to deposit on trabeculae and induce bone loss at cancellous sites. More specifically, aluminum can interfere with osteoblast differentiation and prevent mineralization through inhibiting specific bone cell signaling pathways (Song *et al.*, 2017). This results in bone loss over extended periods of time, especially at cancellous bone sites (Li *et al.*, 2011).

These findings suggest that aluminum was not at high enough concentrations to induce more serious damage to the baculums, or that the duration of aluminum exposure was not long enough to observe long-term damage. If the latter option were true, this may be reflective of the age of the mink, as younger mink would have proportionately lower aluminum concentrations than older mink. These conclusions are further supported by the fact that there were no other relationships between aluminum and baculum and/or femur metrics.

4.7 Rubidium

There were many relationships between bone metrics and rubidium levels relative to other trace elements. Elevated rubidium concentration in the mink livers was associated with reduced structural properties in the baculums including superior-inferior diameter, second moment of area, peak load and work-to-failure. Furthermore, rubidium was inversely correlated with maximum bending moment, connectivity and weight of the femurs. These correlations suggest that rubidium concentration was related bone loss, but there is very little information on the direct effects of rubidium on bone or of rubidium as an endocrine disruptor.

Rubidium is primarily used in specialty glass for fiber optic cables and in photoelectric cells, and may be produced as a by-product during lithium and cesium extraction (Butterman and Reese, 2003). Thus, it is not a commonly discussed trace element when assessing pollutants from the oil mining industry or pulp and paper mills. However, it may be found in excess in potassium and lithium deposits, so it can be released into aquatic ecosystems through mining (Butterman and Reese, 2003).

Rubidium-doped hydroxyapatite has previously been explored as a biomaterial and was found to exhibit reduced material properties of relative to natural hydroxyapatite (Ahmed *et al.*, 2020).

However, the reasons for this have not been studied in detail. There is also evidence for stimulation of potassium excretion and replacement by rubidium, but there are no studies investigating this in the context of bone health or endocrine disruption (Beck *et al.*, 1988). Potassium has been shown to reduce the likelihood of osteoporosis as it increases calcium retention (Ha *et al.*, 2020). Therefore, potassium is an important element for maintaining bone mineralization. If rubidium stimulated potassium excretion, this could imply that calcium retention in the body was reduced, which subsequently led to the elevated calcium levels accompanied by reduced material properties and increased work-to-failure that were observed in those mink. Rubidium can also replace potassium in intracellular fluid (Glendening, Schrenk and Parrish, 1956). At high levels this can lead to decreased overall growth.

With respect to reproductive health, rubidium has demonstrated a negative effect on sperm production and testicular weight. It may also cause reproductive toxicity in catfish (Yamaguchi *et al.*, 2007). These suggest that rubidium may have been able to disrupt sex hormones or sex organ functionality of the mink, but this cannot be confirmed in this present study.

Another explanation for the observed relationships with rubidium is that its presence in the local environment could have been directly accompanied by the presence of another trace element or persistent organic pollutant (POP) with harmful effects on bone health. Based on the results here, rubidium was only correlated with one other element, which was cadmium. Cadmium has been previously identified as a prominent endocrine disruptor with known detrimental effects on bone health (Kazantzis, 2004). However, there was no relationship observed between cadmium and any baculum metrics here. Ultimately, these relationships with rubidium are novel and should be investigated further to determine if there is in fact a significant relationship among them.

4.8 Selenium

Selenium had the strongest relationships with baculum metrics, demonstrating inverse relationships with baculum weight, peak load, stiffness, yield load and mink bodyweight. Selenium is bioaccumulative and typically has been documented as having a positive influence on bone health (Santos *et al.*, 2015). In post-menopausal women, selenium treatment was positively correlated with BMD and inversely correlated with bone remodeling turnover (Wu *et al.*, 2021). This was because in humans at least, osteoblasts exhibit a minimum of nine selenoproteins (Wu *et al.*, 2021). These are proteins containing selenium that help to reduce the amount of reactive oxygen species (ROS). Reactive oxygen species play an important role in osteoporosis pathogenesis by increasing osteoclast formation, inhibiting osteoblast differentiation and increasing osteoblast and osteoclast apoptosis(Domazetovic *et al.*, 2017; Wu *et al.*, 2021). Selenoproteins also play roles in thyroid hormone synthesis, sperm production and fertility (Köhrle *et al.*, 2005). As the synthesis of selenoproteins depends on selenium intake, the presence of selenium helps to mediate osteoclast formation, thereby improving BMD and bone growth by behaving as a type of antioxidant (Zeng, Cao and Combs Jr, 2013). Selenium is also found in bone, but not significantly relative to other organs (Zachara *et al.*, 2001).

Although selenium is a key element involved in antioxidant production, at excess levels it has the opposite effect. A study by Turan et al. (1999) fed rats selenium-deficient and selenium-excess diets and noted reductions in biomechanical properties among both groups accompanied by reductions in crystallinity of the ECM (Turan *et al.*, 2000). Moreover, another study investigating selenium toxicity in fish found that selenium toxicity was linked to skeletal abnormalities (Lemly, 2014). A study investigating birds on a coal mine-affected stream in Alberta noted selenium levels were elevated in eggshells and may have reached ecotoxicological

effects, but they did not investigate any biological effects (Wayland, Kneteman and Crosley, 2006). The influence of selenium on aquatic organisms and aquatic birds has also been demonstrated, whereby studies have found increased mortality, reduced fertility, reduced offspring survival and reduced bodyweight (Hoffman, Heinz and Krynitsky, 1989; Hoffman *et al.*, 1992; Hoffman, 2002). Another study by Hoffman found reductions in alkaline phosphase activity in relation to reduced bone growth for ducklings with selenium toxicity (Hoffman *et al.*, 1992). This was attributed in part due to the oxidative stress caused by increased selenium.

Mining processes have been shown to release selenium into aquatic environments, therefore it is plausible that environmental selenium levels were relatively high in the aquatic environments to which the mink were exposed (Santos *et al.*, 2015). In addition, selenium concentrations are highest in animal products with high protein, which can be attributed to selenium's ability to bioaccumulate. Given that mink are opportunistic carnivores, high levels of selenium in the environment could be reflected in mink. Selenium also had no relationship with liver weight or any other trace elements. Therefore, the reductions in baculum structural properties could have been caused by selenium toxicity. The reductions in bone weight, bodyweight and structural properties all indicate that there was bone loss occurring for mink with greater selenium concentrations. Based on these previous studies, this effect of selenium may have the potential to disrupt reproductive health as well. This warrants further research into the effects of selenium on bone biomechanical properties.

There is potential for selenium to mitigate mercury toxicity and bioaccumulation in organisms, exhibiting protective effects on species growth (Peterson *et al.*, 2009). The two elements are mutually antagonistic, inhibiting toxicity of one another. While mercury is a prominent element found near oil mining activity, there was no observed effect in this research of mercury on bone

metrics and there were no observations supporting a relationship between mercury and selenium. The potential mitigation of mercury should not be ruled out, as element levels may not have been high enough to induce observable changes.

Unlike baculums, selenium had no relationships with femur bending structural properties, but was positively correlated with yield stress and negatively correlated with anterior-posterior diameter. The decrease in diameter would support the findings for baculums in which selenium inhibited bone growth. Moreover, the inverse relationship between yield stress and femur diameters as discussed previously would align with this finding. This would indicate that reductions in femur diameter are also accompanied by increased yield stress. Overall, there is not enough literature to identify the exact mechanism of action of selenium on femurs here, so it should be further investigated.

4.9 Sodium

Sodium was positively correlated with bending modulus and yield stress for baculums. These relationships need to be considered with caution due to the inaccuracies with bending calculations.

In general, the literature on the influence of sodium on bone health is conflicting. Previous studies have demonstrated sodium to have a small protective effect on bone in human males but not females (Greendale *et al.*, 1994; Carbone *et al.*, 2016). However, other studies have demonstrated that sodium intake has a negative effect on bone density and other biomechanical properties, as it depresses bone formation in young and adult rats and humans (Hernandez and Keaveny, 2006; Lu *et al.*, 2011). These effects are primarily observed in cancellous bone where

there is high bone turnover and less so in cortical bone. This relationship exists because generally sodium increases calcium excretion, which is correlated with reduced BMD.

In humans, there is a slight increase in total body BMD associated with increased sodium intake (Carbone *et al.*, 2016). However, sodium intake does not significantly increase the likelihood of osteoporosis, which is characterized by low BMD. Ultimately, there is not enough clear evidence in the literature to support sodium having a positive effect on bone health. Furthermore, the inaccuracies with the bending calculations were likely what contributed most to these findings.

4.10 Magnesium

Magnesium is deposited in the ECM and its release into the bloodstream generally follows bone resorption (Wedig *et al.*, 2006). Typically, low magnesium levels promote osteoporosis, reducing mechanical properties and causing brittle fracture and reductions in bone growth (Boskey *et al.*, 1992; Wedig *et al.*, 2006). One cause of this is the increased osteoclast activity that occurs to alleviate magnesium from the ECM to compensate for low concentrations of it in the body (Boskey *et al.*, 1992). Boskey et al. (1992) examined the effects of magnesium-deficient diets on rats, and tested rat femurs in three-point bending. They found a significant decrease in bone strength, but no significant differences in any other bone mechanical properties. Magnesium toxicity may have similar effects, as it can decrease bone density and compete with calcium for ECM deposition (Wedig *et al.*, 2006).

Here, magnesium had no influence on any bone metric except for connectivity density, as decreasing connectivity density was associated with increased magnesium concentrations. Whether this was caused by magnesium deficiency or toxicity is inconclusive, however the absence of any other relationships between magnesium and bone metrics suggests that any

influence of magnesium on the femur cancellous bone is small. Moreover, the potential influence of magnesium on trabeculae is relatively small, which could potentially be a reflection of magnesium levels in the environment or mink age.

Other Elements

No other elements demonstrated relationships with baculum or femur metrics in this study. This was contrary to another very similar study that found relationships between otter baculum structural properties and strontium, cadmium and tellurium (Thomas *et al.*, 2021). This study collected otters from regions across Alberta and evaluated their baculum biomechanical properties. They found that BMD was negatively correlated with cadmium and tellurium concentrations in the otter livers, indicating that these elements had negative effects on bone health. In addition, peak load was positively correlated with strontium concentrations.

Otters and mink are similar in that they are both subaquatic apex predators with localized home ranges. However, otters have larger home ranges than mink. Unfortunately, there was no information on the mink location at the time of writing, so no comparison between the mink and otter locations could be made to determine whether the discrepancy between trace element effects was due to differences in the distribution of trace elements geographically. The differences between findings may have been due to locational differences but may have also been due to age differences. Generally, older animals will have bioaccumulated greater concentrations of toxins, so long-term effects of trace element exposure can be observed. Thomas *et al.* (2021) did not compare trace element effects between young versus older otters, and only considered older otters for statistical analyses. If the mink in this study were younger, potentially only short-term effects of trace elements on bone health would have been observed.

These effects would have been different and more likely to have been weaker than those effects observed by Thomas *et al*.

4.11 Power Analysis

The power analysis revealed that this study was underpowered with a sample size of 17 for femur bone metrics and 12 for baculum metrics. However, the sample size needed to adequately power the study was a maximum of 23 specimens (for selenium and rubidium effects) and a minimum of 17 (for iron effects). Therefore, increasing the sample size to 23 is the next step for future testing and should be performed to confirm whether selenium toxicity was occurring for these mink.

4.12 Limitations

While this work was able to identify relationships between mink bone properties and trace element concentration levels in their livers, there were shortcomings that affected the data.

Bone health is affected by a wide variety of factors that extend beyond toxin exposure, including diet, age and genetics. As such, bone measures among individuals will generally always have high variability. To overcome this variability, the sample size should have been increased. Eighteen is considered a very small sample size in this field, especially when looking at cumulative effects of compounds on bone health. At a minimum, there should have been at least 30 mink samples. This would have allowed more in-depth statistical analyses to be performed, such as a multivariate analysis or stepwise regression to investigate cumulative effects of trace elements on bones. Increasing the sample size as well as the proportion of male and female mink would have allowed sex differences to be examined. As previously discussed, toxins have

differing effects on male and female bone health. Due to the small sample size in this study, females and males could not be analyzed individually to account for any potential differences in trace element effects. In addition, increasing the number of locations from which the mink were collected would have allowed for a comparative study to investigate geographical differences in trace element distributions, and whether this was reflected in the mink bone metrics. However, this does not mean that this study was invalid. Despite the small sample size, relationships that support the literature were still identified. In addition, this work has laid the groundwork for selecting a bone biomarker of pollutant exposure in mink. All techniques and basis for the tests were developed here and may implemented in future work.

There was also limited information on the mink. Age, home ranges, exact trapping date and diet could not be provided for any of mink. These factors play an enormous role in bone development and in the trace element exposure levels. For instance, without locational data (their home ranges are 1-5km in diameter), the source of trace elements could not be identified and confirmed with concentrations in the mink. The trapping data would have also been important, as seasonal changes affect weather and terrain that would influence the exposure of mink to certain elements. While temperatures during the trapping season ensuring freezing of the carcass upon trapping, scavengers may have left some carcasses in poor conditions (*e.g.*, for those male mink missing baculums). Age is another important factor as it strongly influences the size of bones. Finally, the proportion of male to female mink was not balanced enough to warrant investigation into sex differences. Sex is important to consider as it strongly influences bone size. As well, sex hormones influence bone growth differently in male and female mammals and exists in different proportions in both.

Additionally, this study was somewhat limited in the type of toxins it examined. Many other POPs such as polychlorinated biphenyls (PCBs) and polycyclic aromatic compounds (PAHs) have known detrimental effects on species health and are not naturally found in the environment. Thus, any detection of non-naturally occurring POPs would be indicative of anthropogenic activities affecting the minks. This could have then been compared to bone health to investigate whether the presence of POPs has negative effects on bone health in particular. There is also evidence of the influence of POPs on bone health (Sonne, 2010; Daugaard-Petersen, Langebæk, Frank F. Rigét, *et al.*, 2018; Thomas *et al.*, 2021). Trace elements differ in that they are naturally occurring and are necessary in small amounts for healthy bone development, so anthropogenic activity may not always be the reason for elevated trace element exposure. Overall, incorporating POPs would have allowed this study to be more well-rounded.

There were also limitations in the experimental design. To begin, not all femurs were tested at the same bending span due to the differing sample shipments. The span changes the measured bone properties, as it changes the length of bone subject to bending. In addition, some femurs were mechanically tested before µCT, and some after. This may have caused drying in the femurs, as scan times were long. This may have predisposed them to brittle failure, but this was not checked or confirmed.

Additionally, a beam in bending must meet specific requirements for accurate measurement of its properties according to the ATSM D790 standard (Yalcin, 2018). These bones did not meet all requirements (*e.g.*, a support span-to-depth ratio of 10:1), so measurement of their structural properties should only be examined for relative differences and should not be taken as accurate measurements. As previously discussed, for the calculations of the properties of bones in bending, linear beam theory was used. However, this theory makes several assumptions about

the beam subjected to bending that did not hold for these bones. More specifically, these bones did not meet the support span-to-depth ratio of 10:1. As a result, bones with larger cross-sections had more of the load taken by shear stresses than normal stress. Linear beam theory assumes that all the stress experienced by the specimen in bending is normal bending stress. However, because this was not true for the bones in this study, the calculations for bones with larger cross-sections (experiencing greater shear stresses) would have calculated reduced material properties. This also means that the calculations for bones with relatively smaller cross-sections overestimated material properties. Therefore, material properties of the baculums and femurs in this study should be considered with caution and not be taken as concrete evidence of trace element effects. The calculations of material properties should be revisited and readjusted to account for these assumptions that were not met. Furthermore, bone is not linearly elastic in its plastic deformation region, so calculations of ultimate stress were inaccurate and should be discarded from comparison of bone metrics in this study.

The ability to accurately measure the diaphysis cross-sectional area was also limited. This was because there was not enough time to obtain images of the mid-diaphysis for all bones. So, the diameter was measured and the second moment of area calculated assuming an ellipse shape for femurs and a solid triangle for baculums. This is not as accurate as a μCT scan and cannot consider the individual geometry of every bone. As a result of all these above factors, the material properties should be considered with some degree of caution. However, because all properties were collected in the same way, they can be compared to investigate relative differences among them, which fits well within the scope of this research.

Image analysis also had some sources of error. Analysis of the trabecular structure was limited to the abilities of BoneJ, so the ROI encompassing cancellous bone could not include all trabeculae

in the entire stack. This also introduced a source of error as the ROI was hand-picked every time. However, it was always performed by the same person for increased consistency. The distal end of the femur also demonstrated a reduction in trabeculae towards the interior of each cross-sectional image, observed as a sort of hole. This offset all spacing measurements, increasing the mean and standard deviation (SD). Thus, these values may have been influenced by the size of this hole as opposed to the spacing between trabeculae towards the outer edges of the bone. However, this is the nature of analyzing small bones. Despite these shortcomings, image analysis of the cancellous structure was completed in the same manner for every bone, so comparison of the relative values among mink specimens could be completed.

Overall, results from this study should be taken with a degree of caution due to the limitations and sources of error. Structural properties of the baculums and femurs as well as the cancellous bone properties should only be considered within the context of this research and should not be taken as absolute measurements. They were successfully able to identify differing effects of trace elements on bone health and may be considered as indicators of trace element influence on mink skeletal health. However, material properties for baculums and femurs in bending should be revisited and should not be considered as strong indicators of trace element effects. The techniques used in this study may be used for future evaluation of mink skeletal health within the context of environmental toxin exposure and provide an excellent baseline for future work.

4.13 Impact

There are many studies investigating the influence of POPs on bone health in bioindicator species. Thomas *et al.* (2021) found that otter baculum peak load was most strongly influenced by cadmium and tellurium concentrations. This study also used three-point bending to evaluate

baculum mechanical properties, quantified similar structural properties and looked at otters from Alberta. Comparatively, this research also evaluated the same structural properties of the baculum as this study, except for BMD. The peak load of femurs was also influenced by trace element concentrations, as were baculum structural properties. However, the same trace elements (cadmium and tellurium) were not detected in the mink at relevant concentrations. Some expected relationships were also not present that were identified in this study, but there was no way to control for which elements the mink were exposed to. Furthermore, they did not investigate any material properties or look at femurs. Dauugard-Petersen et al. (2018) looked at baculums of polar bears and found reduced BMD for those polar bears exposed to elevated levels of POPs but did not consider trace elements or biomechanical bone properties. While these studies investigated the relationships between bone and POPs, they did not investigate multiple bone types or assess cancellous bone structures. The American mink is also much more widespread across North America than either the otter or polar bear, so for the purpose of developing a biomarker of pollution exposure, mink are better suited.

Therefore, this research provides the techniques and testing methods necessary for identifying a bone biomarker of pollutant exposure to be implemented in environmental effects monitoring (EEM) programs. These are studies carried out by industries to evaluate the effects of pollutants on fish and aquatic ecosystems to protect them (Government of Canada, 2021). They require regular evaluation of the environment surrounding facilities to ensure that they are complying with existing regulations, and to monitor effects on surrounding ecosystems. They are detailed and comprehensive, defining what is meant by an effect, how to determine whether there is an effect, how/if this effect is related to the pollution produced by the facility under evaluation, and how to determine if this effect is due to a particular stressor (Hewitt *et al.*, 2003). As this

research demonstrates the effects of trace elements on bone health metrics in mink, combined with population monitoring of mink it may be used as a baseline for measuring whether facilities are affecting terrestrial and aquatic wildlife. Thus, this research was an important first step towards the development of EEM programs of oil sands mining and pulp and paper mills in Canada.

4.14 Future Directions

This research sets the groundwork for future identification of a bone biomarker. Relationships between bone metrics and trace elements were identified that support the literature, which is indicative that trace elements may be affecting the bone health of mink nearby oil sands and pulp and paper mills. The presence of more novel and unexpected relationships also warrant further investigation.

Due to the small sample size, variability in the data, and the inability to control for factors such as age and location, relationships between bone metrics and trace elements that were present were not strong enough to confidently identify any definitive linear relationships, as the R^2 values were not above 0.8 (a relative threshold for determining the tightness of the linear fit). In fact, most were quite low. This could be overcome by increasing the sample size to 23 at least, or 30 to perform more in-depth analyses controlling for multiple factors. The incorporation of an increased number of locations evaluating multiple types of industry would also provide an excellent method of comparison for investigating effects of different compounds, and how these relate to the industries' effluent production.

Future work should also focus on reducing the variability in experimental methods. Diaphysis µCT scans should also be collected for accurate measurement of the second moment of area of

all long bones. It may also be beneficial to choose a cancellous site that is not influenced by the presence of a growth plate, such as a vertebra. Most importantly, BMD should be calculated as it can provide insight into the bone mineral content, which is crucial for the identification of changes in bone remodeling and mineralization.

Investigating other compounds in addition to trace elements would provide a well-rounded understanding of the presence of pollutants in the regions selected and how they may influence bone health. Sex differences could also be investigated, as endocrine disruptors have different effects on male versus female sex hormones. Finally, age is another crucial factor to consider to distinguish between young versus adult mink. Bone growth is regulated by different endocrines in young versus adult mink and controlling for age could aid in determining the effects of long- and short-term exposure to pollutants.

4.15 Conclusion

In summary, this research provides the groundwork for future work in developing a bone biomonitoring tool for EEM programs. It has presented the relationships between mink bone health metrics and trace element exposure levels from mink nearby oil sands mining and pulp and paper mill industries, providing insight into the pollutants that aquatic and terrestrial mammals are exposed to. This was the first study to evaluate mink bone as a biomarker of pollutant exposure using both mechanical testing and imaging techniques. It assessed cortical and cancellous bone of baculums and femurs, comparing the effects on reproductive and non-reproductive bones with different functionality. The results present unique findings unlike previous literature and are an excellent baseline for incorporation and consideration for EEM.

Future work should use these methods to identify the best bone biomarkers of POP exposure in mink, as they are a promising species for EEM programs in Canada.

References

Ahmad, S.U. *et al.* (2003) “Environmental pollutant Aroclor 1242 (PCB) disrupts reproduction in adult male rhesus monkeys (Macaca mulatta),” *Environmental Research*, 93(3), pp. 272–278. doi:https://doi.org/10.1016/S0013-9351(03)00110-5.

Ahmed, M.K. *et al.* (2020) “Physical and biological changes associated with the doping of carbonated hydroxyapatite/polycaprolactone core-shell nanofibers dually, with rubidium and selenite,” *Journal of Materials Research and Technology*, 9(3), pp. 3710–3723. doi:https://doi.org/10.1016/j.jmrt.2020.01.108.

Alfvén, T. *et al.* (2000) “Low-Level Cadmium Exposure and Osteoporosis,” *Journal of Bone and Mineral Research*, 15(8), pp. 1579–1586. doi:10.1359/jbmr.2000.15.8.1579.

Ali, M. and Sreekrishnan, T.R. (2001) “Aquatic toxicity from pulp and paper mill effluents: a review,” *Advances in Environmental Research*, 5(2), pp. 175–196. doi:10.1016/S1093-0191(00)00055-1.

Allen, E.W. (2008) “Process water treatment in Canada’s oil sands industry: I. Target pollutants and treatment objectives,” *Journal of Environmental Engineering and Science*, 7(2), pp. 123–138. doi:10.1139/S07-038.

Andersson, A.-M. *et al.* (2012) *The impacts of endocrine disrupters on wildlife, people and their environments - The Weybridge+15 (1996–2011) report*. doi:10.2800/41462.

Antony Jesu Prabhu, P. *et al.* (2016) “Responses in Micro-Mineral Metabolism in Rainbow Trout to Change in Dietary Ingredient Composition and Inclusion of a Micro-Mineral Premix,” *PLOS ONE*, 11(2), p. e0149378. Available at: https://doi.org/10.1371/journal.pone.0149378.

Arnold, M. *et al.* (2017) “Microindentation - a tool for measuring cortical bone stiffness? A systematic review,” *Bone & joint research*. 2017/09/18, 6(9), pp. 542–549. doi:10.1302/2046-3758.69.BJR-2016-0317.R2.

Atanassova, N. *et al.* (2000) “Comparative Effects of Neonatal Exposure of Male Rats to Potent and Weak (Environmental) Estrogens on Spermatogenesis at Puberty and the Relationship to Adult Testis Size and Fertility: Evidence for Stimulatory Effects of Low Estrogen Levels*,” *Endocrinology*, 141(10), pp. 3898–3907. doi:10.1210/endo.141.10.7723.

Aulerich, R.J. *et al.* (1971) “Effects of feeding coho salmon and other Great Lakes fish on mink reproduction.,” *Canadian journal of zoology*, 49(5), pp. 611–616. doi:10.1139/z71-098.

Aulerich, R.J. and Ringer, R.K. (1977) “Current status of PCB toxicity to mink, and effect on their reproduction,” *Archives of Environmental Contamination and Toxicology*, 6(1), pp. 279–292. doi:10.1007/BF02097769.

Baatrup, E. and Junge, M. (2001) “Antiandrogenic pesticides disrupt sexual characteristics in the adult male guppy Poecilia reticulata.,” *Environmental Health Perspectives*, 109(10), pp. 1063–1070. doi:10.1289/ehp.011091063.

Basu, N. *et al.* (2007) “Mink as a sentinel species in environmental health,” *Environmental Research*, 103(1), pp. 130–144. doi:10.1016/j.envres.2006.04.005.

Beck, F.X. *et al.* (1988) “Renal excretion of rubidium and potassium: an electron microprobe and clearance study.,” *Kidney international*, 34(4), pp. 455–462. doi:10.1038/ki.1988.202.

Beier, E.E. *et al.* (2013) “Heavy Metal Lead Exposure, Osteoporotic-like Phenotype in an Animal Model, and Depression of Wnt Signaling,” *Environmental Health Perspectives*, 121(1), pp. 97–104. doi:10.1289/ehp.1205374.

Betts, J.G. *et al.* (2013) *Anatomy and Physiology*. Houston, Texas: OpenStax. Available at: https://openstax.org/books/anatomy-and-physiology.

Boskey, A.L. *et al.* (1992) “Effect of short-term hypomagnesemia on the chemical and mechanical properties of rat bone,” *Journal of Orthopaedic Research*, 10(6), pp. 774–783. doi:10.1002/jor.1100100605.

Boutroy, S. *et al.* (2005) “In Vivo Assessment of Trabecular Bone Microarchitecture by High-Resolution Peripheral Quantitative Computed Tomography,” *The Journal of Clinical Endocrinology & Metabolism*, 90(12), pp. 6508–6515. doi:10.1210/jc.2005-1258.

Bouxsein, M.L. *et al.* (2010) “Guidelines for assessment of bone microstructure in rodents using micro–computed tomography,” *Journal of Bone and Mineral Research*, 25(7), pp. 1468–1486. doi:https://doi.org/10.1002/jbmr.141.

Brankovič, J. *et al.* (2019) “Lactational exposure to dioxin-like polychlorinated biphenyl 169 and nondioxin-like polychlorinated biphenyl 155: Effects on rat femur growth, biomechanics and mineral composition.,” *Ecotoxicology and environmental safety*, 180, pp. 106–113. doi:10.1016/j.ecoenv.2019.04.076.

Brezner, E., Terkel, J. and Perry, A.S. (1984) “The effect of Aroclor 1254 (PCB) on the physiology of reproduction in the female rat—I,” *Comparative Biochemistry and Physiology Part C: Comparative Pharmacology*, 77(1), pp. 65–70.

Brodziak-Dopierala, B. *et al.* (2009) “Interactions Between Concentrations of Chemical Elements in Human Femoral Heads,” *Archives of Environmental Contamination and Toxicology*, 57(1), pp. 203–210. doi:10.1007/s00244-008-9228-0.

Bursian, S.J. *et al.* (2013) “Dietary exposure of mink (Mustela vison) to fish from the upper Hudson River, New York, USA: Effects on organ mass and pathology,” *Environmental Toxicology and Chemistry*, 32(4), pp. 794–801. doi:10.1002/etc.2114.

Butterman, W.C. and Reese, R.G. (2003) “Mineral Commodity Profiles Rubidium,” *U.S. Geological Survey Open-File Report 03-045*, pp. 1–11. Available at: http://pubs.usgs.gov/of/2003/of03-045/of03-045.pdf.

Cao, J. *et al.* (2003) “Expression of RANKL and OPG Correlates With Age-Related Bone Loss in Male C57BL/6 Mice,” *Journal of Bone and Mineral Research*, 18(2), pp. 270–277. doi:https://doi.org/10.1359/jbmr.2003.18.2.270.

Carbone, L. *et al.* (2016) “Sodium Intake and Osteoporosis. Findings From the Women’s Health Initiative,” *The Journal of clinical endocrinology and metabolism*. 2016/02/10, 101(4), pp. 1414–1421. doi:10.1210/jc.2015-4017.

Carmouche, J.J. *et al.* (2005) “Lead exposure inhibits fracture healing and is associated with increased chondrogenesis, delay in cartilage mineralization, and a decrease in osteoprogenitor frequency,” *Environmental health perspectives*, 113(6), pp. 749–755.

Carter, D.R. and Hayes, W.C. (1977) “The compressive behavior of bone as a two-phase porous structure,” *Journal of Bone Joint Surgery*, 59, pp. 954–962.

CCME (2021) *Guidelines - Canadian Environmental Quality Guidelines (CEQGs) provide science-based goals for the quality of aquatic and terrestrial ecosystems.* Available at: https://ccme.ca/en/current-activities/canadian-environmental-quality-guidelines.

Chan, H.M. *et al.* (2003) “Impacts of mercury on freshwater fish-eating wildlife and humans,” *Human and Ecological Risk Assessment*, 9(4), pp. 867–883.

Christian, S. *et al.* (2004) “Is Bone Mineral Composition Disrupted by Organochlorines in East Greenland Polar Bears (Ursus maritimus)?,” *Environmental Health Perspectives*, 112(17), pp. 1711–1716. doi:10.1289/ehp.7293.

Colborn, T. and Clement, C. (1992) *Chemically-induced alterations in sexual and functional development: the wildlife/human connection*. Princeton Scientific Pub. Co.

Currey, J.D. (2012) “The structure and mechanics of bone,” *Journal of Materials Science*, 47(1), pp. 41–54. doi:10.1007/s10853-011-5914-9.

Dane, H. and Sisman, T. (2020) “Effects of heavy metal pollution on hepatosomatic index and vital organ histology in Alburnus mossulensis from Karasu River,” *Turkish Journal of Veterinary and Animal Sciences*, 44, pp. 607–617. doi:10.3906/vet-1904-50.

Daugaard-Petersen, T., Langebæk, R., Rigét, Frank F., *et al.* (2018) “Persistent organic pollutants and penile bone mineral density in East Greenland and Canadian polar bears (Ursus maritimus) during 1996–2015,” *Environment International*, 114(February), pp. 212–218. doi:10.1016/j.envint.2018.02.022.

Daugaard-Petersen, T., Langebæk, R., Rigét, Frank F, *et al.* (2018) “Persistent organic pollutants, skull size and bone density of polar bears (Ursus maritimus) from East Greenland 1892–2015 and Svalbard 1964–2004,” *Environmental Research*, 162(Complete), pp. 74–80. doi:10.1016/j.envres.2017.12.009.

Domazetovic, V. *et al.* (2017) “Oxidative stress in bone remodeling: role of antioxidants,” *Clinical cases in mineral and bone metabolism : the official journal of the Italian Society of*

Osteoporosis, Mineral Metabolism, and Skeletal Diseases. 2017/10/25, 14(2), pp. 209–216. doi:10.11138/ccmbm/2017.14.1.209.

Dongre, N.N. *et al.* (2013) "Biochemical effects of lead exposure on battery manufacture workers with reference to blood pressure, calcium metabolism and bone mineral density," *Indian journal of clinical biochemistry : IJCB*. 2012/07/27, 28(1), pp. 65–70. doi:10.1007/s12291-012-0241-8.

Doube, M. *et al.* (2010) "BoneJ: Free and extensible bone image analysis in ImageJ," *Bone*, 47(6), pp. 1076–1079. doi:https://doi.org/10.1016/j.bone.2010.08.023.

Elefteriou, F. (2008) "Regulation of bone remodeling by the central and peripheral nervous system," *Archives of Biochemistry and Biophysics*, 473(2), pp. 231–236. doi:10.1016/j.abb.2008.03.016.

Ethier, C.R. and Simmons, C.A. (2007) *Introductory biomechanics: from cells to organisms*. Cambridge University Press.

Flora, G., Gupta, D. and Tiwari, A. (2012) "Toxicity of lead: a review with recent updates," *Interdisciplinary toxicology*, 5(2), p. 47.

Fox, G.A. (2001) "Effects of endocrine disrupting chemicals on wildlife in Canada: Past, present and future," *Water Quality Research Journal of Canada*, 36(2), pp. 233–251. doi:10.2166/wqrj.2001.014.

Glendening, B.L., Schrenk, W.G. and Parrish, D.B. (1956) "Effects of Rubidium in Purified Diets Fed Rats," *The Journal of Nutrition*, 60(4), pp. 563–579. doi:10.1093/jn/60.4.563.

González-Riola, J. *et al.* (1997) "Effect of Lead on Bone and Cartilage in Sexually Mature Rats: A Morphometric and Histomorphometry Study," *Environmental Research*, 74(1), pp. 91–93. doi:https://doi.org/10.1006/enrs.1997.3760.

Gosselin, P. *et al.* (2010) "Environmental and Health Impacts of Canada's Oil Sands Industry; Royal Society of Canada: Ottawa, Ontario, Canada, 2010," *The Royal Society of Canada, Ottawa, ON, Canada* [Preprint].

Government of Canada (2021) *Environmental Effects Monitoring*. Available at: https://www.canada.ca/en/environment-climate-change/services/managing-pollution/environmental-effects-monitoring.html.

Goyer, R.A. (1997) "TOXIC AND ESSENTIAL METAL INTERACTIONS," *Annual Review of Nutrition*, 17(1), pp. 37–50. doi:10.1146/annurev.nutr.17.1.37.

Greendale, G.A. *et al.* (1994) "Dietary Sodium and Bone Mineral Density: Results of a 16-Year Follow-up Study," *Journal of the American Geriatrics Society*, 42(10), pp. 1050–1055. doi:https://doi.org/10.1111/j.1532-5415.1994.tb06208.x.

Guggenbuhl, P. *et al.* (2008) "Iron inhibits hydroxyapatite crystal growth in vitro," *Metabolism*, 57(7), pp. 903–910.

Ha, J. *et al.* (2020) “The association of potassium intake with bone mineral density and the prevalence of osteoporosis among older Korean adults,” *Nutrition research and practice*. 2020/01/21, 14(1), pp. 55–61. doi:10.4162/nrp.2020.14.1.55.

Hart, N.H. *et al.* (2017a) “Mechanical basis of bone strength: influence of bone material, bone structure and muscle action,” *Journal of musculoskeletal & neuronal interactions*, 17(3), pp. 114–139. Available at: https://pubmed.ncbi.nlm.nih.gov/28860414.

Hart, N.H. *et al.* (2017b) “Mechanical basis of bone strength: influence of bone material, bone structure and muscle action,” *Journal of musculoskeletal & neuronal interactions*, 17(3), pp. 114–139. Available at: https://pubmed.ncbi.nlm.nih.gov/28860414.

Headley, J. v *et al.* (2001) “Preliminary characterization and source assessment of PAHs in tributary sediments of the Athabasca River, Canada,” *Environmental Forensics*, 2(4), pp. 335–345. doi:https://doi.org/10.1006/enfo.2001.0064.

Heaton, S. *et al.* (1995) “Dietary exposure of mink to carp from Saginaw Bay, Michigan. 1. Effects on reproduction and survival, and the potential risks to wild mink populations,” *Archives of Environmental Contamination and Toxicology*, 28(3), pp. 334–343. doi:10.1007/BF00213111.

Hernandez, C.J. and Keaveny, T.M. (2006) “A biomechanical perspective on bone quality,” *Bone*, 39(6), pp. 1173–1181. doi:10.1016/j.bone.2006.06.001.

Hernández-Gil, F.-T.I. *et al.* (2004) “Physiological bases of bone regeneration II. The remodeling process,” *Medicina Oral, Patología Oral y Cirugía Bucal (Internet)*, 11(2), pp. 151–157. Available at: http://scielo.isciii.es/scielo.php?script=sci_arttext&pid=S1698-69462006000200012.

Hewitt, L.M. *et al.* (2003) “A Proposed Framework for Investigation of Cause for Environmental Effects Monitoring,” *Human and Ecological Risk Assessment: An International Journal*, 9(1), pp. 195–211. doi:10.1080/713609859.

Hoffman, D.J. *et al.* (1992) “Interactive effects of selenium, methionine, and dietary protein on survival, growth, and physiology in mallard ducklings,” *Archives of Environmental Contamination and Toxicology*, 23(2), pp. 163–171. doi:10.1007/BF00212270.

Hoffman, D.J. (2002) “Role of selenium toxicity and oxidative stress in aquatic birds,” *Aquatic Toxicology*, 57(1), pp. 11–26. doi:https://doi.org/10.1016/S0166-445X(01)00263-6.

Hoffman, D.J., Heinz, G.H. and Krynitsky, A.J. (1989) “Hepatic glutathione metabolism and lipid peroxidation in response to excess dietary selenomethionine and selenite in mallard ducklings,” *Journal of Toxicology and Environmental Health, Part A Current Issues*, 27(2), pp. 263–271.

Huiskes, R. *et al.* (2000) “Effects of mechanical forces on maintenance and adaptation of form in trabecular bone,” *Nature*, 405(6787), pp. 704–706. doi:10.1038/35015116.

Ilich, J.Z. and Kerstetter, J.E. (2000) “Nutrition in Bone Health Revisited: A Story Beyond Calcium,” *Journal of the American College of Nutrition*, 19(6), pp. 715–737. doi:10.1080/07315724.2000.10718070.

Inkapool, L. (2018) *Bone properties of mink (Neovison vison) exposed to environmentally relevant levels of PCB*.

Jolliffe, I.T. and Cadima, J. (2016) “Principal component analysis: a review and recent developments,” *Philosophical Transactions of the Royal Society A: Mathematical, Physical and Engineering Sciences*, 374(2065), p. 20150202. doi:10.1098/rsta.2015.0202.

Kamali, M. and Khodaparast, Z. (2015) “Review on recent developments on pulp and paper mill wastewater treatment.,” *Ecotoxicology and environmental safety*, 114, pp. 326–342. doi:10.1016/j.ecoenv.2014.05.005.

Kazantzis, G. (2004) “Cadmium, osteoporosis and calcium metabolism.,” *Biometals : an international journal on the role of metal ions in biology, biochemistry, and medicine*, 17(5), pp. 493–498. doi:10.1023/b:biom.0000045727.76054.f3.

Keaveny, T.M. *et al.* (2001) “Iomechanics of.”

Kelly, E.N. *et al.* (2009) “Oil sands development contributes polycyclic aromatic compounds to the Athabasca River and its tributaries,” *Proceedings of the National Academy of Sciences*, 106(52), pp. 22346 LP – 22351. doi:10.1073/pnas.0912050106.

Khan, I.A. and Thomas, P. (2001) “Disruption of Neuroendocrine Control of Luteinizing Hormone Secretion by Aroclor 1254 Involves Inhibition of Hypothalamic Tryptophan Hydroxylase Activity1,” *Biology of Reproduction*, 64(3), pp. 955–964. doi:10.1095/biolreprod64.3.955.

Köhrle, J. *et al.* (2005) “Selenium, the Thyroid, and the Endocrine System,” *Endocrine Reviews*, 26(7), pp. 944–984. doi:10.1210/er.2001-0034.

Kourtis, L.C., Carter, D.R. and Beaupre, G.S. (2014) “Improving the estimate of the effective elastic modulus derived from three-point bending tests of long bones,” *Annals of biomedical engineering*, 42(8), pp. 1773–1780.

Kucera, E. (1983) “Mink and otter as indicators of mercury in Manitoba waters,” *Canadian Journal of Zoology*, 61(10), pp. 2250–2256. doi:10.1139/z83-297.

Kurek, J. *et al.* (2013) “Legacy of a half century of Athabasca oil sands development recorded by lake ecosystems,” *Proceedings of the National Academy of Sciences of the United States of America*, 110(5), pp. 1761–1766. doi:10.1073/pnas.1217675110.

Lanyon, L. and Skerry, T. (2001) “Postmenopausal osteoporosis as a failure of bone’s adaptation to functional loading: a hypothesis.,” *Journal of bone and mineral research : the official journal of the American Society for Bone and Mineral Research*, 16(11), pp. 1937–1947. doi:10.1359/jbmr.2001.16.11.1937.

Larivière, S. (1999) *Mustela vison*. Soc.

Lemly, A.D. (2014) “Teratogenic effects and monetary cost of selenium poisoning of fish in Lake Sutton, North Carolina,” *Ecotoxicology and Environmental Safety*, 104(Complete), pp. 160–167. doi:10.1016/j.ecoenv.2014.02.022.

Li, H. *et al.* (2008) “Micro-computed tomography for small animal imaging: Technological details,” *Progress in Natural Science*, 18(5), pp. 513–521. doi:https://doi.org/10.1016/j.pnsc.2008.01.002.

Li, X. *et al.* (2011) “Effects of Aluminum Exposure on Bone Mineral Density, Mineral, and Trace Elements in Rats,” *Biological Trace Element Research*, 143(1), pp. 378–385. doi:10.1007/s12011-010-8861-4.

Lidsky, T.I. and Schneider, J.S. (2003) “Lead neurotoxicity in children: basic mechanisms and clinical correlates,” *Brain*, 126(1), pp. 5–19.

Lind, P.M. *et al.* (2003) “Bone Mineral Density in Male Baltic Grey Seal (Halichoerus grypus),” *Ambio*, 32(6), pp. 385–388. doi:10.1579/0044-7447-32.6.385.

Lind, P.M. *et al.* (2004a) “Abnormal bone composition female juvenile American alligators from a pesticide-polluted lake (Lake Apopka, Florida),” *Environmental Health Perspectives*, 112(3), pp. 359–362. doi:10.1289/ehp.6524.

Lind, P.M. *et al.* (2004b) “Abnormal bone composition female juvenile American alligators from a pesticide-polluted lake (Lake Apopka, Florida),” *Environmental Health Perspectives*, 112(3), pp. 359–362. doi:10.1289/ehp.6524.

Link, T.M. *et al.* (1998) “A comparative study of trabecular bone properties in the spine and femur using high resolution MRI and CT,” *Journal of Bone and Mineral Research*, 13(1), pp. 122–132. doi:10.1359/jbmr.1998.13.1.122.

Lu, L. *et al.* (2011) “The influence of dietary sodium on bone development in growing rats,” *Archives of Animal Nutrition*, 65(6), pp. 486–496. doi:10.1080/1745039X.2011.629805.

Lyons, W.R., Abernathy, E. and Gropper, M. (1950) “Effects of Androgen and Somatotrophin on the Os Penis of the Rat.,” *Proceedings of the Society for Experimental Biology and Medicine*, 73(2), pp. 193–197. doi:10.3181/00379727-73-17623.

Madill, R.E.A. *et al.* (2001) “Preliminary risk assessment of the wet landscape option for reclamation of oil sands mine tailings: bioassays with mature fine tailings pore water,” *Environmental Toxicology: An International Journal*, 16(3), pp. 197–208.

Maly, I.P., Eppler, E. and Müller-Gerbl, M. (2018) “High metabolic activity of tissue-nonspecific alkaline phosphatase not only in young but also in adult bone as demonstrated using a new histochemical detection protocol,” *General and Comparative Endocrinology*, 258, pp. 109–118. doi:https://doi.org/10.1016/j.ygcen.2017.05.008.

Mandalunis, P.M. and Ubios, A.M. (2005) “Experimental renal failure and iron overload: a histomorphometric study in rat tibia,” *Toxicologic pathology*, 33(3), pp. 398–403.

Masliyah, J. *et al.* (2004) “Understanding water-based bitumen extraction from athabasca oil sands,” *Canadian Journal of Chemical Engineering*, 82(4), pp. 628–654. doi:10.1002/cjce.5450820403.

Masuo, Y. and Ishido, M. (2011) “Neurotoxicity of Endocrine Disruptors: Possible Involvement in Brain Development and Neurodegeneration,” *Journal of Toxicology and Environmental Health, Part B*, 14(5–7), pp. 346–369. doi:10.1080/10937404.2011.578557.

Medeiros, D.M. *et al.* (2002) “Bone Morphology, Strength and Density Are Compromised in Iron-Deficient Rats and Exacerbated by Calcium Restriction,” *The Journal of Nutrition*, 132(10), pp. 3135–3141. doi:10.1093/jn/131.10.3135.

Meng Bao, C. le *et al.* (2013) “Advances in Bone Tissue Engineering,” in *Regenerative Medicine and Tissue Engineering*. doi:10.5772/55916.

van der Meulen, M.C.H., Jepsen, K.J. and Mikić, B. (2001) “Understanding bone strength: Size isn’t everything,” *Bone*, 29(2), pp. 101–104. doi:10.1016/S8756-3282(01)00491-4.

Morgan, E.F., Unnikrisnan, G.U. and Hussein, A.I. (2018) “Bone Mechanical Properties in Healthy and Diseased States,” *Annual review of biomedical engineering*, 20, pp. 119–143. doi:10.1146/annurev-bioeng-062117-121139.

Nasoori, A. (2020) “Formation, structure, and function of extra-skeletal bones in mammals,” *Biological Reviews*, 95(4), pp. 986–1019. doi:https://doi.org/10.1111/brv.12597.

Nordin, M. and Frankel, V.H. (2001) *Basic biomechanics of the musculoskeletal system*. Lippincott Williams & Wilkins.

O’Brien, D.J., Kaneene, J.B. and Poppenga, R.H. (1993) “The use of mammals as sentinels for human exposure to toxic contaminants in the environment,” *Environmental Health Perspectives*, 99(10), pp. 351–368. doi:10.1289/ehp.9399351.

Osterhoff, G. *et al.* (2016) “Bone mechanical properties and changes with osteoporosis,” *Injury*, 47 Suppl 2(Suppl 2), pp. S11–S20. doi:10.1016/S0020-1383(16)47003-8.

Ottinger, M.A. *et al.* (2008) “Neuroendocrine and behavioral effects of embryonic exposure to endocrine disrupting chemicals in birds,” *Brain Research Reviews*, 57(2), pp. 376–385.

Pandit, D.N. and Gupta, M.L. (2019) “Heapto-somatic index, gonado-somatic index and condition factor of Anabas testudineus as bio-monitoring tools of nickel and chromium toxicity,” *International Journal of Innovations in Engineering and Technology*, 12(3), pp. 25–28.

Peterson, S.A. *et al.* (2009) “Selenium and mercury interactions with emphasis on fish tissue,” *Environmental Bioindicators*, 4(4), pp. 318–334.

Pokhrel, D. and Viraraghavan, T. (2004) “Treatment of pulp and paper mill wastewater—a review,” *Science of the total environment*, 333(1–3), pp. 37–58.

R Core Team (2021) “R: A language and environment for statistical computing. R Foundation for Statistical Computing.” Vienna, Austria. Available at: https://www.r-project.org/.

Ritter, L. (1998) “Persistent organic pollutants,” *International Programme on Chemical Safety (IPCS) within the framework of the Inter-Organization Programme for the Sound Management of Chemicals (IOMC), 1998* [Preprint].

Ritter, L., Solomon, K.R. and Forget, J. (2011) “Persistent Organic Pollutants - An Assessment Report on: DDT-Aldrin-Dieldrin-Endrin-Chlordane-Heptachlor-Heptachlorobenzene-Mirex-Tozapene-Polychlorinated Biphenyls-Dioxins and Furans,” *Chemosphere*, p. 43 pp. Available at: http://www.ncbi.nlm.nih.gov/pubmed/22018961.

Robling, A.G., Castillo, A.B. and Turner, C.H. (2006) “Biomechanical and molecular regulation of bone remodeling.,” *Annual review of biomedical engineering*, 8, pp. 455–498. doi:10.1146/annurev.bioeng.8.061505.095721.

Rodríguez, J. and Mandalunis, P.M. (2018) “A review of metal exposure and its effects on bone health,” *Journal of Toxicology*, 2018. doi:10.1155/2018/4854152.

Rzymski, Piotr *et al.* (2015) “Impact of heavy metals on the female reproductive system,” *Annals of Agricultural and Environmental Medicine*, 22(2), pp. 259–264. doi:10.5604/12321966.1152077.

Santos, S. *et al.* (2015) “Selenium contaminated waters: An overview of analytical methods, treatment options and recent advances in sorption methods,” *Science of the Total Environment*, 521–522(Complete), pp. 246–260. doi:10.1016/j.scitotenv.2015.03.107.

Schindler, D. (2010) “Tar sands need solid science,” *Nature*, 468(7323), pp. 499–501. doi:10.1038/468499a.

Schneider, C.A., Rasband, W.S. and Eliceiri, K.W. (2012) “NIH Image to ImageJ: 25 years of image analysis,” *Nature Methods*, 9(7), pp. 671–675. doi:10.1038/nmeth.2089.

Seeram, E. (2015) *Computed Tomography-E-Book: Physical Principles, Clinical Applications, and Quality Control*. Elsevier Health Sciences.

Silva, M.J. *et al.* (1994) “Direct and computed tomography thickness measurements of the human, lumbar vertebral shell and endplate,” *Bone*, 15(4), pp. 409–414. doi:10.1016/8756-3282(94)90817-6.

Siu, W.S. *et al.* (2004) “A study of trabecular bones in ovariectomized goats with micro-computed tomography and peripheral quantitative computed tomography,” *Bone*, 35(1), pp. 21–26. doi:10.1016/j.bone.2004.03.014.

Skordis, N. and Toumba, M. (2011) “Bone disease in thalassaemia major: recent advances in pathogenesis and clinical aspects.,” *Pediatric endocrinology reviews: PER*, 8, pp. 300–306.

Song, M. *et al.* (2017) “Aluminum trichloride inhibits the rat osteoblasts mineralization in vitro,” *Biological trace element research*, 175(1), pp. 186–193.

Sonne, C. *et al.* (2006) “Xenoendocrine Pollutants May Reduce Size of Sexual Organs in East Greenland Polar Bears (Ursus maritimus),” *Environmental Science & Technology*, 40(18), pp. 5668–5674. doi:10.1021/es060836n.

Sonne, C. (2010) “Health effects from long-range transported contaminants in Arctic top predators: an integrated review based on studies of polar bears and relevant model species,” *Environment international*, 36(5), pp. 461–491.

Sonne, C. *et al.* (2012) “Two decades of biomonitoring polar bear health in Greenland: a review,” *Acta Veterinaria Scandinavica*, 54(1), p. S15. doi:10.1186/1751-0147-54-S1-S15.

Sonne, C. *et al.* (2015) “Penile density and globally used chemicals in Canadian and Greenland polar bears,” *Environmental Research*, 137, pp. 287–291. doi:https://doi.org/10.1016/j.envres.2014.12.026.

Souza-Monteiro, D. *et al.* (2021) “Long-term exposure to low doses of aluminum affects mineral content and microarchitecture of rats alveolar bone,” *Environmental Science and Pollution Research*, 28(33), pp. 45879–45890. doi:10.1007/s11356-021-13937-z.

Syncrude Canada, Ltd. (2020) *Responsible Oil Sands Development*. Available at: https://www.syncrude.ca/our-process/understanding-our-process/.

Tête, N. *et al.* (2013) “Can Body Condition and Somatic Indices be Used to Evaluate Metal-Induced Stress in Wild Small Mammals?,” *PloS one*, 8(6), pp. e66399–e66399. doi:10.1371/journal.pone.0066399.

Thomas, P.J. *et al.* (2021) “Co-exposures to trace elements and polycyclic aromatic compounds (PACs) impacts North American river otter (Lontra canadensis) baculum,” *Chemosphere*, 265, p. 128920. doi:https://doi.org/10.1016/j.chemosphere.2020.128920.

Tillitt, D.E. *et al.* (1995) “Dietary exposure of mink to carp from Saginaw Bay. 3. Characterization of dietary exposure to planar halogenated hydrocarbons, dioxin equivalents, and biomagnification,” *Environmental science & technology*, 30(1), pp. 283–291.

Timoshenko, S. (1953) “History of strength of materials McGraw-Hill book company,” *Inc., New York/Toronto/London* [Preprint].

Tomaszewska, E. *et al.* (2016) “Alteration in bone geometric and mechanical properties, histomorphometrical parameters of trabecular bone, articular cartilage, and growth plate in adolescent rats after chronic co-exposure to cadmium and lead in the case of supplementation with green, bl,” *Environmental Toxicology and Pharmacology*, 46, pp. 36–44. doi:https://doi.org/10.1016/j.etap.2016.06.027.

Tomaszewska, E. *et al.* (2017) “DON-induced changes in bone homeostasis in mink dams,” *Journal of Veterinary Research (Poland)*, 61(3), pp. 357–362. doi:10.1515/jvetres-2017-0047.

Toppari, J. (2002) “Environmental endocrine disrupters and disorders of sexual differentiation,” in *Seminars in reproductive medicine*. Copyright© 2002 by Thieme Medical Publishers, Inc., 333 Seventh Avenue, New …, pp. 305–312.

Turan, B. *et al.* (2000) “A biomechanical and spectroscopic study of bone from rats with selenium deficiency and toxicity,” *Biometals*, 13(2), pp. 113–121. doi:10.1023/A:1009206206324.

U.S. Department of Health and Human Services, P.H.S. (no date) “Agency for Toxic Substances and Disease Registry.” Atlanta, GA. Available at: http://www.atsdr.cdc.gov/toxpro2.html.

Wayland, M., Kneteman, J. and Crosley, R. (2006) “The American Dipper as a Bioindicator of Selenium Contamination in a Coal Mine-Affected Stream in West-Central Alberta, Canada,” *Environmental Monitoring and Assessment*, 123(1), pp. 285–298. doi:10.1007/s10661-006-9197-6.

Wedig, K.E. *et al.* (2006) “Skeletal demineralization and fractures caused by fetal magnesium toxicity,” *Journal of Perinatology*, 26(6), pp. 371–374. doi:10.1038/sj.jp.7211508.

Wirth, J.J. and Mijal, R.S. (2010) “Adverse Effects of Low Level Heavy Metal Exposure on Male Reproductive Function,” *Systems Biology in Reproductive Medicine*, 56(2), pp. 147–167. doi:10.3109/19396360903582216.

Wong, A.K.O. *et al.* (2015) “Bone lead (Pb) content at the tibia is associated with thinner distal tibia cortices and lower volumetric bone density in postmenopausal women,” *Bone*, 79, pp. 58–64. doi:https://doi.org/10.1016/j.bone.2015.05.010.

Wu, C.-C. *et al.* (2021) “Selenium status is independently related to bone mineral density, FRAX score, and bone fracture history: NHANES, 2013 to 2014,” *Bone*, 143, p. 115631. doi:https://doi.org/10.1016/j.bone.2020.115631.

Yalcin, D. (2018) *Bend Testing, Equipment, and ASTM Test Methods*.

Yamaguchi, S. *et al.* (2007) “Effects of lead, molybdenum, rubidium, arsenic and organochlorines on spermatogenesis in fish: Monitoring at Mekong Delta area and in vitro experiment,” *Aquatic Toxicology*, 83(1), pp. 43–51. doi:https://doi.org/10.1016/j.aquatox.2007.03.010.

Yang, J., Pham, S.M. and Crabbe, D.L. (2003) “High-resolution micro-CT evaluation of mid- to long-term effects of estrogen deficiency on rat trabecular bone1,” *Academic Radiology*, 10(10), pp. 1153–1158. doi:10.1016/S1076-6332(03)00109-0.

Yang, X. *et al.* (2018) “Bone impairment caused by AlCl3 is associated with activation of the JNK apoptotic pathway mediated by oxidative stress,” *Food and Chemical Toxicology*, 116, pp. 307–314. doi:https://doi.org/10.1016/j.fct.2018.04.057.

Zachara, B.A. *et al.* (2001) “Tissue level, distribution, and total body selenium content in healthy and diseased humans in Poland.,” *Archives of environmental health*, 56(5), pp. 461–466. doi:10.1080/00039890109604483.

Zeng, H., Cao, J.J. and Combs Jr, G.F. (2013) “Selenium in bone health: roles in antioxidant protection and cell proliferation,” *Nutrients*, 5(1), pp. 97–110. doi:10.3390/nu5010097.

Zhang, Y. *et al.* (2016) “Airborne Petcoke Dust is a Major Source of Polycyclic Aromatic Hydrocarbons in the Athabasca Oil Sands Region,” *Environmental Science & Technology*, 50(4), pp. 1711–1720. doi:10.1021/acs.est.5b05092.

Zofková, I., Nemcikova, P. and Matucha, P. (2013) “Trace elements and bone health,” *Clinical Chemistry and Laboratory Medicine (CCLM)*, 51(8), pp. 1555–1561. doi:doi:10.1515/cclm-2012-0868.

Appendix A – Glossary of Anatomical Terms

All definitions were retrieved from the Anatomy and Physiology textbook (Betts *et al.*, 2013).

Anterior	Front of the body
Baculum	Penile bone (only present in certain species)
Cancellous bone	Porous osseus structure that supports weight distributions within a cortical bone shell
Cortical bone	Dense osseus tissue comprising the diaphysis of long bones and the outer shell of all bones
Diaphysis	Tubular shaft between the ends of long bones
Distal	Position further from the main trunk of the body
Epiphysis	The wide sections at the top and bottom of long bones
Femur	Thigh bone
Haversian canal	Central canal running down each osteon
Inferior	Below the body
Lateral	Side of the body/direction towards the side of the body
Lateral condyle	Smooth bony projection forming the lateral and posterior sides of the distal end of the femur
Lesser trochanter	On the medial side of the femur, it is a spinous process below the neck of the femur
Medial	Positioning towards middle of the body
Medial condyle	The main bony projection on the medial side of the distal end of the femur

Osteoblast	A bone cell responsible for bone formation
Osteoclast	A bone cell responsible for resorbing/taking away bone material
Osteocyte	The most common type of bone cell responsible for intercellular signaling
Osteon	Concentric rings of calcified extracellular matrix. Also termed lamellae, osteons are the primary structural components of bone structures
Periosteum	A thin membrane covering the outside of bones
Posterior	Back of the body
Proximal	Position closer to the main trunk of the body
Superior	Above the body
Trabeculae	Arches/lattice plates of cancellous bone

Appendix B – Further Reading

The following is additional reading on the reproductive effects of different EDCs on species, reviewing their influence at different stages in the mating cycle.

Reproductive Effects of EDCs

Many studies have investigated the cause-and-effect relationship between pollutant exposure and reproductive failure in animals. While some laboratory studies and controlled feeding trials have established this relationship, the exact mechanisms of action are not well-understood. Moreover, it is difficult to detect this relationship in wild animals simply because there are a multitude of factors that will contribute to reproduction in wild populations (*e.g.*: habitat loss and natural cycles) (Fox, 2001). However, the overall current literature does indicate that environmental EDCs produced as a result of industrial activities do impair reproductive success for many species.

The mechanisms of disruption by EDCs that lead to impaired reproduction are quite complex because of the multiplicity of endocrine pathways that have potential to affect reproduction (Khan and Thomas, 2001). Thus, it is important to first determine the precise endocrine pathways that are disrupted by EDCs. In general, the degree to which reproduction is impaired depends on several factors: the degree of EDC exposure, the length of exposure and the toxicity of the EDCs involved. However, one of the most important considerations is the time of exposure; whether an organism is exposed to EDCs pre- or post-natal has different consequences on the survivability of that organism. What follows is a summary of EDC effects on reproductive and health with an emphasis on effects observed in the American mink.

Mating Effects

Adverse effects of EDCs on mating behaviour have important consequences on successful reproduction. A study with female rats fed a diet of Aroclor 1254 at levels equivalent to polychlorinated biphenyl (PCB) concentrations found in mammals in heavily contaminated areas of nature, found this PCB to concentrate in the liver, fat and brain tissues (Brezner, Terkel and Perry, 1984). Results indicate that these mothers had shortened time for sexual receptivity and reduced sexual receptivity, leading to reduced mating (Brezner, Terkel and Perry, 1984). This was attributed to the disturbance of regular hormonal fluctuations that take place during mating by the chemicals, such as reductions in progesterone (Brezner, Terkel and Perry, 1984). However, alterations in mating behaviour are not just isolated to female organisms. EDCs such as vinclozolin and other OCs have been found to affect normal male courtship behaviour in male guppies as a result of demasculinization effects (Baatrup and Junge, 2001). Such effects occur because of the antiandrogenic actions of these EDCs, which affect the male organism's reproductive capability (Ottinger *et al.*, 2008; Masuo and Ishido, 2011).

Further studies reveal similar trends with respect to antiandrogenic effects of EDCs. Ahmad et al. (2001) and (2003) investigated the effects of Aroclor 1242 and 1254 ingestion for 6 months on male rhesus monkeys, specifically observing effects on reproductive capacity. They noted significant decreases in testicular size, testosterone and spermatogenic activity in treated monkeys, as well as serious structural changes in testicles and accessory organs. These results were attributed to the estrogenic activity of Aroclor 1242, which lead to infertility. This and other studies contribute to the current understanding that EDCs (specifically PCBs, furans, and certain OCs) can lead to decreased sperm motility, concentration, and reduced semen quality in

mammals (Atanassova *et al.*, 2000; Baatrup and Junge, 2001; Toppari, 2002; Ahmad *et al.*, 2003).

In mink, similar findings have been established, all indicating that increased PCB exposure increases the likelihood of reproductive failure (Aulerich *et al.*, 1971; Aulerich and Ringer, 1977; Tillitt *et al.*, 1995). Aulerich and Ringer (1977) demonstrated that reproductive failure occurred in mink fed salmon from the Great Lakes that were contaminated from PCBs. (Heaton *et al.*, 1995)also found that when mink diets were supplemented by 40% with fish from the PCB-contaminated Saginaw Bay in Michigan, litter sizes and successful mating significantly decreased. In addition, the relationship between PCB exposure and reproductive defects is proportionate, meaning that longer PCB exposure will worsen reproductive effects even further (Bursian *et al.*, 2013).

Effects on Fetal Exposure

Studies that have performed feeding trials have found significantly increased kit mortality and decreased litter sizes for female mink and rats, when fed increasing proportions of PCB-contaminated diets (Brezner, Terkel and Perry, 1984; Heaton *et al.*, 1995; Basu *et al.*, 2007). For example, Heaton et al. (1995) found that litter sizes were significantly smaller, few live kits were born, and no kits survived beyond 24 hours after birth. Even 10% PCB contamination in their diets resulted in decreased bodyweights and kit survival only to 3 to 6 weeks after birth. In addition, even as the concentration of PCBs diminished in fish over time, the PCB congeners in the fish were much more persistent and harmful to mink. So, much smaller concentrations of these congeners still contributed to observed reproductive failure (Heaton *et al.*, 1995).

Findings also reveal that the relationship between EDC exposure and reproduction is exacerbated from adult to child, indicating that prenatal effects should not be underestimated, and that effects

can be transferred between generations (Masuo and Ishido, 2011). This is due primarily to the fact that many of these EDCs will cross the placenta and be secreted in mothers' milk (Brezner, Terkel and Perry, 1984; Masuo and Ishido, 2011). Moreover, the later in life mink are exposed to EDCs, the less severe the effects are for them, but the more severe implications are for their offspring (Tillitt *et al.*, 1995; Bursian *et al.*, 2013). Unfortunately, this relationship has only been established with respect to maternal EDC exposure, not paternal exposure.

Appendix C – Calculations

The following are sample calculations for baculums in three-point bending and femur second moment of area calculations.

C. 1 Baculum Calculations

Span for all specimens: $L = 18mm$

Second moment of area: $I = \frac{bh^3}{36}$, where *b* is the base length (mm) and *h* is the height (mm) of the triangle.

Bending Moment: $M = \frac{PL}{2}$, where P is load (N) and L (mm) is span.

Stress: $\sigma = \frac{My}{I}$, where *y* is the deflection of the beam from the neutral axis (mm).

Centroid: Assuming a triangular cross-section and a material of uniform density, the centroid is located at $\frac{b}{2}$ and $\frac{h}{3}$.

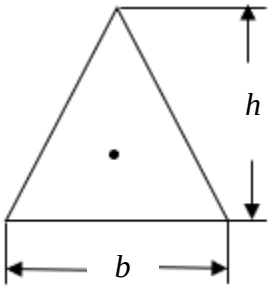

Figure 1.0.1*: Cross-sectional area of the baculum.*

Example 1: Specimen no. 1718-460-1

$b = 2.95mm$

$h = 2.29mm$

$P_{max} = 53.4137N$

$\delta_{max} = 1.90mm$

Position of neutral axis:

$$y = \frac{2.29}{3}$$

$$y = 0.763mm$$

Second moment of area:

$$I = \frac{bh^3}{36}$$

$$I = \frac{(2.95)(2.29)^3}{36}$$

$$I = 0.984mm^4$$

Bending moment:

$$M = \frac{PL}{2}$$

$$M = \frac{(53.4137)(18)}{2}$$

$$M = 480.723\ N \cdot mm$$

Ultimate stress:

$$\sigma = \frac{My}{I}$$

$$\sigma = \frac{(480.723)(0.763)}{0.984}$$

$$\sigma = 373\ MPa$$

Young's modulus:

$$\delta = \frac{FL^3}{48EI}$$

$$E = \frac{FL^3}{48I\delta}$$

$$E = \frac{(53.4137)(18^3)}{48(0.984)(1.90)}$$

$$E = 3.47\ GPa$$

C. 2 Femur Calculations

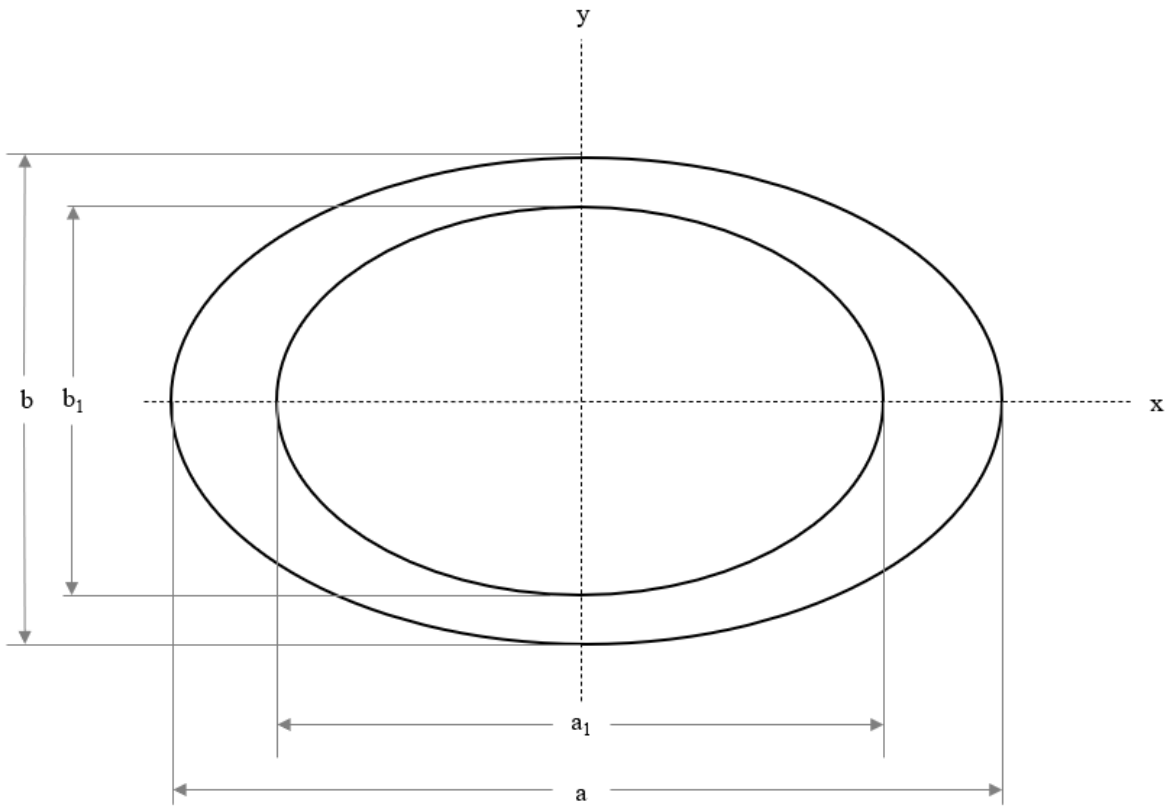

Figure 1.0.2: *The cross section of a femur approximated as an ellipse.*

Second moment of area calculation in the y-direction according to Figure 1a. For the femurs, this was the medial-lateral axis:

$$I_y = \frac{\pi(a^3 b - a_1^3 b_1)}{64}$$

Here, *a* and a_1 are the diaphysis inner and outer diameters in the anterior-posterior directions. The medial-lateral inner and outer diameters are denoted by *b* and b_1. All calculations for bending moment, ultimate stress and elastic modulus were calculated in the same way for

baculums and femurs, with the exception that the position of the neutral axis was taken as the radius of the femur measures to the outer edge of the cortical bone.

Appendix D – Code

The following is the Python code (three-point bend test analysis) followed by R code (statistical analysis).

D. 1 Python Code

```
# -*- coding: utf-8 -*-
"""
Created on Sat Nov 20 22:08:09 2021

@author: gabby
"""

import pandas as pd

#Compliance Correction:
compliance =
pd.read_excel(r'C:\Users\gabby\Documents\MASc_project\Results\Ariana_3ptbe
ndtestsfemur\female_femur_compliance.xlsx')

import matplotlib.pyplot as plt
import numpy as np
from sympy import S, symbols, printing
from scipy.signal import find_peaks

x_min = compliance['Displacement(E1LMTU3045:Digital Position) (mm)'][2738]
xc = compliance['Displacement(E1LMTU3045:Digital Position)
(mm)'][2738:]*(-1) + x_min
yc = compliance['Load(E1LMTU3045:Load) (N)'][2738:]*(-1)
plt.plot(yc, xc)
plt.xlabel('force(N)')
plt.ylabel('displacement(mm)')
plt.show()

p = np.polyfit(yc, xc, 5)
f = np.poly1d(p)


print(f)

x_new = np.linspace(300, .0005, 50)
y_new = f(x_new)

x = symbols("x")
poly = sum(S("{:6.2f}".format(v))*x**i for i, v in enumerate(p[::-1]))
eq_latex = printing.latex(poly)
```

```
#^ here, y is displacement and x is force

plt.plot(x_new, y_new) #label="${}$".format(eq_latex))
plt.plot(yc, xc)
plt.legend(fontsize="small")
plt.show()

#now take equation and find the corrected displacement for a baculum bend
test
df =
pd.read_csv(r'C:\Users\gabby\Documents\MASc_project\Results\3ptbendtestsfe
mur\Femur 1718-451-3\Test5.Stop (2).csv')
force=df['Load(E1LMTU3045:Load) (N)']*-1
t=df['Total Time (s)']
min_disp=max(df['Displacement(E1LMTU3045:Digital Position) (mm)'])
d=df['Displacement(E1LMTU3045:Digital Position) (mm)']*-1 + min_disp
plt.plot(d, force)
plt.show()

plt.plot(force)
plt.show()
plt.plot(d)
plt.show()

x_comp = force
y_comp = f(force)
cd = d - y_comp
plt.plot(force, cd)
plt.show()

plt.plot(cd, force)
plt.plot(d, force)
plt.xlabel('Corrected Displacement (mm)')
plt.ylabel('Force (N)')
plt.show()

#cd is corrected displacement

#plot force, time and corrected displacement
plt.plot(t, force, color = 'blue', linewidth = 1, linestyle = '-') #plot
force vs time
plt.xlabel('Time(s)')
plt.ylabel('Force(N)')
plt.show()
plt.plot(cd, force, color='green') #plot force vs. displacement
plt.xlabel('Displacement(mm)')
plt.ylabel('Force(N)')
plt.show()
plt.plot(t, cd)
plt.show()

#calculate ultimate stress
y=5.647157/2
I=24.44403427
```

```
M=(force*30)/4
stress=(M*y)/I
print (max(M))
#ultimate stress
ultstress=max(stress)
print ('ultimate stress:', ultstress)
print('peak load', max(force))

#find min and max of last 3 loading cycles:
plt.plot(force[7000:10000])
plt.show()
peaks2, _ = find_peaks(force[7000:9500], height=0)
print (peaks2)
#plt.plot(peaks2, '*')
plt.plot(force[8757:9118])
plt.show()

#input the max and min of the last 3 loading cycles below to plot only
last 3 cycles.
#Subtract 0.5 to zero the force values, and subtract the lowest
displacement value to
#zero the displacement values:
cycle8f = force[7325:7689]-0.5
cycle8def = cd[7325:7689]-(cd[7325])
cycle9f = force[8050:8402]-0.5
cycle9def = cd[8050:8402]-(cd[8050])
cycle10f = force[8757:9118]-0.5
cycle10def = cd[8757:9118]-(cd[8757])
plt.plot(cycle8def, cycle8f, color='green')
plt.plot(cycle9def, cycle9f, color='blue')
plt.plot(cycle10def, cycle10f, color='red')
plt.xlabel('deflection(mm)')
plt.ylabel('Force(N)')
plt.show()

#find slope of last 3 loading cycles
z1 = np.polyfit(cycle8def, cycle8f, 1)
p1 = np.poly1d(z1)
plt.plot(cycle8def,p1(cycle8def),"g--",
label="y=%.6fx+%.6f"%(z1[0],z1[1]))
z2 = np.polyfit(cycle9def, cycle9f, 1)
p2 = np.poly1d(z2)
plt.plot(cycle9def, p2(cycle9def),'b--', label =
"y=%.6fx+%.6f"%(z2[0],z2[1]))
z3 = np.polyfit(cycle10def, cycle10f, 1)
p3 = np.poly1d(z3)
plt.plot(cycle10def, p2(cycle10def),'r--', label =
"y=%.6fx+%.6f"%(z3[0],z3[1]))
plt.legend(loc='best')
plt.xlabel('deflection(mm)')
plt.ylabel('Force(N)')
plt.show()

#find youngs modulus
```

```
Y1=(30**3)*z1[0]/(48*I)
Y2=(30**3)*z2[0]/(48*I)
Y3=(30**3)*z3[0]/(48*I)
print (Y1, Y2, Y3)
ym = [Y1, Y2, Y3]
E=sum(ym)/3
print ('Youngs modulus', E)

#to find strain, use E=stress/strain
strain = stress/E
plt.plot(strain, stress)
plt.show()

plt.plot(stress)
plt.show()

#plot line on last 3 cycles of stress curve
stress8 = stress[7325:7689]
stress8t = t[7325:7689]
stress9 = stress[8050:8402]
stress9t = t[8050:8402]
stress10 = stress[8757:9118]
stress10t = t[8757:9118]
z4 = np.polyfit(stress8t, stress8, 1)
p4 = np.poly1d(z4)
plt.plot(stress8t, p4(stress8t),"g--", label="y=%.6fx+%.6f"%(z4[0],z4[1]))
z5 = np.polyfit(stress9t, stress9, 1)
p5 = np.poly1d(z5)
plt.plot(stress9t, p5(stress9t),'b--', label =
"y=%.6fx+%.6f"%(z5[0],z5[1]))
z6 = np.polyfit(stress10t, stress10, 1)
p6 = np.poly1d(z6)
plt.plot(stress10t, p6(stress10t),'r--', label =
"y=%.6fx+%.6f"%(z6[0],z6[1]))
plt.legend(loc='best')
plt.show()

#find stiffness from force-displacement curve - last 3 loading cycles
stiff8 = force[7325:7689]
stiff8d =cd[7325:7689]-cd[7325]
stiff9 = force[8050:8402]
stiff9d = cd[8050:8402]-cd[8050]
stiff10 = force[8757:9118]
stiff10d = cd[8757:9118]-cd[8757]

s1 = np.polyfit(stiff8d, stiff8, 1)
t4 = np.poly1d(s1)
plt.plot(stiff8d, t4(stiff8d),"g--", label="y=%.6fx+%.6f"%(s1[0],s1[1]))
s5 = np.polyfit(stiff9d, stiff9, 1)
t5 = np.poly1d(s5)
plt.plot(stiff9d, t5(stiff9d),'b--', label = "y=%.6fx+%.6f"%(s5[0],s5[1]))
s6 = np.polyfit(stiff10d, stiff10, 1)
t6 = np.poly1d(s6)
```

```
plt.plot(stiff10d, t6(stiff10d),'r--', label =
"y=%.6fx+%.6f"%(s6[0],s6[1]))
plt.legend(loc='best')
plt.show()

stiff_slopes = [s1[0], s5[0], s6[0]]
avgstiffslope = sum(stiff_slopes)/3
print ('stiffness', avgstiffslope)

#find slope of original line along linear portion of stress curve
slopes = [z4[0], z5[0], z6[0]]
avgslope = sum(slopes)/3
print (avgslope)
#find b of original line
x = np.linspace(0, 150, 100)
r = stress[9800]
v = t[9800]
b=r-avgslope*v
print (b)
#find x-intercept of original line:
y=avgslope*x+b
b=r-avgslope*v
x_int = (-b)/avgslope
print ('x-intercept', x_int)

y=avgslope*t+b
plt.plot(t[:],y[:])
plt.plot(t, stress)
plt.ylim(ymin=0)
plt.show()

#find time that corresponds to 0.02% strain
plt.plot(t, strain)
plt.show()
plt.plot(strain)
plt.show()

def condition(x): return 0.00201 > x > 0.001999

output = [idx for idx, element in enumerate(strain) if condition(element)]
print (output)

plt.plot(strain[3337:3674])
plt.show()

def condition(x): return 0.00004 > x > 0.000

output = [idx for idx, element in enumerate(strain) if condition(element)]
print (output)

plt.plot(strain, stress)
plt.xlabel('strain')
plt.ylabel('stress(MPa)')
plt.show()
```

```
ss = strain[3337:3674]
print ('number of data point for 0.002 strain:', len(ss))

#offset line on stress curve by number of data points
# find how much time corresponds to number of data points
print (t[0])
print(t[len(ss)])
j=t[len(ss)]-t[0]
print (j)

#new x intercept:
x3 = x_int + j
print ('new x-intercept:', x3)

#remember:
x_new = np.linspace(0,10,100)
#input new x intercept to find new y=mx+b
b_new = 0-avgslope*x3
print(b_new)
#new equation:
y_new = avgslope*t + b_new
print (y_new)
y_new2 = avgslope*x_new + b_new

#plot new equation on time vs stress graph
plt.plot(t[:15000], stress[:15000], label = 'stress curve')
plt.plot(x_new, y_new2, color = 'g')
plt.plot(t, y_new, label = 'offset line', color = 'red')
plt.xlabel('time(s)')
plt.ylabel('stress(MPa)')

plt.legend(loc='best')
plt.show()

#find where new line intercepts stress curve
plt.plot (t[:12500], y_new[:12500], '--')
plt.plot (t[:15000], stress[:15000], color = 'green')
plt.ylim(ymin=0)
plt.xlabel('Time(s)')
plt.ylabel('Stress(MPa)')
idx = np.argwhere(np.diff(np.sign(stress - y_new))).flatten()
plt.plot(t[idx], stress[idx], 'ro')
plt.show()
print ('intersection points')
print (idx)

print ('yield stress:', stress[idx])
print ('yield strength', force[idx])
```

D. 2 R Code

```
#######################################################
# Testing stats code
# Date: November 25, 2021,
# By: Ariana Fraschetti
#Notes:
#############################################################
#load libraries
library(ggplot2)
library(reshape2)
library(dplyr)
library(ggpubr)
library(sjPlot)
library(factoextra)
library(corrplot)
library(psych)
library(ade4)
library(adegraphics)
library(vegan)
library(MASS)
library(ggfortify)
library(sjPlot)
library("Hmisc")
library(lmtest)
library(devtools)

setwd("C:/Users/gabby/Documents/MASc_project/Results")

test <- read.csv("R_test.csv", header=TRUE)
dataset<- read.csv("Master_Spreadsheet_Thesis_stats_analysis.csv", header =
TRUE)
#investigate histograms of all data
hist(dataset)
#create data set with specimen number, sex, and all numeric variables for
baculum + tox data
bac_tox_data <- dataset[c(1, 3, 5, 7:13, 16:18),c(1:4, 22:33, 40:41, 44,
48:65, 68, 71)]
#normalize
bac_tox_logdata <- data.frame(bac_tox_data[,c(1)],
log10(bac_tox_data[,c(2:39)]))
#check for outliers and check with shapiro-wilks
boxplot(bac_tox_data$BacW)
shapiro.test(bac_tox_data$BacW)
#Run pca for bac and element data
bac_tox_pca <- prcomp(bac_tox_logdata[,c(2:39)], center = TRUE,scale. = TRUE)
```

```
test <- read.csv("R_test.csv", header=TRUE)
dataset<- read.csv("Master_Spreadsheet_Thesis_stats_analysis.csv", header =
TRUE)
#investigate histograms of all data
hist(dataset)
#create data set with specimen number, sex, and all numeric variables for
baculum + tox data
bac_tox_data <- dataset[c(1, 3, 5, 7:13, 16:18),c(1:4, 22:33, 40:41, 44,
48:65, 68, 71)]
#normalize
bac_tox_logdata <- data.frame(bac_tox_data[,c(1)],
log10(bac_tox_data[,c(2:39)]))
#check for outliers and check with shapiro-wilks
boxplot(bac_tox_data$BacW)
shapiro.test(bac_tox_data$BacW)
#Run pca for bac and element data
bac_tox_pca <- prcomp(bac_tox_logdata[,c(2:39)], center = TRUE,scale. = TRUE)
pca1=fviz_pca_biplot(bac_tox_pca, axes = c(1,2),
                     geom=c("point", "text"),
                     label = "var",
                     pointsize = 3,
                     select.var = list(contrib=10))+
                     labs(title ="PCA 1: Baculum Metrics and Trace Elements")+
                     theme(text = element_text(size = 15))

summary(bac_tox_pca)
#contribution of the variables
PCA1pc1=fviz_contrib(bac_tox_pca, "var", axes = 1, title=" ", fill = "navy",
border = "navy")
PCA1pc1
PCA1pc2=fviz_contrib(bac_tox_pca, "var", axes = 2, title=" ", fill =
"darkgoldenrod1", border = "darkgoldenrod1")
PCA1pc2
PCA1pc3=fviz_contrib(bac_tox_pca, "var", axes = 3, title=" ", fill = "coral1")
PCA1pc3
PCA1pc4=fviz_contrib(bac_tox_pca, "var", axes = 4, title=" ", fill = "cyan4")
PCA1pc4
PCA1pc5=fviz_contrib(bac_tox_pca, "var", axes = 5, title=" ", fill =
"darkslategray1")
PCA1pc5
#dataset of all femur and tox metrics (include sex) and log transform
fem_tox_data <- dataset[c(1:12, 14:18), c(1:5, 8:12, 14:21, 34:41, 44, 48:65,
68, 71)]
fem_tox_logdata <- data.frame(fem_tox_data[,c(1,5)],
log10(fem_tox_data[,c(2:4, 6:47)]))
#check normality: shapiro wilks and boxplot
boxplot(fem_tox_logdata$FemLen)
shapiro.test(fem_tox_data$FemL)
#Run pca for femur and tox data
fem_tox_pca <- prcomp(fem_tox_logdata[,c(3:47)], center = TRUE,scale. = TRUE)
pca2=fviz_pca_biplot(fem_tox_pca, axes = c(1,2),
                     geom=c("point", "text"),
                     col.ind = fem_tox_logdata$Sex,
```

```
                    col.var = "navy",
                    label = "var",
                    pointsize = 3,
                    palette = c("firebrick1", "dodgerblue"),
                    select.var = list(contrib=5))+
      labs(title ="PCA 2: Femur Metrics and Trace Elements")+
      theme(text = element_text(size = 15)) +
      scale_shape_manual(values=c(19,19))

summary(fem_tox_pca)
#contribution of the variables
PCA1pc1=fviz_contrib(fem_tox_pca, "var", axes = 1, title=" ", fill = "navy",
border = "navy")
PCA1pc1
PCA1pc2=fviz_contrib(fem_tox_pca, "var", axes = 2, title=" ", fill =
"darkgoldenrod1", border = "darkgoldenrod1")
PCA1pc2
PCA1pc3=fviz_contrib(fem_tox_pca, "var", axes = 3, title=" ", fill = "coral1")
PCA1pc3
PCA1pc4=fviz_contrib(fem_tox_pca, "var", axes = 4, title=" ", fill = "cyan4")
PCA1pc4
PCA1pc5=fviz_contrib(fem_tox_pca, "var", axes = 5, title=" ", fill =
"darkslategray1")
PCA1pc5
PCA1pc6=fviz_contrib(fem_tox_pca, "var", axes = 6, title=" ", fill =
"forestgreen")
PCA1pc6
PCA1pc7=fviz_contrib(fem_tox_pca, "var", axes = 7, title=" ", fill =
"darkslateblue")
PCA1pc7
PCA1pc8=fviz_contrib(fem_tox_pca, "var", axes = 8, title=" ", fill =
"mediumpurple1")
PCA1pc8
#correlation matrix for baculums and tox only
btcor <- cor((bac_tox_logdata[,2:39]), use = "pairwise.complete.obs")
pval <- corr.test(bac_tox_logdata[,2:39], use = "pairwise.complete.obs")$p
corrplot(btcor, type="lower", p.mat=pval, insig="blank", number.cex = 0.8,
sig.level = 0.05, tl.col = "black")
#correlation matrix for femurs and tox only
ftcor <- cor((fem_tox_logdata[,3:47]), use = "pairwise.complete.obs")
pval <- corr.test(fem_tox_logdata[,3:47], use = "pairwise.complete.obs")$p
corrplot(ftcor, type="lower", p.mat=pval, insig="blank", number.cex = 0.8,
sig.level = 0.05, tl.col = "black")

#correlation matrix for femurs and baculums
#create new dataframe
bac_fem_data <- data.frame(dataset[c(1:12, 14:18),c(1,5)], dataset[c(1:12,
14:18),c(2:4, 8:39)])
bac_fem_logdata <- data.frame(bac_fem_data[,c(1:2)],
log10(bac_fem_data[,c(3:37)]))
#matrix
bfcor <- cor((bac_fem_logdata[,3:37]), use = "pairwise.complete.obs")
pval <- corr.test(bac_fem_logdata[,3:37], use = "pairwise.complete.obs")$p
```

```
corrplot(bfcor, type="lower", p.mat=pval, insig="blank", number.cex = 0.8,
sig.level = 0.05, tl.col = "black")

#regressions
#define plot that will display all data:
ggplotRegression <- function (fit) {

require(ggplot2)

ggplot(fit$model, aes_string(x = names(fit$model)[1], y = names(fit$model)
[2])) +
  geom_point(size = 3) +
  stat_smooth(method = "lm", col = "red") +
  labs(title = paste("Adj R2 = ",signif(summary(fit)$adj.r.squared, 5),
                     " Slope =",signif(fit$coef[[2]], 5),
                     " P =",signif(summary(fit)$coef[2,4], 5))) +
                     theme_classic()
}

ggplotRegression2 <- function (fit) {

require(ggplot2)

ggplot(fit$model, aes_string(x = names(fit$model)[1], y = names(fit$model)
[2])) +
  geom_point(aes(color = Sex, shape = Sex)) +
  stat_smooth(method = "lm", col = "navy") +
  labs(title = paste("Adj R2 = ",signif(summary(fit)$adj.r.squared, 5),
                     " Slope =",signif(fit$coef[[2]], 5),
                     " P =",signif(summary(fit)$coef[2,4], 5))) +
                     theme_classic()
}
ggplotRegression3 <- function (fit) {
require(ggplot2)

ggplot(fit$model, aes_string(x = names(fit$model)[1], y = names(fit$model)
[2])) +
  geom_point() +
  stat_smooth(method = "lm", col = "cyan4") +
  labs(title = paste("Adj R2 = ",signif(summary(fit)$adj.r.squared, 5),
                     " Slope =",signif(fit$coef[[2]], 5),
                     " P =",signif(summary(fit)$coef[2,4], 5))) +
                     theme_classic()
}
```

```
ggplotRegression4 <- function (fit) {

require(ggplot2)

ggplot(fit$model, aes_string(x = names(fit$model)[1], y = names(fit$model)
[2])) +
  geom_point() +
  stat_smooth(method = "lm", col = "green") +
  labs(title = paste("Adj R2 = ",signif(summary(fit)$adj.r.squared, 5),
                     " Slope =",signif(fit$coef[[2]], 5),
                     " P =",signif(summary(fit)$coef[2,4], 5))) +
                     theme_classic()
}
ggplotRegression5 <- function (fit) {

require(ggplot2)

ggplot(fit$model, aes_string(x = names(fit$model)[1], y = names(fit$model)
[2])) +
  geom_point() +
  stat_smooth(method = "lm", col = "midnightblue") +
  labs(title = paste("Adj R2 = ",signif(summary(fit)$adj.r.squared, 5),
                     " Slope =",signif(fit$coef[[2]], 5),
                     " P =",signif(summary(fit)$coef[2,4], 5))) +
                     theme_classic()
}
#1. BACULUM METRICS
#structural properties and bone geometry
ba <- lm(BacSI ~ BacPL, data = bac_tox_logdata)
bb <- lm(BacSt ~ BacW, data = bac_tox_logdata)
bag <- ggplotRegression(ba)
bbg <- ggplotRegression2(bb)

ggarrange(bag, bbg,
          labels = c("A", "B"),
          ncol = 2, nrow = 1)

#Ca and Fe
bc <- lm(Ca ~ BacE, data = bac_tox_logdata)
bd <- lm(Ca ~ BacYS, data = bac_tox_logdata)
be <- lm(Ca ~ BacWtF, data = bac_tox_logdata)
bf <- lm(Fe ~ BacE, data = bac_tox_logdata)
bg <- lm(Fe ~ BacYS, data = bac_tox_logdata)

bcg <- ggplotRegression(bc)
bdg <- ggplotRegression2(bd)
beg <- ggplotRegression3(be)
bfg <- ggplotRegression4(bf)
bgg <- ggplotRegression5(bg)
```

```
ggarrange(bcg, bdg, beg, bfg, bgg,
          labels = c("A", "B", "C", "D", "E"),
          ncol = 2, nrow = 3)

bptest(bc)
bptest(bd)
bptest(be)
bptest(bf)
bptest(bg)

#Pb
bh <- lm(Pb ~ BacWtF, data=bac_tox_logdata)
bhg <- ggplotRegression(bh)
bptest(bh)

#Rb
bi <- lm(Rb ~ BacSI, data = bac_tox_logdata)
bj <- lm(Rb ~ BA, data=bac_tox_logdata)
bk <- lm(Rb ~ BacPL, data = bac_tox_logdata)
bl <- lm(Rb ~ BacWtF, data = bac_tox_logdata)

big <- ggplotRegression(bi)
bjg <- ggplotRegression2(bj)
bkg <- ggplotRegression3(bk)
blg <- ggplotRegression4(bl)

ggarrange(big, bjg, bkg, blg,
          labels = c("A", "B", "C", "D"),
          ncol = 2, nrow = 2)

#Se

bm <- lm(Se ~ BacW, data = bac_tox_logdata)
bn <- lm(Se ~ BacPL, data=bac_tox_logdata)
bo <- lm(Se ~ BacSt, data = bac_tox_logdata)
bp <- lm(Se ~ BacYL, data = bac_tox_logdata)
bq <- lm(Se ~ BW, data = bac_tox_logdata)

bmg <- ggplotRegression(bm)
bng <- ggplotRegression2(bn)
bog <- ggplotRegression3(bo)
bpg <- ggplotRegression4(bp)
bqg <- ggplotRegression5(bq)

ggarrange(bmg, bng, bog, bpg, bqg,
          labels = c("A", "B", "C", "D", "E"),
          ncol = 2, nrow = 3)

#Na
br <- lm(Na ~ BacE, data = bac_tox_logdata)
bs <- lm(Na ~ BacYS, data=bac_tox_logdata)
bt <- lm(Na ~ BacUS, data = bac_tox_logdata)
```

```
#bt did not pass homoscedasticity test

brg <- ggplotRegression(br)
bsg <- ggplotRegression2(bs)

ggarrange(brg, bsg,
          labels = c("A", "B"),
          ncol = 2, nrow = 2)

#FEMUR AND TRACE ELEMENTS

#Con ~ PL
fa <- lm(Con ~ FemLen, data = fem_tox_logdata)
fb <- lm(Con ~ FemPL, data=fem_tox_logdata)
fgh <- ggplot(fem_tox_logdata, aes(x = FemLen, y = Con)) +
geom_point(aes(shape = Sex, color = Sex), size = 3) + stat_smooth(method =
"lm", col = "red") + theme_classic() +
 labs(title = paste("Adj R2 = ",signif(summary(fa)$adj.r.squared, 5),
                    " Slope =",signif(fa$coef[[2]], 5),
                    " P =",signif(summary(fa)$coef[2,4], 5))) +
                    theme_classic()
fbg <- ggplot(fem_tox_logdata, aes(x = FemPL, y = Con)) + geom_point(aes(shape
= Sex, color = Sex), size = 3) + stat_smooth(method = "lm", col = "red") +
theme_classic() +
 labs(title = paste("Adj R2 = ",signif(summary(fb)$adj.r.squared, 5),
                    " Slope =",signif(fb$coef[[2]], 5),
                    " P =",signif(summary(fb)$coef[2,4], 5))) +
                    theme_classic()

ggarrange(fgh, fbg,
          labels = c("A", "B"),
          ncol = 2, nrow = 1)
#Ys ~ FA
fc <- lm(FA ~ FemYS, data= fem_tox_logdata)
fcg <- ggplot(fem_tox_logdata, aes(x = FA, y = FemYS)) + geom_point(aes(shape
= Sex, color = Sex), size = 3) + stat_smooth(method = "lm", col = "red") +
theme_classic() +
 labs(title = paste("Adj R2 = ",signif(summary(fb)$adj.r.squared, 5),
                    " Slope =",signif(fb$coef[[2]], 5),
                    " P =",signif(summary(fb)$coef[2,4], 5))) +
                    theme_classic()

#Tb.th
fg <- lm(Al ~ Tb.Th, data= fem_tox_logdata)
bptest(fg)

ggplot(fem_tox_logdata, aes(x = Al, y = Tb.Th)) + geom_point(aes(color = Sex),
size = 3) + stat_smooth(method = "lm", col = "red") + theme_classic()
```

```
#Fe
fe <- lm(Fe ~ FA, data=fem_tox_logdata)
feg <- ggplot(fem_tox_logdata, aes(x = Fe, y = FA)) + geom_point(aes(shape =
Sex, color = Sex), size = 3) + stat_smooth(method = "lm", col = "red") +
theme_classic() +
 labs(title = paste("Adj R2 = ",signif(summary(fe)$adj.r.squared, 5),
                    " Slope =",signif(fe$coef[[2]], 5),
                    " P =",signif(summary(fe)$coef[2,4], 5))) +
                    theme_classic()

ff <- lm(Fe ~ FemSt, data=fem_tox_logdata)
ffg <- ggplot(fem_tox_logdata, aes(x = Fe, y = FemSt)) + geom_point(aes(shape
= Sex, color = Sex), size = 3) + stat_smooth(method = "lm", col = "red") +
theme_classic() +
 labs(title = paste("Adj R2 = ",signif(summary(ff)$adj.r.squared, 5),
                    " Slope =",signif(ff$coef[[2]], 5),
                    " P =",signif(summary(ff)$coef[2,4], 5))) +
                    theme_classic()
fg <- lm(Fe ~ FemBenMom, data =fem_tox_logdata)
fgg <- ggplot(fem_tox_logdata, aes(x = Fe, y = FemYS)) + geom_point(aes(shape
= Sex, color = Sex), size = 3) + stat_smooth(method = "lm", col = "red") +
theme_classic() +
 labs(title = paste("Adj R2 = ",signif(summary(fg)$adj.r.squared, 5),
                    " Slope =",signif(fg$coef[[2]], 5),
                    " P =",signif(summary(fg)$coef[2,4], 5))) +
                    theme_classic()

fh <- lm(Fe ~ FemYL, data = fem_tox_logdata)
fhg <- ggplot(fem_tox_logdata, aes(x = Fe, y = FemYL)) + geom_point(aes(shape
= Sex, color = Sex), size = 3) + stat_smooth(method = "lm", col = "red") +
theme_classic() +
 labs(title = paste("Adj R2 = ",signif(summary(fh)$adj.r.squared, 5),
                    " Slope =",signif(fh$coef[[2]], 5),
                    " P =",signif(summary(fh)$coef[2,4], 5))) +
                    theme_classic()

ggarrange(feg, ffg, fgg, fhg,
          labels = c("A", "B", "C", "D"),
          ncol = 2, nrow = 2)

#the rest of bone metrics and trace elements
fi <- lm(Mg ~ ConDen, data = fem_tox_logdata)
fk <- lm(Rb ~ Con, data = fem_tox_logdata)

fig <- ggplot(fem_tox_logdata, aes(x = Mg, y = ConDen)) + geom_point(aes(shape
= Sex, color = Sex), size = 3) + stat_smooth(method = "lm", col = "red") +
theme_classic() +
 labs(title = paste("Adj R2 = ",signif(summary(fi)$adj.r.squared, 5),
                    " Slope =",signif(fi$coef[[2]], 5),
                    " P =",signif(summary(fi)$coef[2,4], 5))) +
                    theme_classic()
```

```
fkg <- ggplot(fem_tox_logdata, aes(x = Rb, y = Con)) + geom_point(aes(shape =
Sex, color = Sex), size = 3) + stat_smooth(method = "lm", col = "red") +
theme_classic() +
 labs(title = paste("Adj R2 = ",signif(summary(fk)$adj.r.squared, 5),
                    " Slope =",signif(fk$coef[[2]], 5),
                    " P =",signif(summary(fk)$coef[2,4], 5))) +
                    theme_classic()
ggarrange(fig, fkg,
          labels = c("A", "B", "C"),
          ncol = 2, nrow = 1)
#Rb and Se
fl <- lm(Rb ~ FemBenMom, data = fem_tox_logdata)
fm<- lm(Rb ~ Con, data = fem_tox_logdata)
fn <- lm(Se ~ FemYS, data = fem_tox_logdata)
fo<- lm(Se ~ FemAP, data = fem_tox_logdata)
fp <- lm(Rb ~ FemW, data=fem_tox_logdata)

flg <- ggplot(fem_tox_logdata, aes(x = Rb, y = FemBenMom)) +
geom_point(aes(shape = Sex, color = Sex), size = 3) + stat_smooth(method =
"lm", col = "red") + theme_classic() +
 labs(title = paste("Adj R2 = ",signif(summary(fl)$adj.r.squared, 5),
                    " Slope =",signif(fl$coef[[2]], 5),
                    " P =",signif(summary(fl)$coef[2,4], 5))) +
                    theme_classic()
fmg <- ggplot(fem_tox_logdata, aes(x = Rb, y = Con)) + geom_point(aes(shape =
Sex, color = Sex), size = 3) + stat_smooth(method = "lm", col = "red") +
theme_classic() +
 labs(title = paste("Adj R2 = ",signif(summary(fm)$adj.r.squared, 5),
                    " Slope =",signif(fm$coef[[2]], 5),
                    " P =",signif(summary(fm)$coef[2,4], 5))) +
                    theme_classic()
fng <- ggplot(fem_tox_logdata, aes(x = Se, y = FemYS)) + geom_point(aes(shape
= Sex, color = Sex), size = 3) + stat_smooth(method = "lm", col = "red") +
theme_classic() +
 labs(title = paste("Adj R2 = ",signif(summary(fn)$adj.r.squared, 5),
                    " Slope =",signif(fn$coef[[2]], 5),
                    " P =",signif(summary(fn)$coef[2,4], 5))) +
                    theme_classic()
fog <- ggplot(fem_tox_logdata, aes(x = Se, y = FemAP)) + geom_point(aes(shape
= Sex, color = Sex), size = 3) + stat_smooth(method = "lm", col = "red") +
theme_classic() +
 labs(title = paste("Adj R2 = ",signif(summary(fo)$adj.r.squared, 5),
                    " Slope =",signif(fo$coef[[2]], 5),
                    " P =",signif(summary(fo)$coef[2,4], 5))) +
                    theme_classic()
```

```
fpg <- ggplot(fem_tox_logdata, aes(x = Rb, y = FemW)) + geom_point(aes(shape =
Sex, color = Sex), size = 3) + stat_smooth(method = "lm", col = "red") +
theme_classic() +
 labs(title = paste("Adj R2 = ",signif(summary(fp)$adj.r.squared, 5),
                    " Slope =",signif(fp$coef[[2]], 5),
                    " P =",signif(summary(fp)$coef[2,4], 5))) +
                    theme_classic()

ggarrange(flg, fmg, fpg, fng, fog,
          labels = c("A", "B", "C", "D", "E"),
          ncol = 2, nrow = 3)

#relationships between bac and fem metrics

bfa <- lm(Tb.Th ~ BacSt, data= bac_fem_logdata)
bfb <- lm(Tb.Sp ~ BacYL, data = bac_fem_logdata)

bfag <- ggplot(bac_fem_logdata, aes(x = Tb.Th, y = BacSt)) + geom_point(size =
3) + stat_smooth(method = "lm", col = "red") + theme_classic() +
 labs(title = paste("Adj R2 = ",signif(summary(bfa)$adj.r.squared, 5),
                    " Slope =",signif(bfa$coef[[2]], 5),
                    " P =",signif(summary(bfa)$coef[2,4], 5))) +
                    theme_classic()
bfbg <- ggplot(bac_fem_logdata, aes(x = Tb.Sp, y = BacYL)) + geom_point(size =
3) + stat_smooth(method = "lm", col = "red") + theme_classic() +
 labs(title = paste("Adj R2 = ",signif(summary(bfb)$adj.r.squared, 5),
                    " Slope =",signif(bfb$coef[[2]], 5),
                    " P =",signif(summary(bfb)$coef[2,4], 5))) +
                    theme_classic()
ggarrange(bfag, bfbg,
          labels = c("A", "B"),
          ncol = 2, nrow = 1)

#POWER ANALYSIS
library(pwr)
#power analysis for iron and baculum yield stress:
pwr.f2.test(u=1, f2 = 0.69, sig.level = 0.007875, power = 0.80)
pwr.f2.test(u=1, f2 = 0.59, sig.level = 0.026179, power = 0.80)
pwr.f2.test(u=1, f2 = 0.5, sig.level = 0.02346, power = 0.80)
pwr.f2.test(u=1, f2 = 0.467, sig.level = 0.03367, power = 0.80)

#aluminum and lead
pwr.f2.test(u=1, f2 = 0.611, sig.level = 0.014702, power = 0.80)
pwr.f2.test(u=1, f2 = 0.6102, sig.level = 0.015801, power = 0.80)

#rubidium
pwr.f2.test(u=1, f2 = 0.7243, sig.level = 0.0046507, power = 0.80)
pwr.f2.test(u=1, f2 = 0.65746, sig.level = 0.012, power = 0.80)
pwr.f2.test(u=1, f2 = 0.584, sig.level = 0.0081394, power = 0.80)
pwr.f2.test(u=1, f2 = 0.5019, sig.level = 0.023205, power = 0.80)
```

```
#selenium
pwr.f2.test(u=1, f2 = 0.7658, sig.level = 0.0022334, power = 0.80)
pwr.f2.test(u=1, f2 = 0.737, sig.level = 0.003769, power = 0.80)
pwr.f2.test(u=1, f2 = 0.727, sig.level = 0.0044544, power = 0.80)
pwr.f2.test(u=1, f2 = 0.4315, sig.level = 0.047457, power = 0.80)

#Na and Mg
pwr.f2.test(u=1, f2 = 0.61036, sig.level = 0.020681, power = 0.80)
pwr.f2.test(u=1, f2 = 0.6006, sig.level = 0.022912, power = 0.80)
pwr.f2.test(u=1, f2 = 0.4387, sig.level = 0.044395, power = 0.80)
```

Appendix E – Additional Results

The following are supplementary results including a table of mink specimen basic information and an image of the femur diaphysis cross-section.

Table E.1*: Collection information of the mink specimens. ECCC provided some morphological and locational information of the mink, including their body and liver weights, sex, collection site and province in which they were collected.*

Specimen ID/No.	Bodyweight (kg)	Liver weight (g)	Hepatosomatic index (HSI)	Sex	Collection site	Province
1718-451-1	0.66	32.8	4.97	Male	RFMA #137	Alberta
1718-451-2	0.54	18	3.33	Female	RFMA #137	Alberta
1718-451-3	0.68	34.5	5.07	Male	RFMA #137	Alberta
1718-451-5	0.62	34.5	5.56	Female	RFMA #174	Alberta
1718-456-1	0.9	39.7	4.41	Male	RFMA #174	Alberta
1718-456-3	0.42	23.2	5.52	Female	RFMA #174	Alberta
1718-456-4	0.66	21.1	3.20	Male	RFMA #137	Alberta
1718-456-5	0.76	30.3	3.99	Male	RFMA #137	Alberta
1718-460-1	0.78	42.7	5.47	Male	RFMA #174	Alberta
1718-460-2	0.7	29.6	4.23	Male	RFMA #137	Alberta
1718-460-3	0.52	21.2	4.08	Male	RFMA #137	Alberta
1718-460-5	1.08	42.2	3.91	Male	RFMA #174	Alberta
1718-418	0.94	61.7	6.56	Male	RFMA #2317	Alberta
JPK-02	0.77	32.9	4.27	Male	RFMA #592	Alberta
1718-425	0.86	43.1	5.01	Male	RFMA #592	Alberta
QC1954	0.74	54.6	7.38	Male	Wakefield	Quebec
QC1955	0.78	41.6	5.33	Male	Wakefield	Quebec
QC1958	0.66	46.4	7.03	Male	Wakefield	Quebec

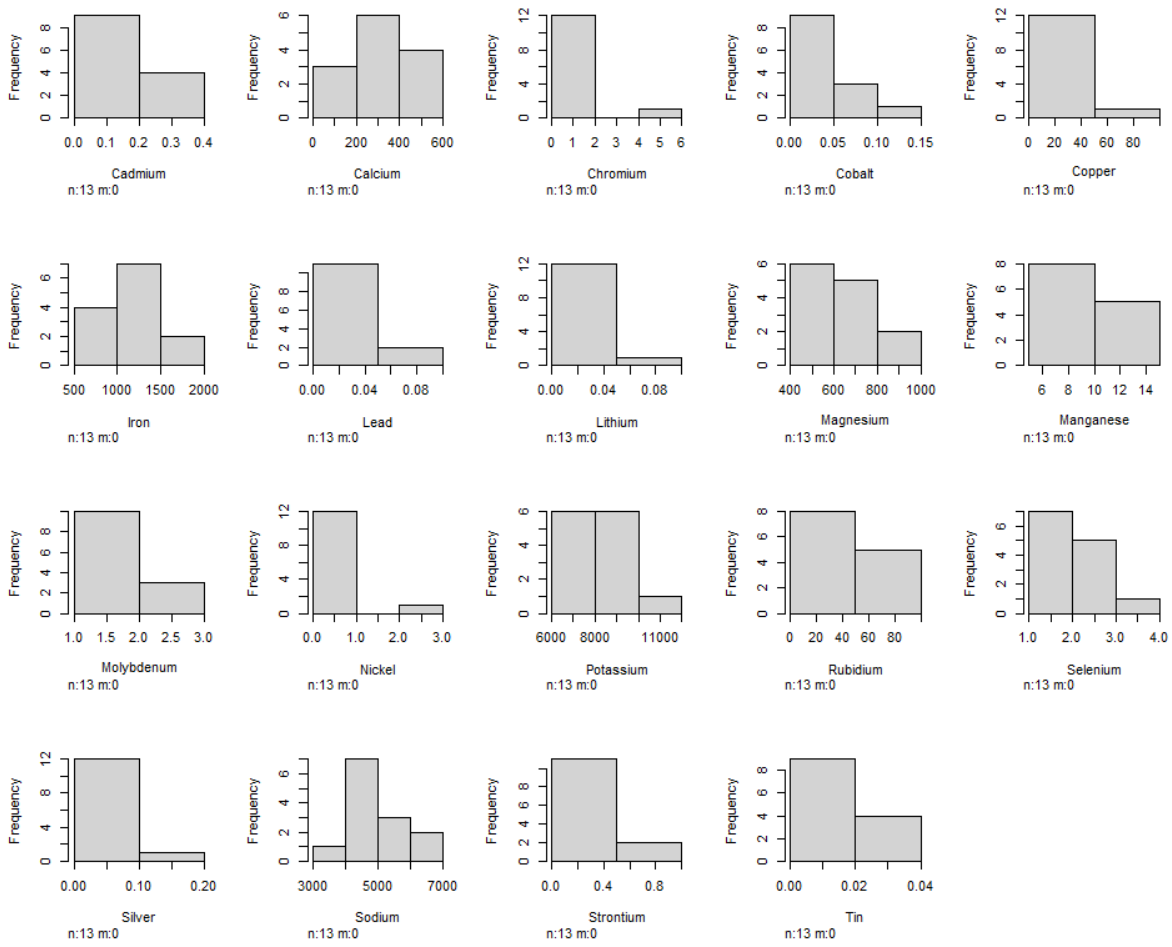

Figure E.1: *Sample histograms of the trace element concentrations*.
The majority of variables exhibited non-normal distributions.

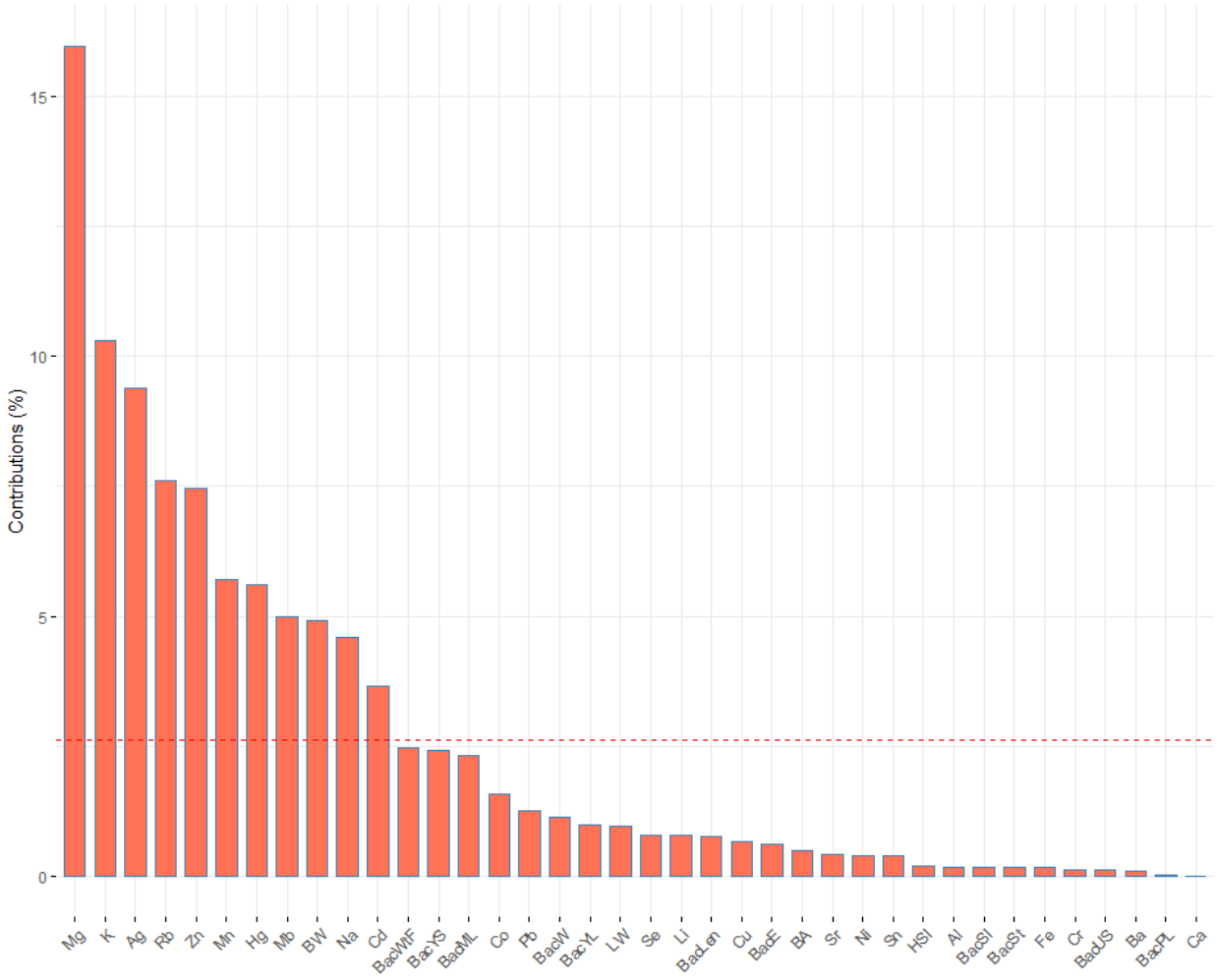

Figure E.2: *Percent contribution of each variable to the third principal component of PCA 1*. This principal component accounted for 13% of the variability in data.

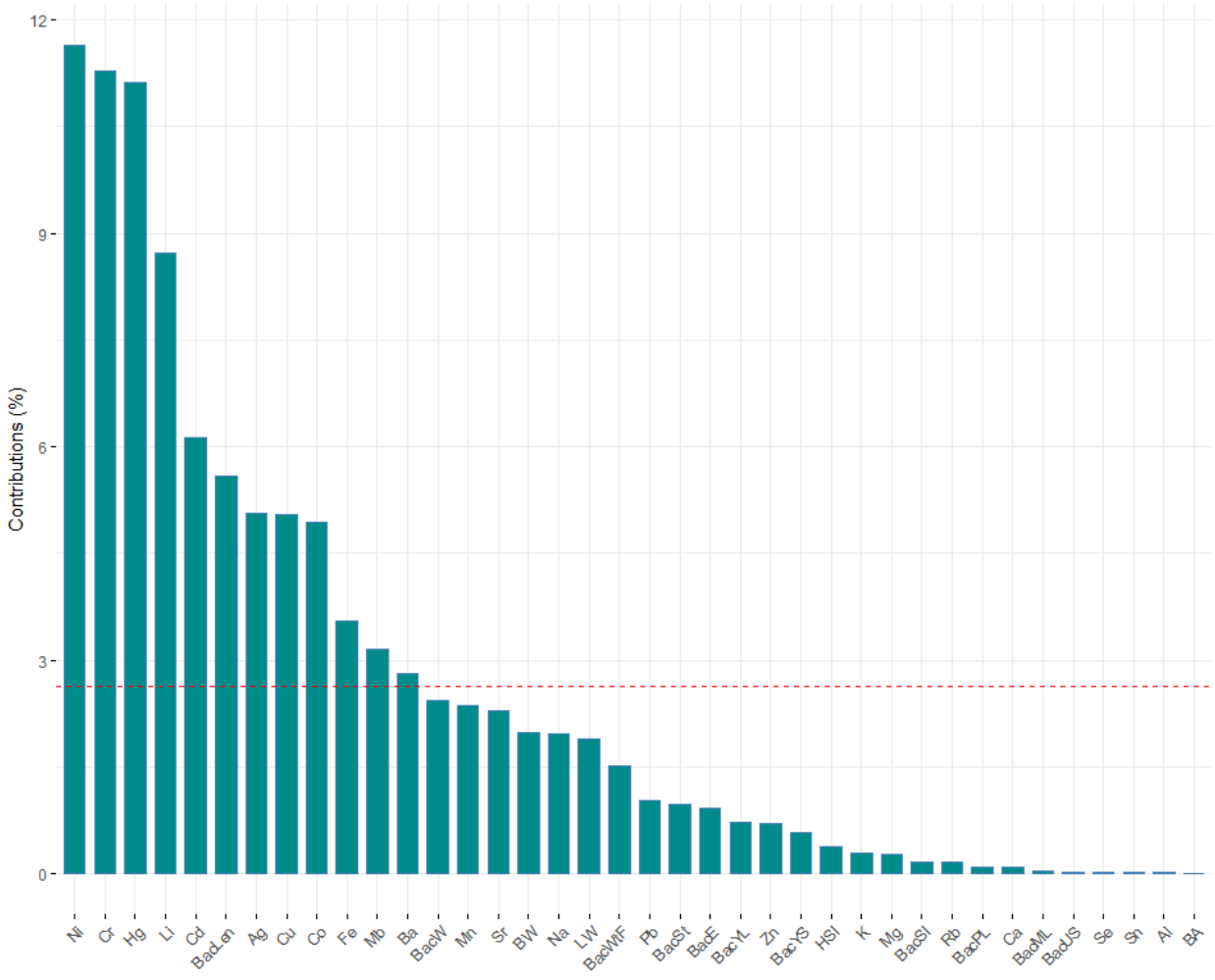

Figure E.3: *Percent contribution of each variable to the fourth principal component of PCA 1.* This principal component accounted for 10% of the variability in data.

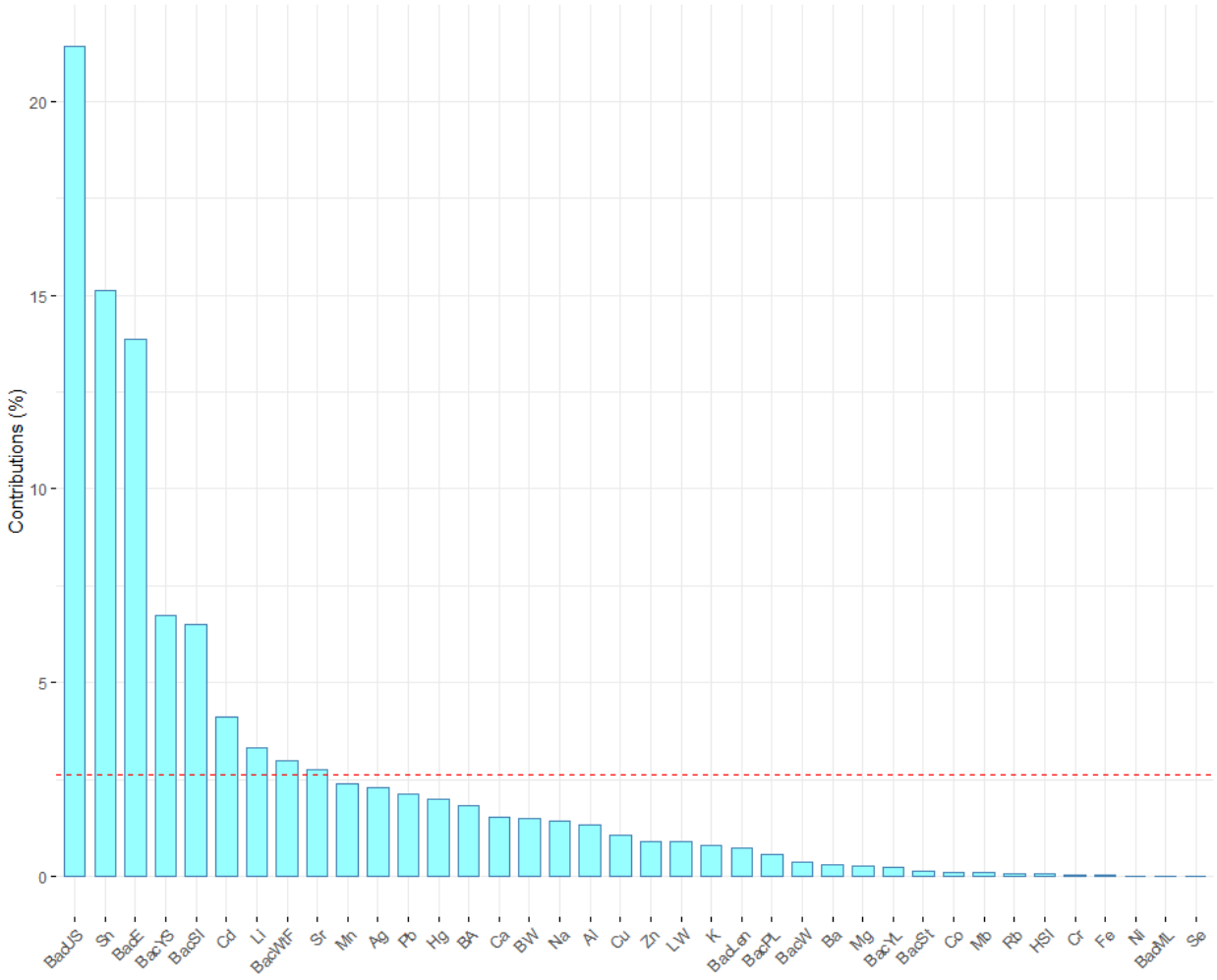

Figure E.4: *Percent contribution of each variable to the fifth principal component of PCA 1*. This principal component accounted for 6% of the variability in data.

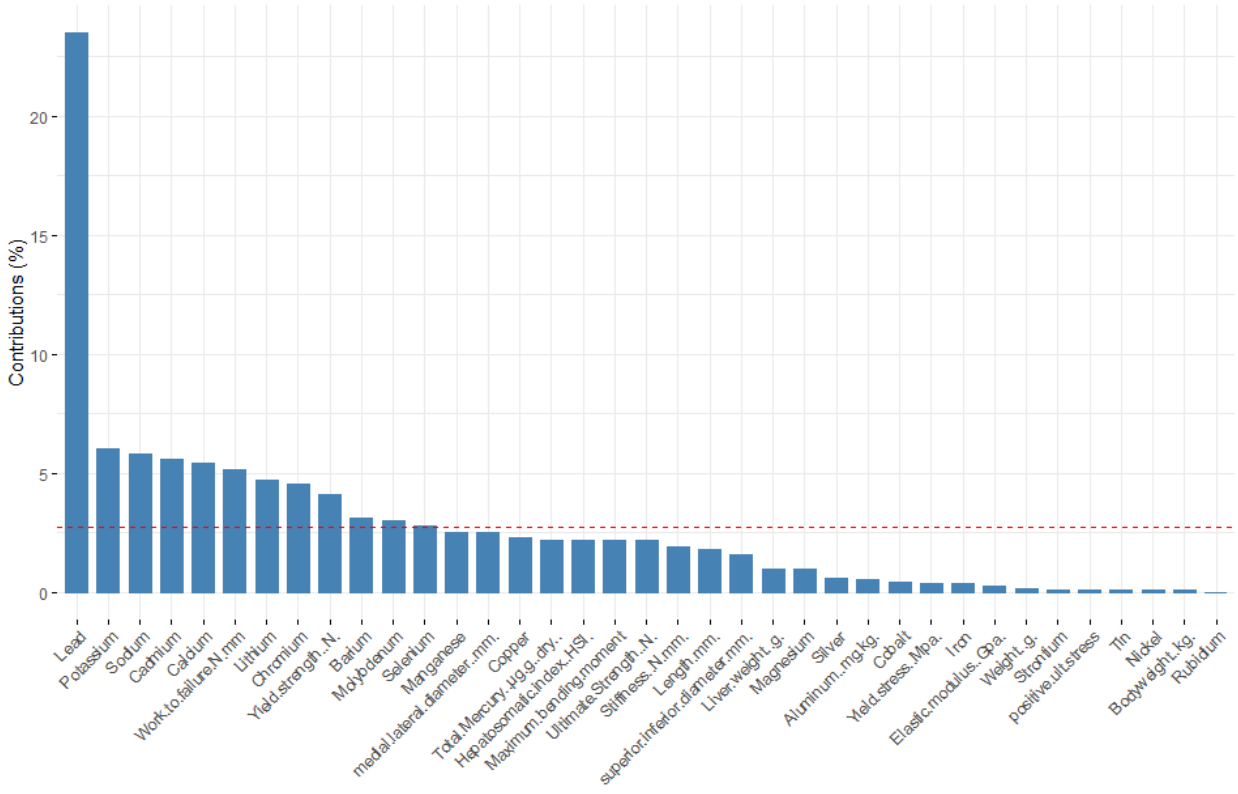

Figure E.5: *Percent contribution of each variable to the fifth principal component pf PCA 1*. This principal component accounted for 4.4% of the variability in data.

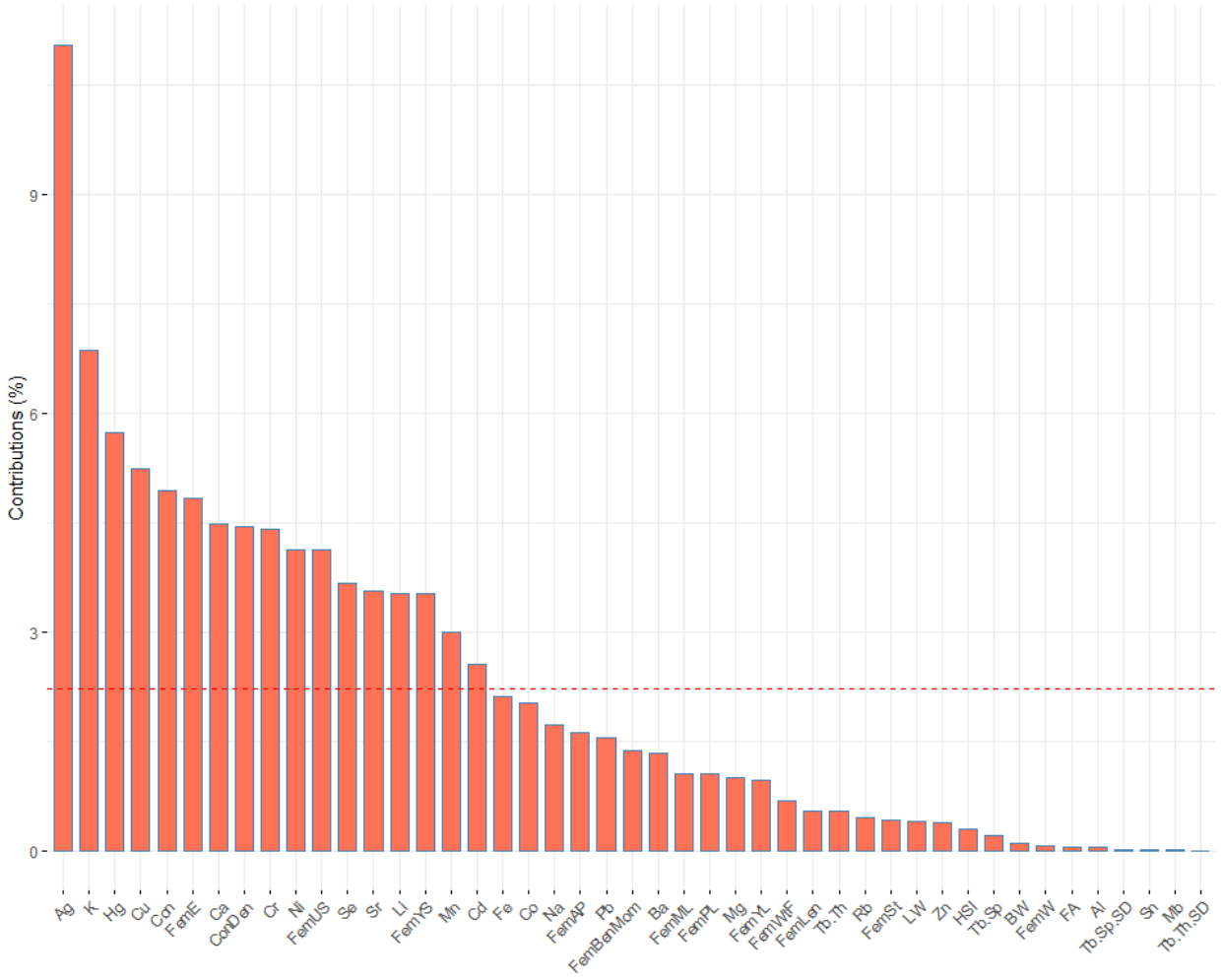

Figure E.6: *The third principal component of PCA 2*. This accounted for 13% of the variation in data.

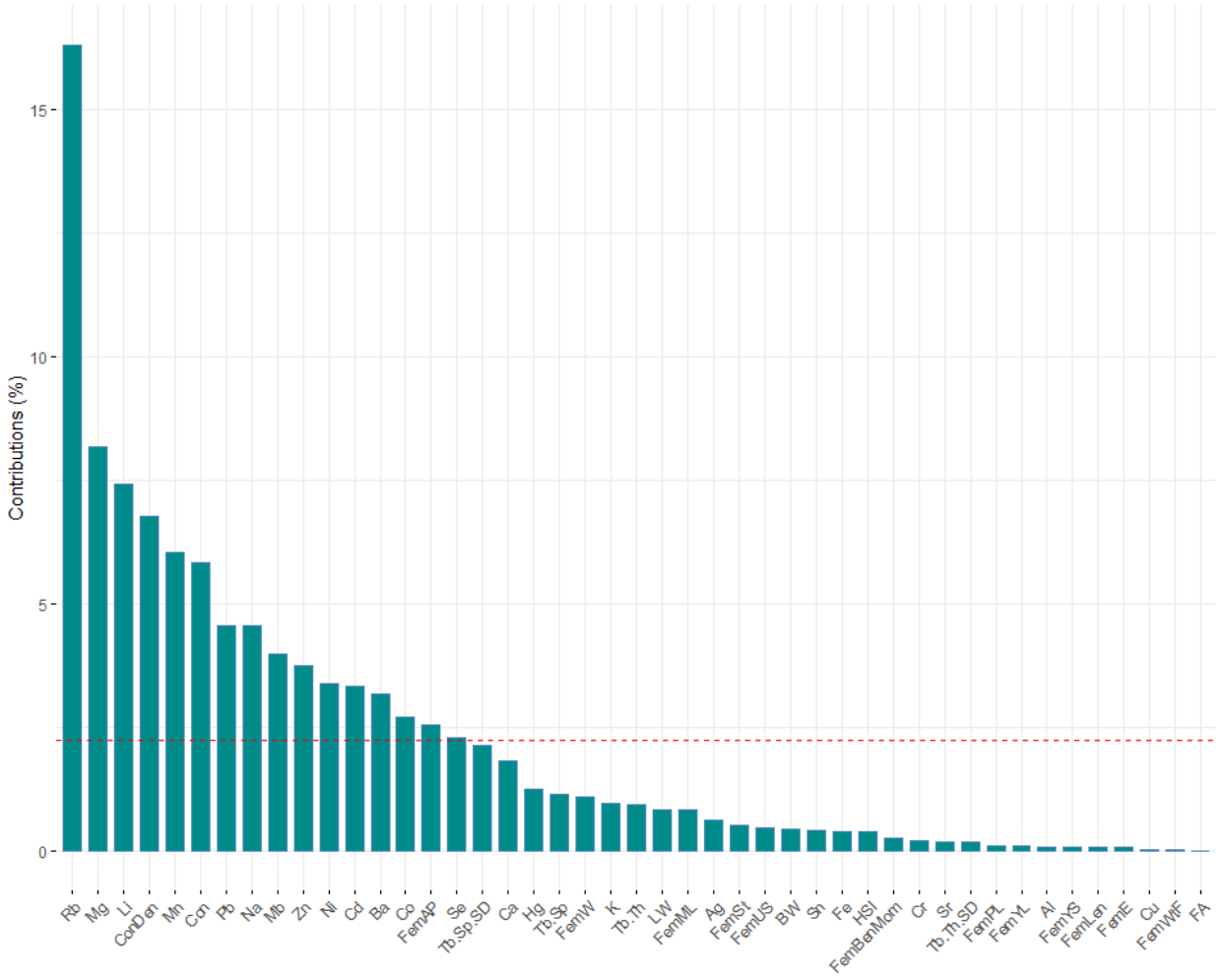

Figure E.7: *The fourth principal component of PCA 2*. This accounted for 9% of the variation in the data.

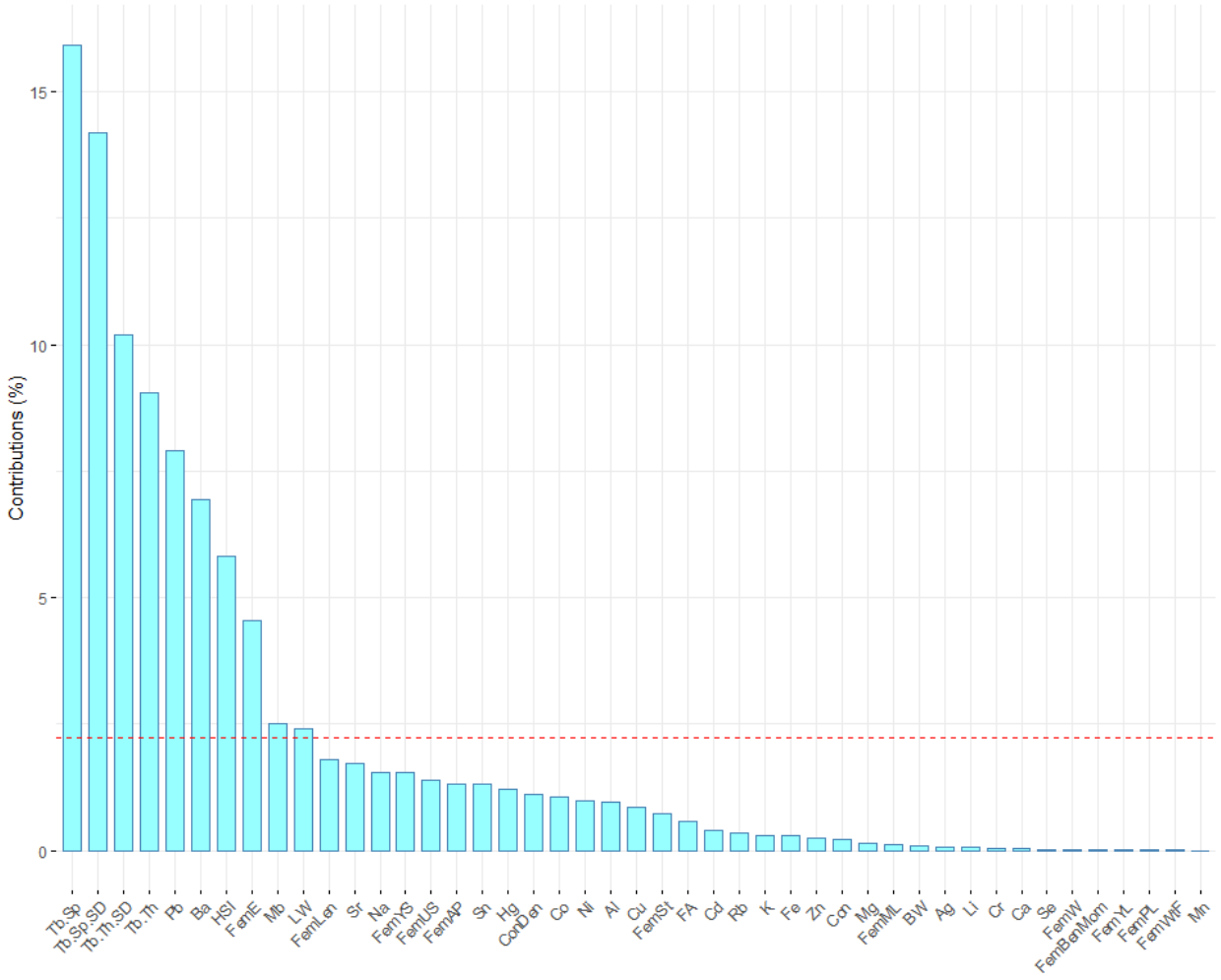

Figure E.8: *The fifth principal component of PCA 2*. This accounted for 7% of the variation in data.

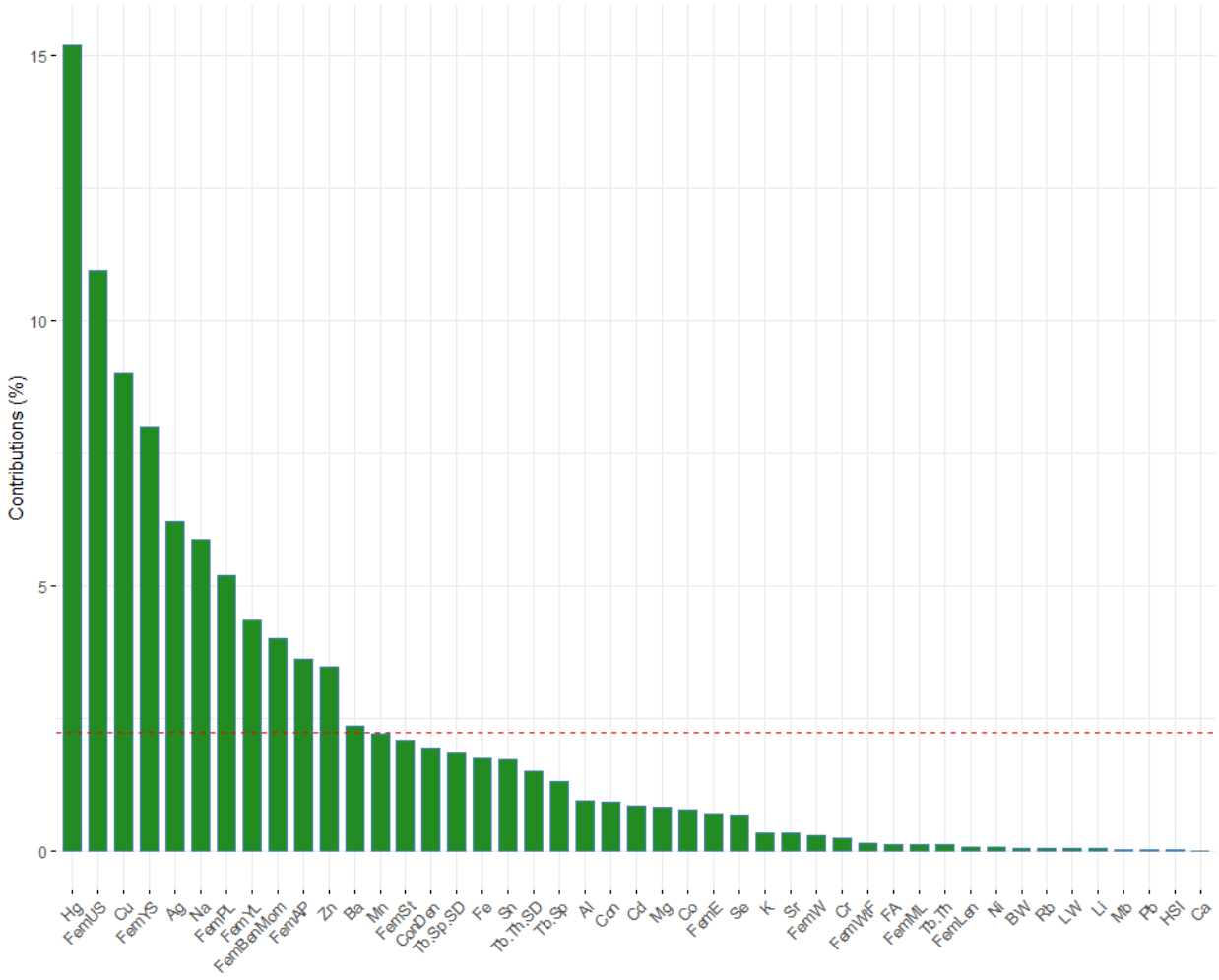

Figure E.9: *the sixth principal component of PCA 2.* This accounted for 5% of the variation in the data.

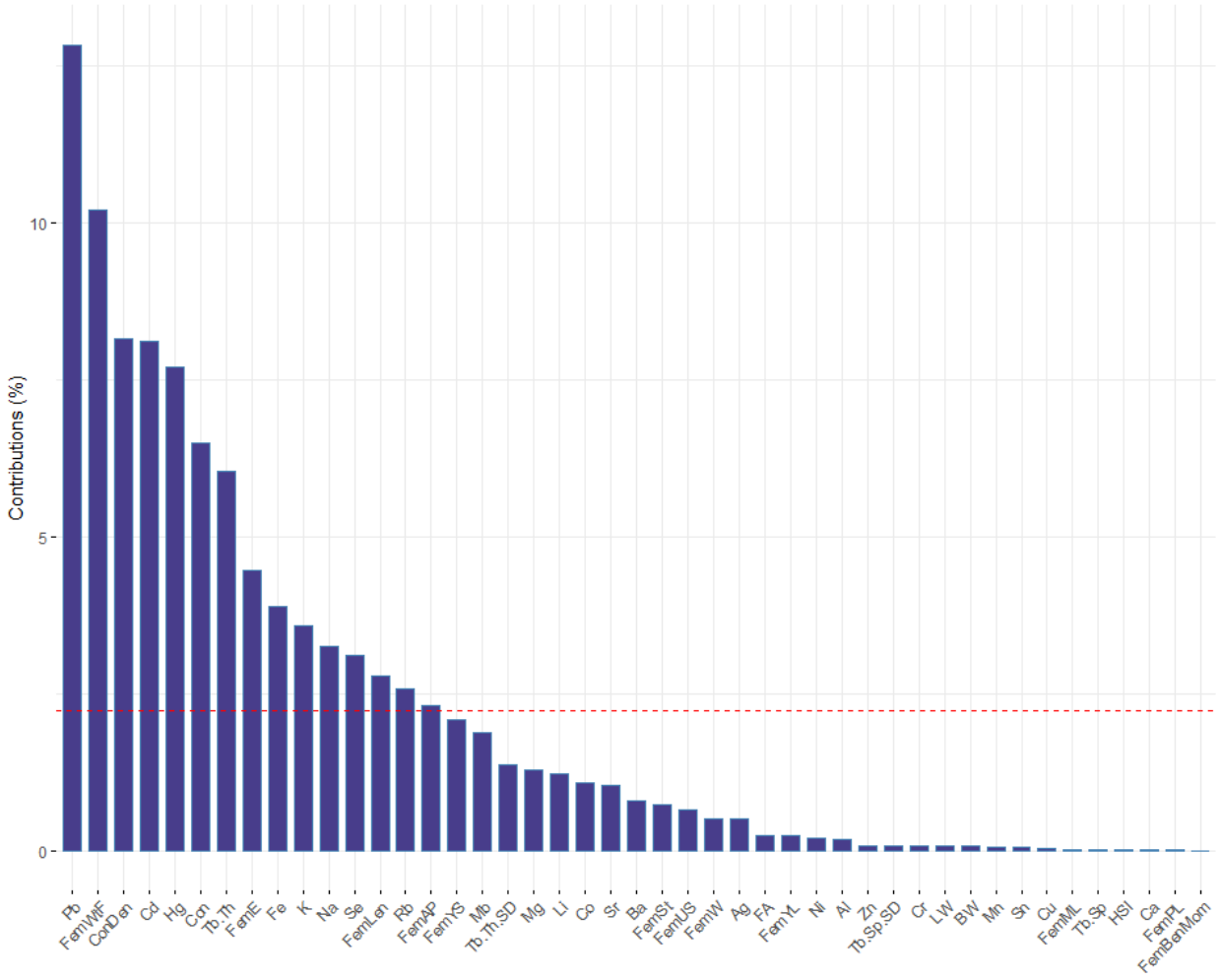

Figure E.10: *The seventh principal component of PCA 2*. This accounted for 4% of the variation in data.

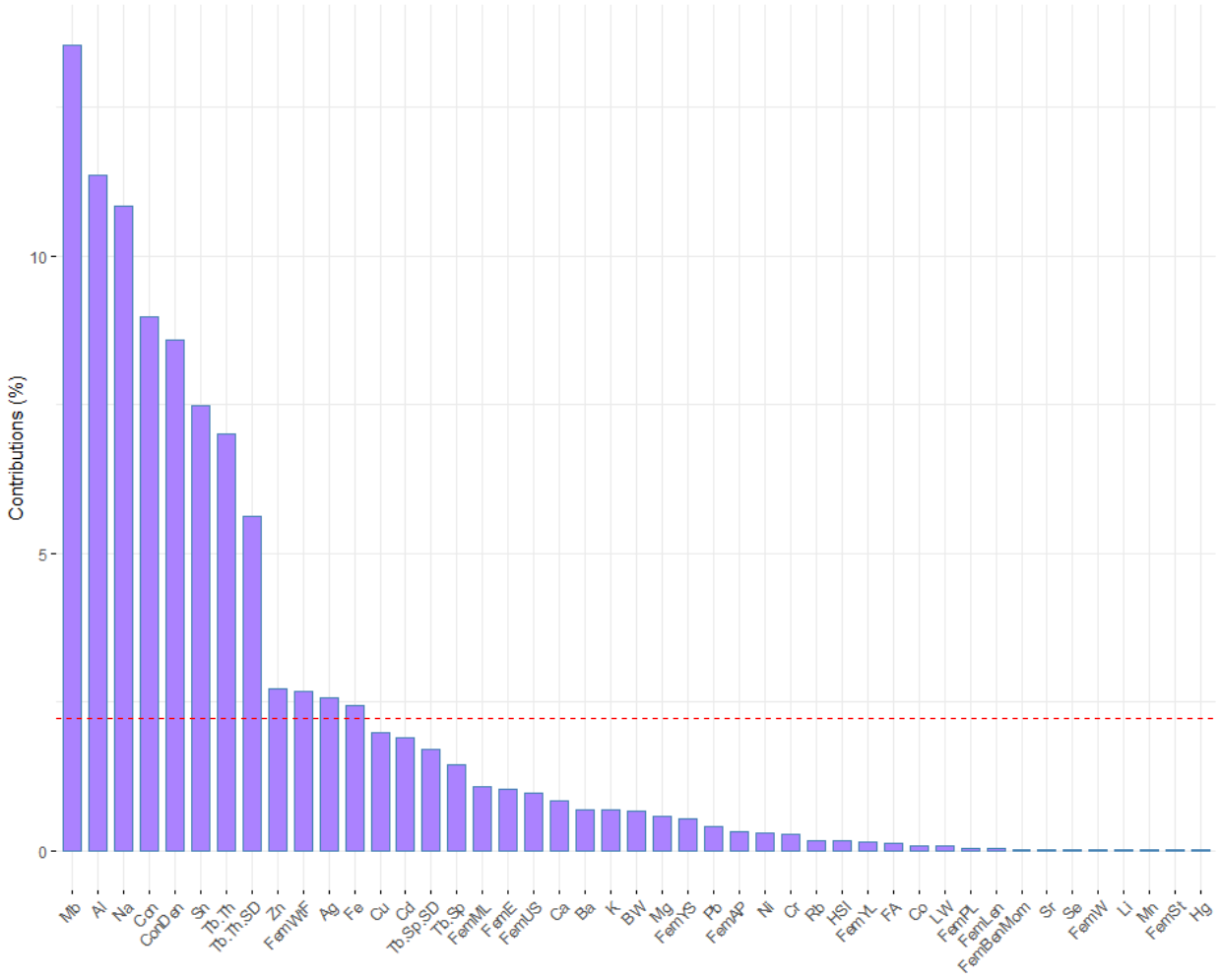

Figure E.11: *The eight principal component of PCA 2*. This accounted for 3% of the variation in the data.

Appendix F – Power Analysis Results

Table F.1: *The minimum sample sizes needed for a power of 0.80. Only significant relationships between trace elements and bone metrics are listed.*

Relationship	R^2	P-value	Minimum Sample Size
Iron and baculum yield stress	0.48	0.0079	20
Iron and baculum bending modulus	0.35	0.026	17
Iron and femur second moment of area	0.25	0.023	20
Iron and femur yield load	0.22	0.034	19
Iron and femur yield stress	0.21	0.036	19
Iron and femur stiffness	0.20	0.042	19
Lead and baculum work-to-failure	0.38	0.015	19
Aluminum and baculum work-to-failure	0.37	0.016	19
Aluminum and connectivity	0.21	0.036	19
Rubidium and baculum work-to-failure	0.52	0.0047	21
Rubidium and baculum second moment of area	0.43	0.012	19
Rubidium and baculum peak load	0.36	0.024	17
Rubidium and trabecular connectivity	0.34	0.0081	23
Rubidium and femur weight	0.25	0.023	23
Rubidium and maximum bending moment	0.18	0.050	21
Sodium and baculum bending modulus	0.37	0.021	17
Sodium and baculum yield stress	0.36	0.023	17
Magnesium and connectivity density	0.19	0.044	19
Selenium and baculum stiffness	0.59	0.0022	23
Selenium and baculum peak load	0.54	0.0038	21
Selenium and bodyweight	0.53	0.0045	21
Selenium and baculum yield load	0.50	0.0063	20
Selenium and baculum weight	0.47	0.0082	19
Selenium and femur yield stress	0.19	0.047	19